



**TURUN
YLIOPISTO**

STUDIES ON CATIONIC POLYTHIOPHENES WITH HYDROGEN-BONDING DONOR CAPABILITIES

Sergio Ulises Espinosa Domínguez

University of Turku

Faculty of Science and Engineering
Department of Chemistry
Doctoral programme in Physical and
Chemical Sciences

Supervised by

Professor Carita Kvarnström
Department of Chemistry
University of Turku
Turku, Finland

Adjunct Professor Pia Damlin
Department of Chemistry
University of Turku
Turku, Finland

Reviewed by

Adjunct Professor Sami Hietala
Department of Chemistry
University of Helsinki
Helsinki, Finland

Professor Ulrich Scheler
Department of Polyelectrolytes &
Dispersions
Leibniz Institute of Polymer Research
Dresden, Germany

Opponent

Professor Matti Knaapila
Department of Physics
Technical University of Denmark
Copenhagen, Denmark

The originality of this thesis has been checked in accordance with the University of Turku quality assurance system using the Turnitin OriginalityCheck service.

ISBN 978-951-29-7820-5 (PRINT)
ISBN 978-951-29-7821-2 (PDF)
ISSN 0082-7002 (Print)
ISSN 2343-3175 (Online)
Punamusta Oy, Finland 2019

TURUN YLIOPISTO

Luonnontieteiden ja tekniikan tiedekunta

Kemian laitos

SERGIO ULISES ESPINOSA DOMÍNGUEZ: Vetysidosten luovuttajina toimivien kationisten polytiofeenien tutkimus

Väitöskirja, 137 s.

Fysikaalisten ja kemiallisten tieteiden tohtoriohjelma (PCS)

Marraskuu 2019

Tiivistelmä

Tämä projekti keskittyy kationisiin isotiouroniumpolytiofeeneihin (CIT), jotka ovat tiettytyyppisiä konjugoituja polyelektrolyyttejä (CPE). Yleensä CPE:t yhdistävät pii-konjugoidun polymeerirungon funktionalisiin ioniryhmiin, mikä antaa niille kromo- ja fluoroforisia ominaisuuksia sekä myös vesiliukoisuuden. Tämä rakenne tarjoaa CPE:lle sekä konjugoitujen polymeerien pii-pii- ja hydrofobiset vuorovaikutukset että polyelektrolyyttien koordinatiiviset vuorovaikutukset sähköstaattisten voimien ja vetysitoutumisen kautta. Erityisesti polytiofeeni-CPE-proteiinit ovat herkkiä erilaisille ärsykkeille, kuten liuottimelle (solvatokromismi) tai muille molekyyille (affiniteetikromismi), mitä voidaan tutkia fluoresenssin avulla. Näiden ominaisuuksien lisäksi isotiouronium-ryhmän kationinen toiminnallisuus tutkittavissa CIT:issä tarjoaa näille polymeereille hyvät vetysitoutumis- ja donoriominaisuudet. Tässä työssä tutkittiin CIT:n rakenteen vaikutusta erilaisiin ominaisuuksiin, kuten (i) sähköiset ominaisuudet (ionisaatiopotentiaali, elektroniaffiniteetti, optiset siirtymät) ja (ii) polymeeriliuotin, polymeeri-polymeeri ja polymeerin-sammuttajavuorovaikutukset. Lisäksi CIT:ien optisia ominaisuuksia tutkittiin vakiotila-absorptiofluoresenssispektroskooppitekniikoilla molekyylin muutosten seuraamiseksi, kun taas polymeerirakenteen aggregaatiota (ionisten ja hydrofobisten aineosien kanssa) tutkittiin elektronien paramagneettisen resonanssin spektroskopialla. (EPR) Syklistä voltammetriaa, tiheysfunktionaalista teoriaa (DFT) ja molekyylimekaniikkaa (MM) käytettiin täydentävinä työkaluina.

Nämä tulokset palvelevat laajempaa konjugoituneiden polyelektrolyyttien supramolekyylikemian tutkimuskenttää, jossa kaikkien monimutkaisten ilmiöiden mekaniikkaa ei vielä täysin tunneta. Parempi tuntemus hyödyttäisi esimerkiksi anturikehityksessä ja orgaanisessa optoelektronikassa, joissa jo parhaillaan ollaan löytämässä sovelluskohteita useille konjugoituneille polyelektrolyyteille.

Avainsanat: konjugoituneet polyelektrolyytit, kationinen polytiofeeni, isotiouronium, vetysitoutuminen, sivuketjun pituus, UV-Vis, vakiotilafluoresenssi, elektronin paramagneettinen resonanssi, syklinen voltammetria, tiheysfunktionaaliteoria, molekyylimekaniikka

UNIVERSITY OF TURKU
Faculty of Science and Engineering
Department of Chemistry
SERGIO ULISES ESPINOSA DOMÍNGUEZ: Studies on Cationic
Polythiophenes with Hydrogen-Bonding Donor Capabilities
Doctoral Dissertation, 137 pp.
Doctoral programme in Physical and Chemical Sciences (PCS)
November 2019

Abstract

This project focuses on cationic isothiuronium polythiophenes (CITs), a particular type of conjugated polyelectrolytes (CPEs). In general, CPEs combine a pi-conjugated polymer backbone with pendant ionic groups, which gives them chromo- and fluoro-phoric properties, and also water-solubility. This structure provides CPEs with interacting driving forces of conjugated polymers (pi-pi stacking and hydrophobic interactions) and of polyelectrolytes, such as coordination through electrostatic forces and hydrogen bonding (H-bonding). Polythiophene-CPEs in particular, have a high sensitivity to different stimuli, such as solvent (solvatochromism) or other chemical species (affinity chromism), which can be traced by fluorescence. Besides these properties, the isothiuronium cationic functionality in the CITs under study, gives them enhanced hydrogen-bonding (H-bonding) donor capabilities.

The properties in the CITs were utilized for studying how structure influences on functions such as (i) electronic properties (ionization potential, electron affinity, optical transitions and (ii) polymer-solvent, polymer-polymer and polymer-quencher interactions. The optical properties of the CITs were traced by steady-state absorption-fluorescence spectroscopic techniques in order to track molecular changes, while their aggregation was studied by electron paramagnetic resonance (EPR) spectroscopy, using paramagnetic probes with different ionic and hydrophobic constituents. Cyclic voltammetry, density functional theory (DFT) and molecular mechanics (MM) were also used as complementary tools.

These results could be useful to the broad field of supramolecular chemistry of CPEs, some of which complex phenomena is still not completely understood at a mechanistic level. This in turn could benefit fields such as actuators and sensors and organic optoelectronics, research areas which are currently finding applications to several CPEs.

Keywords: Conjugated polyelectrolytes, cationic polythiophene, isothiuronium, hydrogen bonding, side chain length, UV-Vis, steady-state fluorescence, electron paramagnetic resonance, cyclic voltammetry, density functional theory, molecular mechanics

Preface and acknowledgements

This research is the first of its kind in this research group, in which similar CPEs had been studied during the last 20 years, however not with the aims or experimental/computational approaches of the present work.

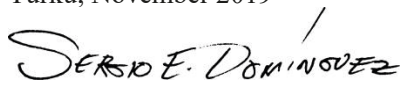
I would like to express my deepest gratitude to my supervisors, Professor Carita Kvarnström and Adjunct Professor Pia Damlin, I was very fortunate in having their permanent guidance and support.

I would also like to extend my gratitude to present and former staff and students in our laboratory, in particular to the students I supervised, for their excellent experimental work: Mia Meriläinen, performing electrochemical measurements, and Antti Vuolle, performing spin-coating, AFM and surface free energy experiments (to be published). I want to also thank Timo Ääritalo for his help with synthesis/purification procedures, to Jaana Rosenberg for her help with MALDI-TOF, Ermei Mäkilä and Martti Kaasalainen (Physics Department), and Michael Kaszuba (Malvern Instruments Ltd.) for their advice on DLS, also to the researchers at University of Urbino, Italy: Prof. Maria Francesca Ottaviani, Ph.D. Michela Cangiotti and Ph.D. Alberto Fattori, for their excellent EPR experiments and analyses, and to the staff at CSC-IT Center for Science, Finland, for computational resources and advisory. I also thank Professors Sergio Revah Moiseev, Mariano Gutiérrez Rojas, Hiram Isaac Beltrán Conde and Gerardo Muñoz Hernández, at UAM, México, and to Prof. Pavel A. Troshin, at the Russian Academy of Sciences, for their support during the process of becoming a doctoral student at University of Turku.

Funding acknowledgements to: (i) The Mexican National Council for Science and Technology (CONACyT) for the international doctoral scholarship no. 310828, (ii) the Turku University Foundation (Turun Yliopistosäätiö), (iii) Real estate Foundation (Kiinteistösäätiö), (iv) the Finnish National Doctoral Programme in Nanoscience (NGS-NANO), and (v) the Doctoral Programme in Physical and Chemical Sciences (PCS) from University of Turku.

I dedicate this work to my Mother and Brother

Turku, November 2019



Sergio Ulises Espinosa Domínguez

Table of Contents

I. List of original publications	8
II. Errata	9
III. Abbreviations	10
IV. Symbols	13
1. Literature review	14
1.1. Conjugated polyelectrolytes and water-soluble polythiophenes	14
1.1.1. Polythiophene as an sp^2 pi-system	16
1.1.2. Electronic transitions in pi systems	19
1.2. Aggregation of conjugated polyelectrolytes and water-soluble polythiophenes	21
1.3. Electron and charge transfer	24
1.4. Conjugated polyelectrolytes with hydrogen-bonding capabilities	28
1.5. Hydrogen-bonding mediated aggregation of ionic polythiophenes	30
1.6. Hydrogen-bonding mediated electron and charge transfer	31
1.7. Role of molecular structure	32
1.8. Role of solvent	33
2. Aims of the Study	35
3. Experimental	36
3.1. Materials	36
3.2. Methods	39
3.2.1. UV-Vis absorption spectrophotometry	39
3.2.2. Steady-state fluorescence spectrophotometry	39
3.2.3. Cyclic voltammetry	40
3.2.4. Electron paramagnetic resonance spectroscopy (EPR)	40
3.2.5. Density functional theory (DFT)	40
3.2.6. Dynamic light scattering (DLS)	40
3.2.7. Synthesis/purification methods and ^1H -NMR	41
3.2.8. Time-of-flight matrix-assisted laser desorption/ionization (MALDI-TOF)	41
4. Results/Discussions	42
4.1. ^1H -NMR and MALDI-TOF	42
4.2. Ionization potential, electron affinity and bandgap	42
4.3. Studies on polymer-solvent and polymer-polymer interactions	48

4.3.1. Disaggregated and aggregated ranges of polymer concentration	48
4.3.2. Effect of spacer length on polymer-solvent interactions	49
4.3.3. Effect of spacer length on relative quantum yields	50
4.3.4. Effect of spacer length and solvent on polymer-polymer interactions	51
4.3.4.1. λ_{max} wavelength and excitation spectra	51
4.3.4.2. λ_{em} wavelengths	54
4.3.4.3. Stokes shifts	55
4.3.4.4. Absorbance and PL intensities	56
4.3.5. EPR study on the effect of spacer length on the concentration-driven aggregation in water	58
4.4. Effect of solvent polarity and hydrogen-bonding capacity on the solution interactions between the PT1:4Fo pair	65
5. Conclusions	72
6. Future perspectives	74
7. List of references	75
Original Publications	85

I. List of original publications

The experimental part of this thesis is based on the following publications, referred to in the text as **Papers I-IV**, which can be found reprinted at the end of this thesis. Papers I-II are reproduced with permission from the Royal Society of Chemistry. Paper III is reproduced with permission from Langmuir 2018, 34 (25), 7364–7378, Copyright 2018, American Chemical Society. Some unpublished material is also included.

I. P. Damlin, M. Hätönen, **S. E. Domínguez**, T. Ääritalo, H. Kivelä and C. Kvarnström, Study of the electrochemical and optical properties of fullerene and methano[60]-fullerenediphosphonate derivatives in solution and as self-assembled structures, RSC Advances 4 (2014) 8391-8401.

II. **S. E. Domínguez**, M. Merilainen, T. Ääritalo, P. Damlin and C. Kvarnström, Effect of alkoxy-spacer length and solvent on diluted solutions of cationic isothiuronium polythiophenes, RSC Advances 7 (2017) 7648-7657.

III. **S. E. Domínguez**, M. Cangiotti, A. Fattori, T. Ääritalo, P. Damlin, M. F. Ottaviani, and C. Kvarnström, Effect of Spacer Length and Solvent on the Concentration-Driven Aggregation of Cationic Hydrogen-Bonding Donor Polythiophenes, Langmuir 34 (25) (2018) 7364–7378.

IV. **S. E. Domínguez**, T. Ääritalo, P. Damlin and C. Kvarnström, Hydrogen-bonding mediated interactions between a water-soluble polythiophene-fullerene pair with two-point hydrogen-bonding capabilities, as a function of fullerene concentration and polarity and hydrogen-bonding capacity of the solvent, *Manuscript submitted to Physical Chemistry Chemical Physics*.

Contribution of the Author:

Paper I: The Author performed part of the experiments on absorption in solution.

Papers II and IV: The Author planned the work together with supervisors, performed or supervised the experimental/computational work, and analyzed the data, wrote the first draft of the manuscript, and finalized it together with co-authors.

Paper III: The Author planned the work together with supervisors and co-authors, performed the experimental/computational work executed in our group, analyzed the data and wrote the first draft of the manuscript, which was then finalized together with co-authors.

II. Errata

In Paper II is stated (quote): “*About tacticity, it is known that oxidative polymerization of alkyl-thiophenes using FeCl_3 minimizes 2,4-linkages, therefore generating mainly head-to-tail (HT) couplings between adjacent thiophene rings, through 2,5-linkages.*”

In this paragraph: (i) The term “tacticity” is incorrect, the correct term is *regioregularity*; (ii) the statement is correct in regard to the minimization of 2,4-linkages, however in order to generate mainly HT regioregularity, it is also required the use of 3-alkoxy-4-methylthiophenes as monomers. For details see section 1.7.

In Paper II, supplementary information, paragraph “Fluorescence quantum yield”, it was mistakenly written Φ_f instead of Φ_r , when referring to the quantum yield of the fluorescence standard quinine sulfate.

In Papers II and III, supplementary information, Tables S1: (i) are reported values of “viscosity”, instead of “dynamic viscosity”; (ii) the units of dynamic viscosity were reported as mPa, instead of the correct mPa s; and (iii) the units of density (g/cm^3) were not mentioned properly.

In Paper III, when referring to polymers, the terms “H-aggregate” or “J-aggregate” were used, instead of the more appropriate “H-like” or “J-like” aggregates.

III. Abbreviations

$^1\text{H-NMR}$	Proton nuclear magnetic resonance
2Fo	[6,6]-bis(diphosphonate)-bromomethanefullerene C_{60}
4Fo	[6,6]-[(bis(diphosphonate))]2-bromomethanefullerene C_{60}
5DSA	5-doxyl-stearic acid
6-31G**	basis set used in the present work
A_{ii}	A_{xx} , A_{yy} and A_{zz} components of the hyperfine coupling tensor A for the coupling between the electron spin and the nitrogen nuclear spin
ACQ	aggregation-caused quenching
AGG	aggregated state, [POL]
Alkox4	[6,6]-bis(diethoxyphosphoryl)-bromomethanefullerene C_{60}
Alkox8	[6,6]-[bis(diisopropoxyphosphoryl)]2-bromomethanefullerene C_{60}
B3LYP	Becke 3-parameter Lee-Yang-Parr hybrid exchange correlation functional
C_{60}	fullerene- C_{60} , [60]fullerene, buckminsterfullerene, buckyball
CAT8	4-octyl-dimethylammonium,2,2,6,6tetramethyl-piperidine-1oxyl bromide
CAT16	4-cetyldimethylammonium,2,2,6,6tetramethyl-piperidine-1oxyl bromide
CC	middle aggregation state, [POL]
CIT	cationic isothiuronium polythiophene
CMC	apparent critical micelle concentration
CP	conjugated polymer
CPE	conjugated polyelectrolyte
CV	cyclic voltammetry or cyclic voltammogram
DFT	density functional theory
DI	1,4-dioxane
DIS	disaggregated state, [POL]
DLS	dynamic light scattering (or photon correlation spectroscopy)
DP	degree of polymerization
E_{00}	energy of the zero-zero (0-0) vibronic transition
E_A	electron affinity

Eg _{EC}	electrochemical bandgap= $I_p - E_A$
Eg _{OPT}	optical bandgap
EPR	electron paramagnetic resonance (spectroscopy)
eV	electron volt
Fc/Fc ⁺	ferrocene/ferrocenium (couple)
FMO	frontier molecular orbital
FRET	fluorescence resonance energy transfer
G09	Gaussian 09 software/package
GPC	gel permeation chromatography
GSQ	General static quenching model, a variation of SV model
H-acceptor	H-bonding acceptor or proton acceptor
H-bond(ing)	Hydrogen bond(ing)
H-donor	H-bonding donor or proton donor or electron acceptor
HOMO	highest occupied molecular orbital
HT	head-to-tail (couplings through 2,5-linkage between thiophene rings)
IC	internal conversion (of an S _n excited state)
I _p	ionization potential
IPA	isopropanol
ITO	indium tin oxide
k _q	specific bimolecular collisional deactivation of electronic energy constant
K _{sv}	Stern-Volmer kinetic interaction constant
LUMO	lowest unoccupied molecular orbital
MALDI-TOF	matrix-assisted laserdesorption ionization time-of flight
MEPS	molecular electrostatic potential surface
mM	milimolar
MM	molecular mechanics
M _n	number-average molecular weight
M _w	weight-average molecular weight
OLED	organic light emitting diodes
OSC	organic solar cell
P3HT	poly-3-hexylthiophene
P3TMA	poly(3-thiophene methyl acetate)
PCM	polarizable continuum model
PET	photoinduced electron transfer
PL ₀	photoluminescence intensity in absence of a quencher
PL	photoluminescence intensity
PT1	poly-3-(N, N-diethyl- S-iso-thiouronium) <i>ethyloxy</i> -4-methylthiophene
PT2	poly-3-(N, N-diethyl- S-iso-thiouronium) <i>hexyloxy</i> -4-methylthiophene
PT3	poly-3-(N, N-diethyl- S-iso-thiouronium) <i>decyloxy</i> -4-methylthiophene

Q1-3	ranges of 4Fo concentration in SV plots of the PT1:4Fo pair
Rh	hydrodynamic radius
R ²	correlation coefficient
S0	ground state
S1	relaxed excited state
SANS	small-angle neutron scattering spectroscopy
SEC	size-exclusion chromatography
Sn	singlet exciton state
SV	Stern-Volmer model (or plot)
TBATFB	tetrabutylammonium tetra-fluoroborate
THF	tetrahydrofuran
TOH	4-hydroxy, 2,2,6,6 tetramethyl-piperidine-1oxyl
UV-Vis	ultraviolet–visible absorption spectrophotometry
Vmax	most positive electrostatic potential
Vmin	most negative electrostatic potential
v/v	volume/volume (mixture)
W-DI	water:1,4-dioxane 50:50 v/v mixture
W-IPA	water:isopropanol 50:50 v/v mixture
W-THF	water:tetrahydrofuran 50:50 v/v mixture

IV. Symbols

\bar{D}	dispersity = M_w/M_n
$[4Fo]$	concentration of the 4Fo fullerene
$[POL]$	concentration of polymer, either PT1 or PT2
δH	H-bonding interactive force of Hansen solubility parameters
ΔE	peak potential difference
ΔG_{CS}	Gibbs free-energy change for charge separation
ΔH	enthalpy change
ΔS	entropy change
$\Delta \nu$	Stokes shift
ε	molar absorption coefficient
η	viscosity
λ_{em}	maximum in photoluminescence
λ_{ex}	excitation wavelength
λ_{exMAX}	maximum in excitation
λ_{max}	maximum in absorbance
π	“pi”, related to pi electronic delocalization, pi systems or pi-pi interactions
τ	microviscosity (interaction) parameter
τ_0	fluorescence lifetime
Φ_f	fluorescence quantum yield

1. Literature review

For the sake of brevity, some of the references cited in Papers I-IV are omitted in here and can be consulted in these papers.

1.1. Conjugated polyelectrolytes and water-soluble polythiophenes

Conjugated polyelectrolytes (CPEs) are conjugated polymers containing ionic (cationic and/or anionic) functionalities, through side groups and/or pendant side chains. Besides the electronic properties and noncovalent interaction forces related to “pi” (π) systems (see next section), these molecules also possess physical-chemical properties of polyelectrolytes, such as solubility in high dielectric media such as water (and other polar solvents), together with the capability of coordination through noncovalent forces such as electrostatic and hydrogen bonding (H-bonding), either with solvent (which plays a role in solubilization) or with other molecules. The ionic groups in CPEs introduce also ion-dipole and ion-ion forces. All of these forces have an impact on their: (i) solubility, (ii) conformation in solution, (iii) aggregation between polymer chains (intermolecular aggregation) and between different segments of the same chain (intramolecular aggregation), and (iv) interactions with other molecules (complex formation and assembly).¹⁻⁴

Other important characteristics of CPEs are the rich synthetic chemistry associated to their organic nature and their processability from solution (e.g. roll-to-roll printing), for optoelectronic applications. In this regard, the first two sets of conjugated polyelectrolytes were reported independently in 1987, by Patil et al.⁵ and Sundaresan et al.,⁶ and were based either on thiophene or pyrrole, respectively, both of them with anionic functionalizations. Some other conjugated backbones functionalized in this way are (not in historical order, some of them used as copolymers): polyacetylenes, polydiacetylenes, polyfluorenes, polyanilines, poly(p-phenylenevinylene)s, poly(p-phenylene ethynylene)s, and poly(fluorene-co-phenylene)s.^{7,8}

Cationic groups are commonly quaternary ammonium (NR_3^+) and pyridinium ($[\text{C}_5\text{H}_5\text{NH}]^+$), while anionic groups include carboxylate (CO_2^-), phosphonate (PO_3^{2-}), and sulfonate (SO_3^-).⁹ Figure 1 shows some examples of reported water soluble ionic polythiophenes, anionic sulfonate (1), anionic phosphonate (2), anionic carboxylate (3), one of the cationic isothiuronium polythiophenes (CITs) studied in the present research (4) and a zwitterionic copolymer (5).

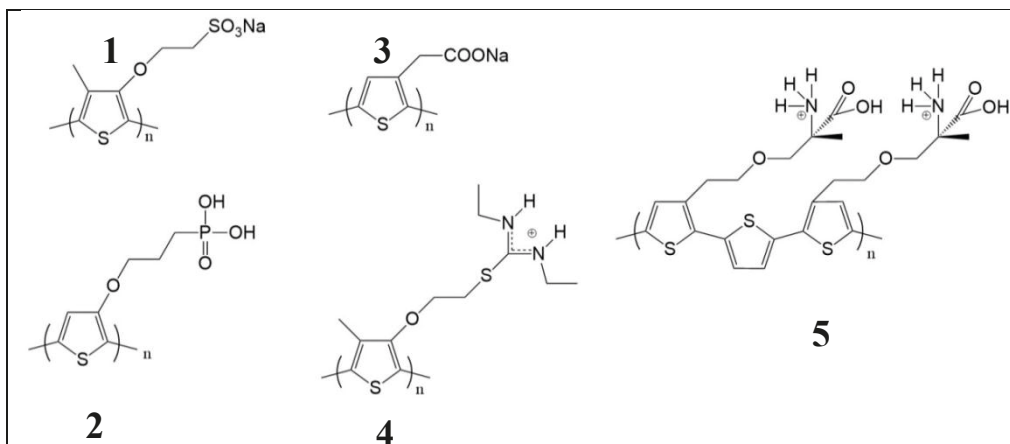


Figure 1. Some previously reported cationic, anionic and zwitterionic polythiophenes. Modified from ^{7,10}.

The possible application for a particular conjugated polyelectrolyte depends on three aspects: (i) the driving-force required (e.g. photons or potential), (ii) the phase of application (i.e. solution or solid-state), and (iii) structural factors, such as the type of conjugated backbone and its ionic nature.

Some CPEs, when in their disaggregated state, display similar photo-physical properties to those of a neutral analog dissolved in a non-polar organic solvent.⁸ In this regard, neutral polythiophenes in solution have a high sensitivity (traceable by fluorescence) to different stimuli, such as temperature (thermo chromism), solvent (solvatochromism), surfactants (surfacto chromism), irradiation (photo chromism) and other chemical species (affinity chromism, i.e. iono chromism).¹¹ This allows to study phenomena involved with the interaction of these molecules, either with themselves (i.e. aggregation) or with other molecules (i.e. solubilization, or complexing), and these properties remain in water-soluble polythiophenes.^{8,11}

These properties are present also in CPEs in general, reason why these molecules are capable of chemical and biological sensing, or as fluorescent probes for imaging studies.^{7,12} This is because it is possible to functionalize them with specific functional groups which can act as “ligands”, which allows following molecular interactions in water or other polar media by tracking photon-driven optical transitions, which are highly sensitive to environmental and structural changes. This is due to the electronic coupling taking place, caused by the proximity of the conjugated units present in their conjugated backbone, which generates light

harvesting followed by intra- and inter-chain energy transfer, which, if changed, even only partially, changes the optical properties in an amplified way.⁷ These changes can be detected by spectrophotometric techniques, which in turn can be steady-state or time-resolved.¹³

Cationic CPEs are particularly useful because of the negatively charged phosphates in either the backbone of DNA,⁷ or biologically important anions such as adenosine phosphates.¹⁴ In this regard, the isothiuronium group in the polymers used in the present work, is ideal for sensing of phosphates, through a double-point H-bonding, as detailed ahead.

CPEs can also interact with multicharged targets, which allow performing imaging studies on biological systems at higher levels of complexity, such as *in vitro* or *in vivo*. It is believed that these molecules have the potential to be used as either delivery systems, due to their hydrophobic backbones, or in photodynamic therapy, due to their sensitization of oxygen and other reactive oxygen species, generating biocidal or tumoricidal activity.^{7,15}

On the other hand, for solid-state applications, water- and/or alcohol-soluble CPEs have been studied as constituents in inorganic optoelectronic devices such as organic light emitting diodes (OLEDs) and organic solar cells (OSCs), because of their solution processability. Solubility is ideal for (i) low-cost, large-scale technologies such as roll-to-roll or ink-jet printing, (ii) control over interfacial mixing during the production of multi-layered devices, especially if other layers are processed from organic solvents, due to the phenomenon known as orthogonal-solubility, compatible with flexible devices, (iii) environmental-friendly character of the solvents,^{16,17} (iv) their unique solid-state-interface properties, which promote surface-dipoles,^{16,18} which in turn can improve charge or hole mobilities when applied as electrode-selective “buffer” layers in OSCs. This has shown to promote simultaneous improvement of two or all three main parameters affecting the performance of OSCs (open-circuit voltage, short-circuit current density and fill factor).^{16,17}

1.1.1. Polythiophene as an sp^2 pi-system

Despite carbon exists only in low concentrations on Earth (c. 0.01 wt%), this element appears in an impressive variety of forms, since it is capable to change its electronic configuration in the ground state ($1s^2 2s^2 2p^2$), into sp^1 , sp^2 or sp^3 “degenerate”, hybrid electronic configurations, that are energetically intermediate between the s- and p- orbitals, and possible to exist due to the very close binding energies between the p electrons. The sp^1 and sp^2 hybridizations generate pi and sigma bonds, however in different ways, presenting different spatial orientations and transitions of their electronic orbitals.¹⁹ In this regard, sp^2 hybridization and its properties are the target in this thesis, since this is the hybridization present in the thiophene rings, which constitute the molecules used in this project.

For the case of hydrocarbons (i.e. molecules consisting only of carbon and hydrogen), the sp^2 hybridization, which generates alternating double and single bonds (C-C=C-C), is present in ethylene ($CH_2=CH_2$), and the archetypical polyacetylene ($CH_3-CH=CH-CH_3$)_n, molecule involved in the Nobel-prize winning research on doping of organic semiconductors.

sp^2 hybridization is also present in the so-called *2D allotropes*, such as polycyclic aromatics (e.g. benzene), in which the atoms are arranged in planar cyclic arrays with $4n+2$ pi electrons (where n is an integer number), in which there is an stabilizing effect thanks to electronic delocalization. For the case of molecules containing heteroatoms different from hydrogen (i.e. oxygen, nitrogen or sulfur), this hybridization is present in molecules such as furan, pyrrole, thiazole, imidazole and thiophene.¹⁹

Figure 2a shows that spatially, the sp^2 hybridization mixes the s orbital with two of the three p-orbitals (p_x , p_y , p_z), generating three hybrid sp^2 -orbitals, with one electron each, and the p_z orbital, which keeps one electron.

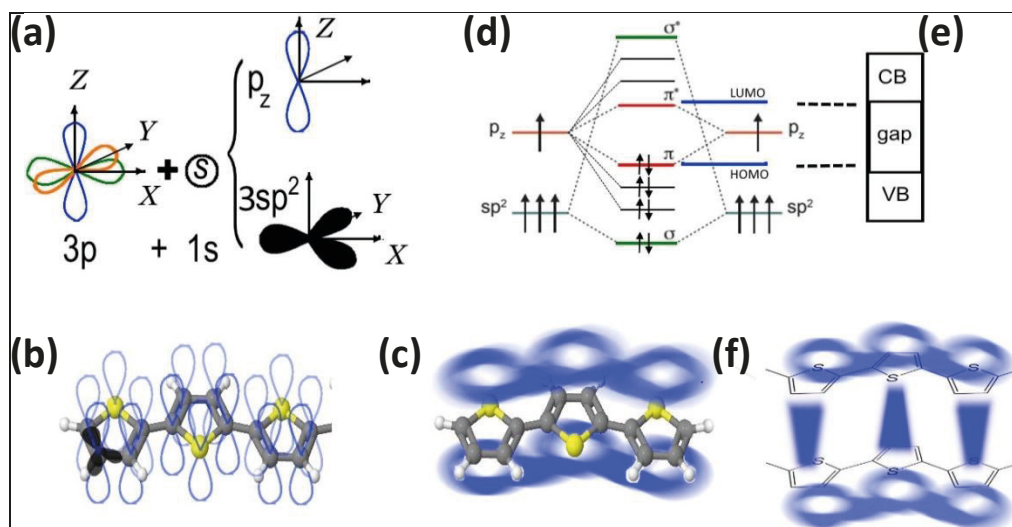


Figure 2. Polythiophenes possess a pi system. Modified from ^{13,20,21}.

As depicted in red in Figure 1b, bonds between two sp^2 orbitals (i.e. sigma (σ) bonds) are formed between C-C and C-H, with the first forming the thiophene ring (and therefore the backbone of a polythiophene). The p_z orbitals lie perpendicularly to the thiophene ring. In Figure 1c is shown the way these p_z orbitals of adjacent carbons combine to form pi bonds.

The thiophene ring is considered aromatic, because the electron pairs on its constituent sulfur atom are highly localized in the pi system. This is the reason why thiophene does not show the reactivity of conventional sulfides (the sulfur atom in thiophenes resists alkylation and oxidation). However, the degree of aromaticity of thiophene is smaller than that of benzene.

Figure 1d shows that energetically, the overlap of two p_z orbitals, each containing one electron, brings about the formation of a bonding pi orbital occupied by two electrons and an unoccupied antibonding state (π^*) separated by an energy gap known as bandgap, while the bond between two sp^2 -orbitals is known as a sigma bond. Both types of bonds generate bonding (σ -, π -) and antibonding (σ^* -, π^* -) states. The bonding pi-orbitals generate the highest occupied molecular orbital (HOMO), while the antibonding π^* -orbitals generate the lowest unoccupied molecular orbital (LUMO).

Energetically, sigma bonds have a strong overlap and large splitting, while pi bonds generate lower overlap, and therefore smaller splitting. This causes pi bonds to generate electronic delocalization through the molecule, generating the so-called pi-system, in which it is not possible to assign pi bonds to a particular carbon. Because of this, pi bonds are drawn as alternating single and double bonds, or through a resonant scheme.

In polythiophenes (and conjugated polymers in general), the extension of the pi system is known as conjugation length, which indicates the unperturbed expansion of the pi system, which can be disrupted by the degree of polymerization (i.e. number of repeating units) or chain distortions, which in turn can be caused by twisting of the backbone or regioregularity. For larger/longer conjugation lengths, the bonding states are populated accordingly and therefore, the energy of the HOMO increases, whereas that of the LUMO decreases. Figure 2e shows that for an “infinite” polymer chain, these would form conduction-like and valence-like bands (CB and VB), respectively.

Notice that this terminology is an analogy to the bands formed in inorganic semiconductors, and such theoretical framework is commonly used since this analogy is useful when interpreting the physical properties of organic semiconducting materials. The “bands” in organic materials present larger anisotropy, due to the soft nature and lack of extended crystalline regions in solids of conjugated polymers, reason why it is more proper to refer to density of states of these materials.^{20,22}

In sp^1 hybridization, present in unidirectional double bonds ($C=C=C$) or alternating triple-single bonds ($C-C\equiv C-C$), the similarity with inorganic semiconductors is larger, since in an infinite $C=C=C$ chain (carbyne), the number of bonding and antibonding states is so large that they form a continuum of energy levels, which is referred to as an energy band.¹⁹

A further discussion on the implications of this in the solid state (e.g. exciton coupling dynamics), is beyond the scope of the present research work and must be omitted in here. However, exciton coupling relates to H- and J-aggregation, which was also studied in this project, for details see section 1.2.

Since the pi electrons in the pi system can not be assigned to a parent atom, the reactivity of a solid in terms of its redox potential is described by parameters such

as ionization potential and electron affinity, which allows the identification of the energy position of the HOMO and LUMO levels, or, in other words, the valence band maximum and conduction band minimum levels.¹⁹ Delocalization also causes pi electrons to be easily polarizable, which generates weak intermolecular interactions known as pi interactions, which in turn generate “pi stacking”, as depicted in Figure 2f.²⁰

1.1.2. Electronic transitions in pi systems

The absorption and emission of photons, together with non-radiative processes (e.g. internal conversion and intersystem crossing) are direct result of light and matter interactions. Figure 3 shows a modified Jablonski diagram, in order to visualize the processes of absorption and emission, their origin and timescales, and how are related to the steady-state spectroscopic output.

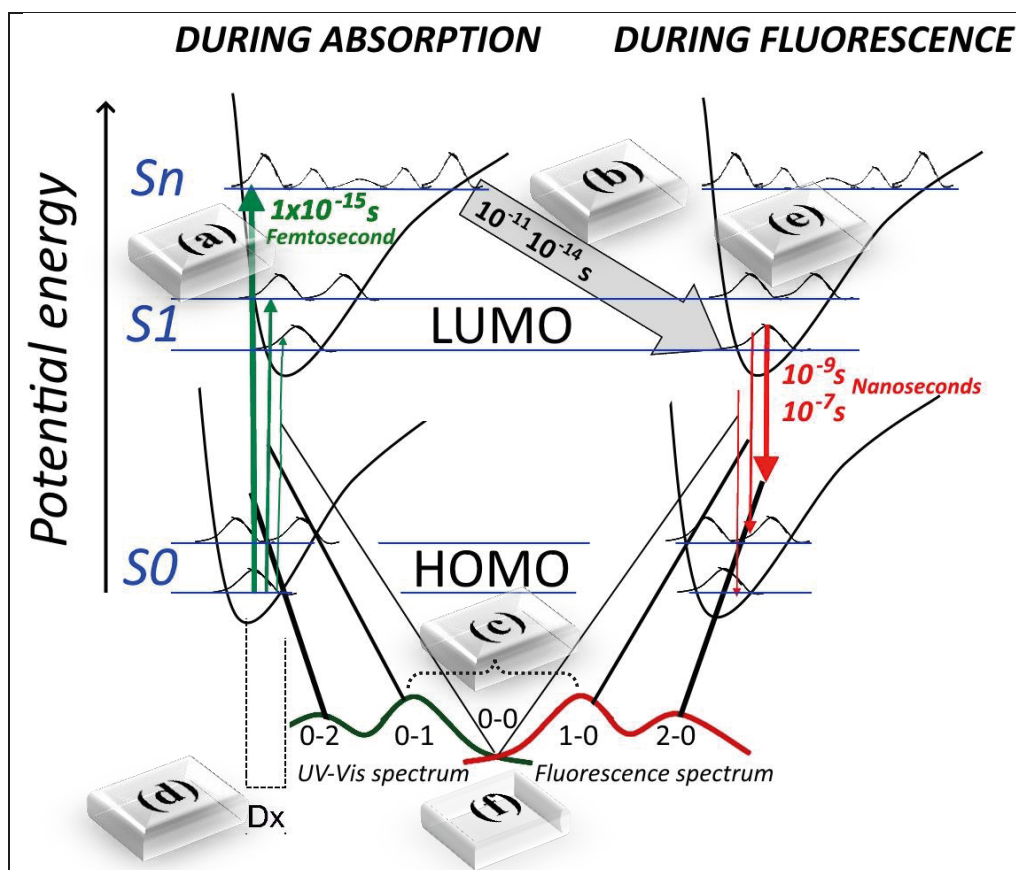


Figure 3. Modified Jablonski diagram, modified from ^{13,20,21}.

As depicted in Figure 3a, absorption involves the photonic excitation of a molecule from its ground state (S_0) to a singlet exciton state (S_n). In pi systems, the $S_0 \rightarrow S_n$

transitions involves predominantly pi-electrons, since the optical transitions with lowest energy have a pi-pi* character. Figure 3b shows the relaxation from S_n to the first excited state (S_1), through picosecond, internal conversion (IC), which is known as the Kasha's rule.²⁰ In regard to the spatial arrangement of the molecule (i.e. its conformation) during this process, the Born-Oppenheimer approximation states that the rearrangement of the electronic-molecular orbitals is much faster (by orders of magnitude) than the rearrangement of the constituent-nuclei of the molecule. Therefore, the spatial location of the atoms in the molecule change *only* during the $S_1 \rightarrow S_0$ relaxation, and not during the $S_n \rightarrow S_0$ one. In other words, the molecular conformation can be considered constant during the absorption process, which is known as the Franck-Condon principle.²⁰ The constant-character of the spatial location of the nuclei during the $S_0 \rightarrow S_1$ transition is represented through straight lines.

Because of the internal $S_n \rightarrow S_1$ relaxation, the fluorescence emission spectrum is shifted to lower energies (i.e. higher nanometer values), which is known as a bathochromic “red” shift, and the resultant difference in wavelength (i.e. energy) between the absorption and emission maxima, is known as Stokes shift, as shown at Figure 3c.²⁰ The shift in the atomic coordinates of the molecule is labeled as “Dx” (Figure 3d).

Every molecule exhibits several vibrational modes, which causes a fine structure of vibronic modes in the fundamental electronic transitions. S_0 and S_n possess particular vibrational and rotational structures, due to the displacement of charge and shift in the atomic coordinates of the molecule (i.e. molecular conformation).²⁰ This is visually represented in Figure 3 as the potential curves for the S_0 and S_1 states, each of them sub-divided to represent their constituent vibronic modes. Each vibronic mode has different values of absolute square of the amplitude of each vibronic-mode wavefunction.

Even if a quantum-mechanical description of these phenomena is beyond the scope of the present work, it can be said that the magnitude of the $S_0 \rightarrow S_n$ transitions is proportional to the overlap of the electronic wavefunctions of both states. This is described at the quantum-mechanic level by the “golden rule” of Fermi. It uses first order perturbation theory to describe the probability of the $S_0 \rightarrow S_n$ transition, as a function of the density of final states and the transition dipole moment, which in turn depends on the wavefunctions of S_0 and S_n .²⁰

Each wavefunction is composed by the wave function of the nucleus of the m-th vibrational level of the n-th electronic state (shown in Figure 3e), and the wave function of the electrons in the n-th electronic state, with the latter being independent of both the spatial coordinates and spin of the electrons. The probability of the $S_0 \rightarrow S_n$ transition is then predicted using: (1) an operator of dipole moment, which when zero, generates a null probability of the $S_0 \rightarrow S_1$ transition (which is known as a dipole-forbidden transitions), and (2) the Franck-Condon factor, which is related to the vibration of the nuclei, and describes the

probability of the excitation of a particular vibrational state during an electronic transition.²¹

The term oscillator strength refers to the probability for a particular vibronic transition, i.e. the amplitude of an electronic transition, after integrating over all frequencies. It is a function of the electron mass, speed of light in vacuum and refractive index, and can be correlated to the transition dipole element.²⁰ Figure 3 shows how the different oscillator strengths of transitions give origin to the shape of absorption and emission spectra.²¹

The extent of displacement between the ground and excited states potentials (i.e. curves in Figure 3) determine the degree of symmetry and overlap between these spectra. With the latter being commonly known as the energy of the zero-zero (0-0) vibronic transition, observed in Figure 3f.¹⁴

The above rules and principles (Kasha's rule, Franck-Condon principle and oscillator strength) were necessary to be introduced since they allow a deeper understanding of the changes in steady-state absorption and fluorescence spectra analyzed in this project.

1.2. Aggregation of conjugated polyelectrolytes and water-soluble polythiophenes

Precise control of solution-phase aggregation of CPEs has been a long time goal because it is related with sensing in solution via conformational changes.²³ Control on aggregation also opens the possibility to specific nanostructuring, desirable for applications involving charge transport, such as (i) sensing in solution¹² and (ii) solid-state optoelectronic devices.¹⁷

However, a clear understanding of aggregation of CPEs is a challenging topic because it depends on the interplay between their molecular structure (rigidity and twisting of the backbone, density and type of ionic functional groups), excluded volume effects, and interaction forces from the backbone (hydrophobic, pi stacking), ionic group (electrostatic, H-bonding, long range ion-ion interactions), together with side-chain hydrophobic interactions with solvent or other polymer chains, since it is known that side chains also play a role in the water-solubility of CPEs.³

All of these factors define the architecture of the aggregates (e.g. disordered clusters to ordered micelles, liquid crystals, and highly structured vesicles), and in consequence, their optical-electrical properties.

Early studies on CPEs showed that in water these molecules present intramolecular aggregation,²⁴⁻²⁶ which decrease properties useful for sensing, such as fluorescence spectra and quantum yields.²⁷ For poly(p-phenylene vinylene) based CPEs, there is

an alignment during aggregation, causing the conjugated units (phenylene) to become almost co-planar in order to optimize hydrophobic and pi stacking interactions, present due to the highly conjugated nature of their backbones. These forces, however seem not to be dominant, probably due to a balance between the tendency of interactions between side chains to limit the structuring, and the competing influence of electrostatic repulsion between side chains and attraction between ionic head groups and counterions, through Coulombic interactions.²⁸

The aggregates of CPEs are usually charged, leading to electrostatically-driven ordering, as observed for poly(3-thiophene methyl acetate) (P3TMA) with different degrees of polymerization, when analyzed with small-angle neutron scattering (SANS) spectroscopy. The data indicated ordering arising from intermolecular electrostatic repulsion, with increasing concentration causing a similar behavior to that of isotropic model for overlapping polyelectrolytes. Electrostatic forces were possible to screen by the addition of salt, causing larger aggregation. On the other hand, ionic forces play a role through counterions, which can decrease optoelectronic or other properties, a fact that can be avoided in zwitterionic CPEs.^{1,3,29,30}

The structure of the aggregates vary widely, being possibly weakly bound, poorly-defined clusters (something commonly formed in water). They can also be more structured, self-assembled aggregates, with 2D or 3D ordering, formed by diblock-CPEs, or in presence of surfactants or (non-conjugated) polyelectrolytes. In fact, it is well known that surfactants offer a reliable platform to control the aggregation of CPEs, due to specific interactions that lead to a variety of structures, that could be useful for sensing.³

Solvents also can tune the aggregation of CPEs, since they can modify the structural order and conjugation length of the backbone.^{8,26} This is discussed in more detail in the section “1.8. Role of solvent” in this thesis, since the use of cosolvents for aggregation control was one of the main strategies used in this research work.

The concept of H- and J-aggregation is an important tool developed to study the self-association of small conjugated molecules (e.g. dyes), either in solution or at the solid-liquid interface. J- and H-aggregation is related to head-to-tail arrangement (end-to-end stacking) or to parallel arrangement (plane-to-plane stacking), respectively, and is useful since these two types of aggregates generate red and blue shifts in the absorption spectra, respectively. This concept was expanded by Spano et al.³¹ to analyze films of polythiophenes, in order to perform structure-function studies in conjugated polymer aggregates, by proposing that for polythiophenes, H- and J-aggregates coexist in the form of “H-J aggregates”, and the contribution of each mode differs in each practical situation. Later, Zhu et al.³² used this concept to study the molecular ordering in solution, of a hydrophilic, thermo-responsive polythiophene, with ethylene oxide side groups, using

synchrotron X-ray scattering and absorption in solution to track co-facial stacking (i.e. [010] ordering) and [100] ordering (i.e. cofacial molecular stacking). The latter analyses were possible because the polymer used presented a clear structuring of both absorption and fluorescence, i.e. these spectra showed more than one clear vibronic transition (e.g., 0–0 and 0–1, see Figure 2), and by comparing the 0–0/0–1 ratio it was possible to estimate the [010] ordering. Such structured spectra is also present in nanofibers or thin films, in which case it is possible to gain understanding on the exciton coupling (i.e. intra- or inter-chain) present, as shown in previous studies on poly-3-hexylthiophene (P3HT), one of the most studied polymers for OSCs applications.^{33–35}

The CITs used in this work do not present such structured spectra, however, in **Paper III** it was possible to discuss their aggregation, as a function of molecular structure and solvent, by using the criterion reported by Deng et al.,³⁶ which analyzes changes in the excitation spectra due to concentration (see section 4 for more details). This criterion was previously used in the research field of ligno-cellulosic materials, specifically to study the aggregation of lignin, through the use of lagnosulfonates as model molecules.

As previously mentioned, the fluorescence of CPEs is sensitive to changes in the surrounding media. Studies on the effect of concentration on fluorescence provide information on aggregation, since these changes cause shortening of the lifetime of the S1 state. Alternately, decreases in the steady-state fluorescence of the fluorophore, can be observed due to either an increase in concentration (aggregation-caused quenching (ACQ) or self-quenching) or due to the presence of other molecules (known as quenchers). Previously, steady-state fluorescence was used to estimate the critical micelle concentration of micelles formed in water by water-soluble block copolymers, using pyrene as fluorescent probe,^{37,38} or following the intrinsic fluorescence of a polythiophene graft polyampholyte,³⁹ in order to estimate the *apparent* critical micelle concentration (CMC). An approach similar to the latter reference was used in **Paper III** in order to study the concentration-driven aggregation of CITs with H-bonding capabilities, in solvents with different polarity/H-bonding capacity.

Electron Paramagnetic Resonance (EPR) spectroscopy also has also demonstrated to be a useful tool to obtain information on the aggregation behavior of dendrons⁴⁰ and surfactant micelles.⁴¹ This technique was also used to study J-type and H-type aggregation of P3HT nanofiber dispersions, as a function of the concentration of a strong charge transfer dopant.⁴² In **Paper III** EPR spectroscopy was used to study the concentration-driven aggregation of cationic polythiophenes in aqueous media.

1.3. Electron and charge transfer

When the presence of a molecule shortens the lifetime of the excited state, or decreases the steady-state fluorescence of a fluorophore, the molecule is acting as a quencher. These ground- or excited-state interactions, and molecular rearrangements (mentioned before) are: (1) Fluorescence resonance energy transfer (FRET), (2) photoinduced electron transfer (PET), (3) static quenching, (4) dynamic quenching or (5) “pseudo-static” quenching.

These mechanisms, and the models used to study them, are described in **Paper IV**, and will be briefly resumed here.

(1) FRET involves the transfer of the excited state energy from the initially excited donor (the fluorophore), to an acceptor, which ideally should be non-fluorescent. This kind of quenching mechanics typically involve an overlap of the emission spectrum of the donor with the absorption spectrum of the acceptor.⁴³ The rate of FRET ($k_t(r)$) is a function of the donor-acceptor distance (r), the orientation factor (κ), and the spectral overlap between the donor emission and the acceptor absorption, expressed by the the overlap integral ($J(\lambda)$).^{4,13}

$$k_{t(r)} \propto \frac{1}{r^6} \kappa^2 J(\lambda) \text{ ----(1)}$$

(2) PET is expected to occur in presence of strong electron-withdrawing quenchers like fullerenes,⁴ and is controlled by the free energy of the reaction, the reorganization energy, and the distance between the donor and acceptor, without requiring intimate molecular contact.⁴⁴ According to the Marcus formulation, PET depends on three parameters: (i) the electronic coupling between donor and acceptor, (J_{DA}); (ii) the reorganization energy of each molecule ($\lambda_{D,A}$); and (iii) the available driving force, i.e. the free-energy change for charge separation (ΔG_{CS}).^{44,45} The latter can be estimated using the Rehm-Weller equation (equation 2), which has been used to analyze systems in solution:^{14,45}

$$\Delta G_{CS} = E_{ox}(D) - E_{red}(A) - E_{00} + C \text{ ----(2)}$$

where ΔG_{CS} is the free energy change for charger separation (which must be negative for PET to occur spontaneously), $E_{ox}(D)$ is the first one-electron oxidation of the donor, $E_{red}(A)$ is the the first one-electron reduction of the acceptor, E_{00} is the energy of the zero-zero vibronic transition of PT1, and C is a term related to Coulombic attraction, which in turn is dependent of the solvent.

(3) Static quenching occurs as a result of the formation of a non-fluorescent fluorophore-quencher complex in the S_0 state (ground state complex), causing a decrease of “free” fluorophore in the system.^{46,47}

(4) Dynamic quenching, occurs due to random diffusive collisions between fluorophore and quencher during the lifetime of the S1 state,⁴⁸ without the formation of a complex between them.⁴⁷

(5) Pseudo-static quenching refers to a phenomenon that occurs when the concentration of quencher increases, which causes an enhancement of its local concentration, causing superlinear quenching (or “superquenching”) which is observed as an upward behavior in the Stern-Volmer plot (see equation 3), indicating the onset of an additional quenching mechanism. Frank and Vavilov,⁴⁶ introduced the concept of “sphere-of-action”, or “quenching sphere”, and that the probability to find the quencher in such sphere at the moment of excitation is a function of both, concentration of quencher and the volume of the sphere.^{13,43,47} Therefore, during a complete fluorophore-quencher interaction the probability of quenching is unity.⁴⁹ Sphere of action quenching has also been named “pseudo” or “false” static quenching, since no ground state complex is formed.⁴⁷

The photo-chemical or -physical phenomena present in static, dynamic or pseudostatic quenching can be explored by using the Stern-Volmer (SV) model:⁵⁰

$$\frac{PL_0}{PL} = 1 + K_{sv}[Q] \text{ ---(3)}$$

where PL_0 and PL are the photoluminescence intensity (PL) at λ_{em} of the fluorophore in absence and presence of a quencher, respectively, $[Q]$ the concentration of quencher, and K_{sv} the Stern-Volmer interaction constant (with units of 1/M), which provides information about quenching efficiency.

Equation 3 was proposed to study a process now referred to as dynamic quenching,⁴³ therefore, this model generates linear SV plots only when the fluorophore-quencher pair interact by dynamic quenching. When the pair interacts partially or totally different to dynamic quenching non-linear Stern-Volmer plots are obtained, showing either up- or down-wards shapes. It is also possible that a linear Stern-Volmer plot, however with an extremely larger value of K_{sv} (e.g. to the power of 10) indicate the presence of static quenching.^{48,51}

For these cases deviating from purely dynamic quenching several variations of the Stern-Volmer model have been proposed and will be briefly presented here, for further details the reader is encouraged to read the references provided.

In the case of linear SV plots, with large K_{sv} values, following can be used:

(i) A modified SV equation is known as Benesi-Hildebrand by plotting $1/[Q]$ and $PL_0/(PL_0-PL)$ as the X and Y axes, respectively. This model has been used to study large water-soluble conjugated molecules such as beta- cyclodextrin polymers⁵² or also systems involving water-soluble fullerene derivatives.⁵³ This model has also been used to analyze proteins such bovine serum albumin,⁵⁴ in literature it can also be found without being labeled as Benesi-Hildebrand, e.g. in reference⁵⁵.

(ii) A modified SV model which allows estimating the number of binding sites, by plotting $\log[Q]$ and $\log[(PL_0/PL) / PL]$ as the X and Y axes, respectively. This model has been used to analyze the quenching of a biocompatible water-soluble anthracenyl polymer,⁴⁸ and a water-soluble cationic piperidine-containing polythiophene.⁵¹

In the case of upward-shaped SV plots, there is a distinction regarding if the $[Q]$ can be considered as “low” or “high”, and this distinction varies in each particular system. At low values of $[Q]$, it is commonly assumed that there exists a combination of static and dynamic quenching,⁵⁶ and also possible quencher-induced aggregation.⁵⁷ If time-resolved fluorescence is not available, it is still possible to distinguish between static and dynamic quenching graphically, by applying the *plotting method* described by Geddes⁴³ and Lakowicz.¹³ This method has been used to analyze the quenching of a poly(para-phenylene ethynylenes) by C_{60} fullerenes.⁴⁷

On the other hand, for upward-shaped SV plots at high values of $[Q]$, it is considered an emergent phenomenon, which involves a crossover from static quenching, due to the increase of the quencher capabilities in the form of a “sphere of effective quenching”. Perrin’s model for a sphere of effective quenching was developed for viscous media or rigid matrices, where the fluorophore and quencher cannot change their positions in space relative to one another during the excited-state lifetime of the fluorophore. This model assumes that a complete quenching occurs if a quencher molecule is located inside a sphere (called the sphere of effective quenching, active sphere or quenching sphere) of volume V_q surrounding the fluorophore.^{58,59} Sphere of action quenching has been also named “pseudo” or “false” static quenching, since no ground state complex is formed.⁴⁷

After assuming that the probability that “n” quenchers lie within V_q follows a Poisson distribution, and since the emission intensity is proportional to PL_0 , then Perrin’s model states that:

$$\frac{PL_0}{PL} = Ae^{V_q N [Q]} + B \quad \text{---(3b)}$$

where A and B are empirical constants, N is Avogadro’s number. This model applies if (i) there is no evidence of ground-state complex formation and (ii) the interactions between the fluorophore and quencher are likely to be non-specific in nature.⁶⁰ This equation can be solved by: (i) estimating empirical values for A and B and then applying the method described by Deshmukh et al.⁶⁰ or (ii) by assuming that $A=1$ and $B=0$, and plotting $[Q]$ and $LN[(PL_0/PL)]$ as the X and Y axes, respectively. In the latter case, the slope of the plot yields $Kp = V_q N$,⁵⁸ which in turn can be associated with the radius of the quenching sphere (R_s) by:⁶¹ $V_q = \frac{4}{3} \pi R_s^3 N$.

Perrin’s model was developed in particular for the interpretation of non-radiative energy transfer in rigid media.⁵⁸ However, remarkably, it has been used to analyze the quenching of small conjugated molecules such as anthracene,⁶¹ pyrene⁵⁶ or

phenanthrene,⁵⁹ and also to analyze quenching of water-soluble poly(phenylenevinylene)s,⁴⁶ and a solution processable fluorescent porous organic polymer.⁶⁰ Some authors suggest the use of a correction factor for polymer-quencher systems, in order to account for the charge-induced enhancement of the local quencher concentration.⁴⁶

Upward-shaped SV plots at high values of [Q] had also been studied assuming purely static-quenching by complexation, since it may also lead to upward curvatures in the SV plots. In these cases, the model for general static quenching (GSQ) can also be used. This model requires the same plotting as the Benesi-Hildebrand method, with $1/[Q]$ and $PL_0/(PL_0-PL)$ as the X and Y axes, respectively. The difference between each of these models is the parameters included in the slope and Y-intercept. These models allow analyzing upward curves because at high values of [Q] the module $1/[Q]$ compresses the values in the X axis around a certain value, while the module $PL_0/(PL_0-PL)$ compresses the values in the Y axis around unity. These two effects cause a linearization of the data.

The model for general static quenching has been used to analyze systems involving pyrene.⁵⁶ However, since the Benesi-Hildebrand has been used for polymeric systems, and the plotting is the same, the model for general static quenching could constitute a tool for internal comparison.

Finally, downward-shaped curves at high [Q] had been interpreted as the possible formation of micelles of a water-soluble fluorene-thiophene diblock copolymer.¹⁴ For such systems, a modified Stern-Volmer relationship known as the *multiequilibrium model* has been used which takes into account diffusion of a quencher into the core of an ionic micelle.¹⁴

For the sake of simplicity after choosing the best fittings to the data, only Perrin's and GSQ models were used in **Paper IV** to study the interactions between a water-soluble polythiophene-fullerene pair.

Another tool to gain insight on the possible dominant mechanism(s), besides the shape of the Stern-Volmer plot, is to evaluate the effect of temperature on the K_{sv} value. A ground-state complex is dissociated due to increases in temperature, causing a decrease in K_{sv}, while for dynamic quenching the case is opposite, higher temperatures increase the number of collisions in the excited state.⁴³

The UV-Vis spectra also provides information, since the presence of quencher causes a distortion in the absorption spectrum of the fluorophore, because a ground-state complex possess its own absorption mechanisms.

Regardless which model provides the best fit, if kinetic constants obtained at different temperatures are available, it is possible to insert these values into the van 't Hoff model, in order to estimate thermodynamic parameters:

$$\ln K = -\frac{\Delta H}{RT} + \frac{\Delta S}{R} \text{ ----(4)}$$

where K is K_{sv} (or the corresponding to a modified model) at the corresponding temperature, $f(T)$ and R is the universal gas constant. DH and DS are estimated then from the slope and intercept from the plot of LnK(T) vs 1/T.⁵¹

In **Paper IV**, the van 't Hoff model was used to perform a thermodynamic analysis on the interactions between a water-soluble polythiophene-fullerene pair.

1.4. Conjugated polyelectrolytes with hydrogen-bonding capabilities

H-bonding is relevant for the field of anion coordination chemistry, since it allows improved complexing with anions, some of which are critical in biology, medicine, catalysis and environmental science. Complexing with anions is challenging due to their varying sizes, shapes and charges, and their pH dependence. However success in synthesis of different receptors (of anions) has been achieved. With neutral and cationic receptors, the interactions with anions are mainly H-bonding and/or electrostatic. Also, since H-bonding can be considered as incipient proton transfer reactions (details after Figure 4),⁶² complexing with anions sometimes involves deprotonation.

For the particular type of receptors used in the present thesis, the work from the groups of Wilcox⁶³ and Hamilton⁶⁴ is relevant. They showed that urea moieties are good anion receptors, particularly oxoanions like CH₃CO₂⁻. In consequence, several *neutral* thio-urea (thiouronium) and *cationic* iso-thio-urea (isothiouronium) receptors have been reported, and both of them allow anion-binding through two-point H-bonding (see Figure 4).⁶⁵

Isothiouroniums, the core of the present thesis work, have received less attention than thiouroniums.⁶⁵ However, the work of Kubo et al.^{57,66,67} increased the interest on isothiouroniums, because in general, these molecules showed stronger binding with several anions. Their affinity is such, that in several cases they allow sensing in aqueous media and other solvents that are prone to compete for intermolecular H-bonding, such as water and hydroxylic solvents, also referred to as “competitive solvents”, in the contexts of molecular recognition,^{64,65} or polymer solvation.⁶⁸

This occurs because S-alkylation of thioureas generates a relatively larger dipole moment and enhanced acidity of the NH residues, reason why isothiurea groups are improved binders to oxoanions, in comparison with thioureas.^{69,70}

Teramae et al.⁷¹ studied the effect of spacer length of alkyl side chains between the isothiouronium group with bibenzene, finding that a methylene side chain causes decomposition in protic and nucleophilic solvents after photoexcitation, while an

ethylene spacer allowed 1:1 complexation of different anions (in order of selectivity): $\text{HPO}_4^{2-} > \text{CH}_3\text{CO}_2^- > \text{H}_2\text{PO}_4^-$, with kinetic interaction constants around 1×10^4 l/M.

Some of these isothiuronium receptors interact with anions through PET, and show increased fluorescence in presence of the anion (i.e. are “turn-on” receptors).⁶⁵

Isothiuroniums were later used, mainly by the same Japanese groups, to bind anions at interfaces, as part of sensing systems together with gold nanoparticles or polythiophene as signal reporter, to template photodimerization⁶⁵ and later to functionalize a polythiophene for sensing of phytate in water.⁵⁷

Figure 4 shows some previously reported thiourea-based molecules (1 to 3), together with an schematic representation of a two-point H-bonding with a carboxylate anion (4).

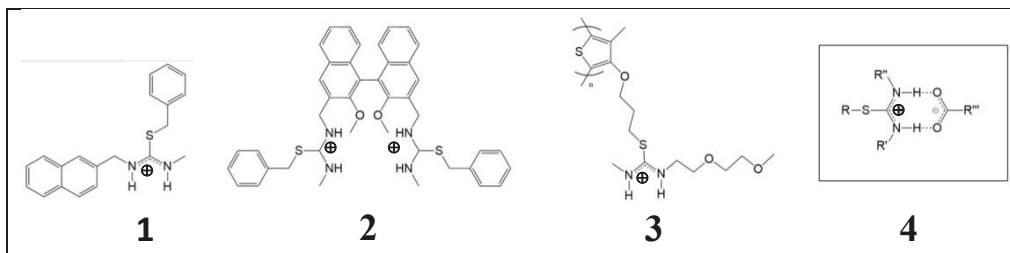


Figure 4. Thiourea based molecules reported by Kubo et al., (1-3) together with an schematic of the isothiurea functionality forming a two-point H-bonding with a carboxylate anion (4). Modified from^{65 57}.

As mentioned before, H-bonds can be considered as incipient proton transfer reactions, and for strong hydrogen bonds, such proton transfer is considered to be in a very advanced state. In a H-bonding, “X-H---A”, X-H is the “proton donor” or “electron acceptor” or “H-bonding donor” while A is the proton acceptor or electron donor or H-bonding acceptor.

The donor can interact with one acceptor (simple H-bond), or, due to its long range, it can interact with two or three acceptors, in the so called bifurcated or two-point, and trifurcated or three-point H-bonds, respectively. H-bonds with more than three acceptors are possible, yet not common since they require very high spatial densities of acceptors.⁶²

A H-bond has several constituents, different in nature. According to Morokuma, the total energy of a H-bond is composed of electrostatic, polarization, charge transfer, dispersion, and exchange repulsion forces, making H-bonds to merge with other types of interactions, such as van der Waals, ionic, cation- π and even covalent (in the solid state).⁶² The contribution of each component vary with the chemical structures of donor and acceptor, and also with the environment, reason

why a H-bond can gradually change into another interaction type. If the polarity of X-H and A is reduced by changing X or A, the electrostatic part of the H-bond will also decrease, while the van der Waals contribution is barely affected, increasing then its relative contribution.⁶²

In regard to the range in distance of an H-bond, the van der Waals cutoff criterion requires the H---A distance to be substantially shorter than the sum of the van der Waals radii of donor and acceptor. However some authors consider this criterion should be avoided since it is too restrictive, and suggest to simply consider that H--A distances up to 3.2 Å as potential H-bonds.⁶²

In regard to the distance dependence of each contribution, from all the components of an H-bond, the electrostatic contribution is the one which decreases the least with distance, making it dominant at long distances, even if charge transfer dominates at optimal geometry: elongation of a H-bond always makes it more electrostatic in nature. However charge transfer and van der Waals terms are always present. For weak H-bonds, dispersion contributes as much as electrostatics. In regard to the geometry of an H-bond, linear H---A angles are statistically favored over bent ones.⁶²

In **Paper IV** a study was performed on the solution-interactions between a water-soluble polythiophene-fullerene pair with two-point hydrogen-bonding capabilities.

1.5. Hydrogen-bonding mediated aggregation of ionic polythiophenes

To the best of the author's knowledge, the study related to water-soluble lignin sulfonates by Deng et al.,³⁶ is the only contribution that can be found about studies on H-bonding mediated, aggregation of macromolecules built from conjugated units, using steady-state fluorescence spectroscopy.

Besides this, only the contribution by Briseno et al.⁷² reported a study on solid-state properties of thiophene oligomers and polymers, "end-functionalized" (see Figure 5) with a phosphonic functionality. It was proposed that the solid state was then tuned by the interaction between adjacent molecules: (a) H-bonding through the phosphonic-phosphonic groups (P-OH---O=P), (b) between terminal thiophene rings, (c) van der Waals forces between adjacent alkyl chains, and (d) pi forces, between adjacent rings (see Figure 5). The polythiophene and the substrate (ZnO nanowire) were proposed to interact through H-bonding. However, in the referred work, neither water was used as solvent, nor the role of the interaction forces in solution were investigated. A modified scheme of this contribution is presented in Figure 5.

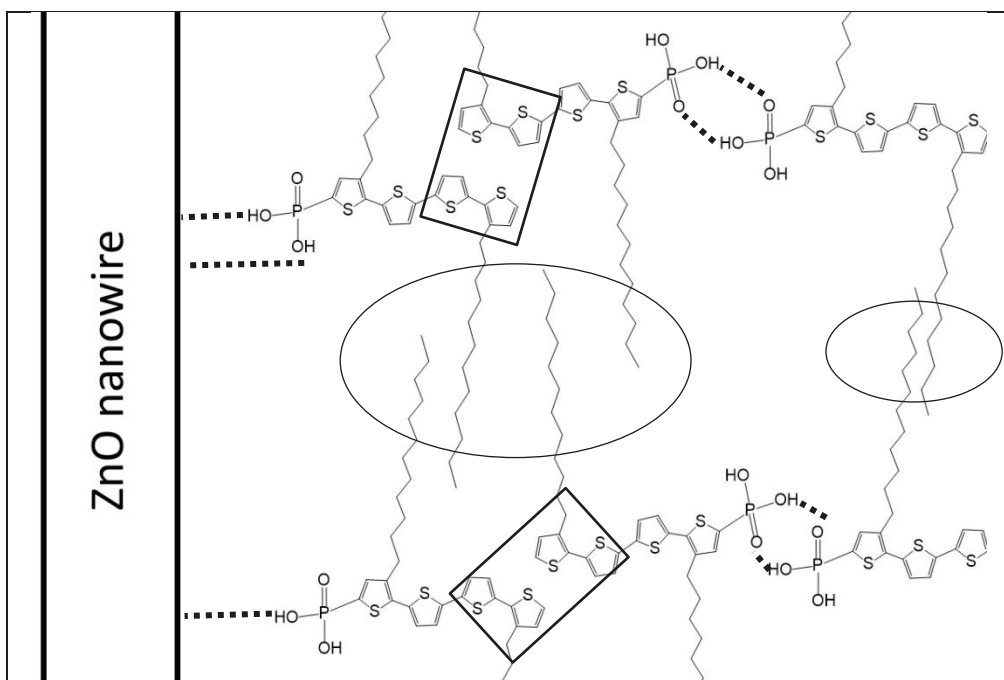


Figure 5. H-bonding (dashed black lines), hydrophobic (in ovals) and π - π (in rectangles) interactions between thiophene oligomers in the solid state. Modified from Briseno et al.⁷²

1.6. Hydrogen-bonding mediated electron and charge transfer

Particularly important for the present project are those works involving water-soluble donor: C_{60} pairs, with two-point, triple-point, or multiple H-bonding capabilities, in order to study the role of H-bonding on the mechanisms of interaction (static and/or dynamic quenching, PET and FRET).⁷³ Most of these water-soluble pairs involve the use of small-molecules as donors, however there are some reports involving the use of CPEs donors.

Paper IV reports a study on the effect of solvent polarity and H-bonding capacity on the interactions between a water-soluble polythiophene: C_{60} donor:acceptor pair. One of the few contributions dealing with solution-phase studies using a similar pair is that of Li et al.⁷⁴ using a polythiophene block copolymer with diamino pyrimidine functional groups (**1** in Figure 6) and a thymine tethered fullerene derivative (**2** in Figure 6). Three-point H-bonding increased the short-range electron transfer. When the donor:acceptor pair was applied in OSC, H-bonding increased the stability of the devices, allowing also control over the morphology, by changing the donor:acceptor ratio.

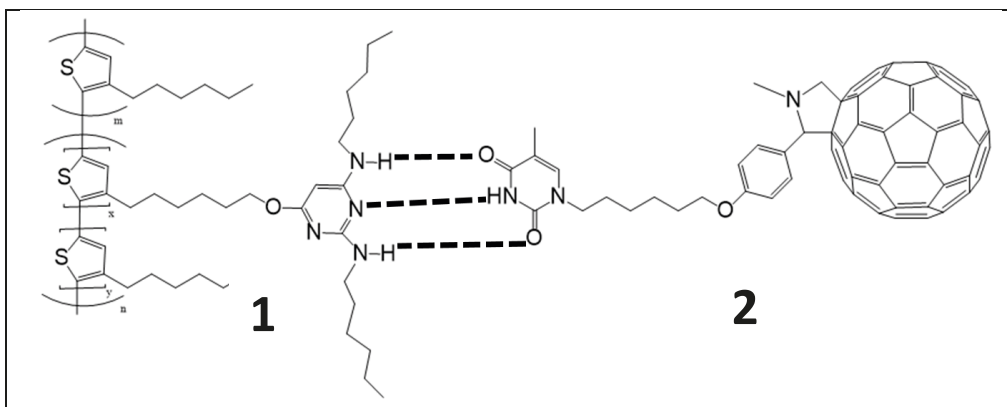


Figure 6. Triple-point H-bonding mediated charge transfer, between a polythiophene block copolymer with diamino pyrimide functional groups (1) and a thymine tethered fullerene derivative (2). Dashed horizontal lines represent the H-bonding. Modified from Li et al.⁷⁴

1.7. Role of molecular structure

The most widely used polymerization methods of poly(3-alkylthiophenes) are either electrochemical, or chemical oxidation. The latter is performed through the Yamamoto and Suzuki coupling reactions or using FeCl_3 as catalyst. Although all of these methods reduce or eliminate 2,4-linkages, they do not solve the lack of regiochemical control over head-to-tail (HT) couplings between adjacent thiophene rings. However, by using monomers that preferentially couple HT, such as 3-alkoxy-4-methylthiophenes, the oxidative polymerization using FeCl_3 results in the formation of regioregular polymers with mainly HT 2,5-linkages.⁷⁵ FeCl_3 -catalyzed polymerization of 3-alkoxy-4-methylthiophenes was also used by Leclerc's group to synthesize different cationic thiophenes,¹⁰ by Minami et al. to polymerize a CIT possessing mainly HT couplings,⁵⁷ and by this group, in order to synthesize the CITs used in the present work (for details see Figure 9 in the methods section).

In neutral conjugated polymers, the attachment of flexible side chains, with different lengths, can improve dramatically the solubility of polythiophenes.^{75,76} Also, the self-assembly of neutral polythiophenes is very sensitive to the placement and nature of the substituent side chains attached to the thiophene ring.⁷⁷ For example, inert side chains reduce the light absorbing and semiconducting properties of copolymers, whereas alkyl or alkoxy groups raise the conformational entropy of the macromolecule in solution and disturb molecular packing. Bulkier branched-alkyl side chain reduces the tendency of the polymer to crystallize and generates a more twisted and less rigid backbone because of steric effects. In turn, these effects reduce the conjugation length and π -stacking.⁷⁸ Side chains also impact on solid-state properties such as crystallinity and backbone orientation. These parameters in turn influence the exciton diffusion and charge transport, affecting the morphology and performance of solid-state applications such as OSCs.⁷⁹

For water soluble polythiophenes, side chain length has shown to have an impact on (i) the isotropic decays and complexity of decay of non-ionic oligo(ethylene oxide) polythiophenes,⁸⁰ (ii) the electronic properties of films of thiophene-containing polymer zwitterions,⁸¹ and (iii) the optoelectronic and photophysical properties of polythiophenes bearing carboxylic acid groups, in solution and as part of OSCs.⁸² Molecular dynamics (MD) simulations have shown that the side chain length of surfactants generates a fine balance between electrostatic and hydrophobic interactions with a CPE.^{3,83}

1.8. Role of solvent

As mentioned in section 1.2., solvents can also tune the aggregation of CPEs, since they can modify the structural order and conjugation length of the polymer backbone.⁸⁴ Also changes in the partitioning between aggregated and nonaggregated forms of the polymer due to solvent can be seen. This is due to conformational changes taking place both in backbone and side chains of CPEs, causing either easy dissolution, with an expanded conformation, or a “collapse” of the backbone and aggregation, both inducing changes in the optical properties of CPEs in solution.³

This is critical for the present project, since the effect of solvent was used: (i) in **Paper II**, in order to study its effect on the Stokes shift values of different CITs, which allowed obtaining information on possible specific solvent–fluorophore interactions by using, for example, the “Stokes shift vs. orientation polarizability” Lippert-Mataga plot, and (ii) in **Paper III**, to exploit the changes in emission spectra with the degree of self-quenching. This resulted in information on the formation, number, and interaction pathways of these type of chromophores.

Some CPEs present important differences in solubility and aggregation in water and alcohols, which is relevant for all the fields of applications commented before in section 1.1. Clusters of CPEs in aqueous media could become completely dissolved by using organic cosolvents, which is probably due to selective solvation, obtained by the ionic groups being surrounded by water-rich regions. This phenomenon could be exploited for sensing or nanostructuring.³

MD simulations have shown that in the aggregation of CPEs, there is a very fine balance between electrostatic and hydrophobic interactions, which are strongly dependent on the side chain length and solvent.³

Solvent also tunes the forces of interaction between donor:acceptor pairs, which has been studied in the context of research of organic photovoltaics. One of the study approaches has been the use of the Hansen solubility parameters to study different donor:acceptor pairs, by correlating the solubility of C₆₀ fullerene in organic solvents and polymers.⁸⁵ However, these studies did not include neither CPEs nor water. In this regard, **Papers III and IV** uses these solubility parameters qualitatively, to point out the H-bonding capacity of the solvents used.

Concerning CPEs, the *ortogonal solubility* between water (or other hydroxylic solvents) and organic solvents, during ink-jet or screen printing processing of multi-layer organic photovoltaics, is being exploited, since such orthogonality between solvents provides control over the morphology and efficiency of these devices.⁸⁶ Also, the use of CPEs as electrode selective “buffer” layers in OSCs is an active research field, since it allows simultaneously improvement of open circuit voltage, short-circuit current, and fill factor.¹⁷

On the other hand, *cosolvents* have been used to gain information on H-bonding, for example, a study using methanol–dimethylformamide mixtures, which provide information on the H-bonding interactions and dipole association during polymer intermolecular interactions.⁸⁷ The intermolecular complex between the two solvents interferes with the hydrogen-bonding effect that typically yields a nanoribbon morphology for such a molecule.

It is also known that mixed solvents generate preferential solvation of certain parts of the polymer, such as backbone and attached functional group, in certain component of the binary mixture.⁸⁸

It is worth to mention that just like the effect of solvents alone, the effect of cosolvents has been also extensively studied in the field of organic photovoltaics (field in which cosolvents are known as “*additives*”).

In this context, cosolvents provide larger control than solvents alone on the interactions between donor:acceptor pairs since cosolvents provide control over the solid-state properties of the films present in these devices. The formation of films depend on two groups of parameters: (i) the kinetic parameters defining the drying kinetics of the mixture (e.g. vapor pressure of solvents and deposition conditions), and (ii) the thermodynamic parameters in solution, which involves solubility and interactions between donors and acceptors.⁸⁹ From these approaches, and due to the solid-state nature of these devices, the research concerning point “i” dominates the current research,^{89,90} while the studies involving the effect of cosolvents on the thermodynamics in solution (i.e. point “ii”) is largely missing, even more in environmentally friendlier water-soluble donor:acceptor systems.

Papers II and III discuss the role of the side chain length on polymer-solvent and polymer-polymer interactions of CITs, when interacting in pure water or water-cosolvent mixtures.

2. Aims of the Study

The aims of this work were to study H-bonding-influenced polymer-solvent, polymer-polymer and polymer-quencher interactions of cationic isothiuronium polythiophenes (CITs). These aims were achieved by exploiting the structural properties of the CITs: Firstly, their chromo- and fluoro-phoric optical properties allowed the use of steady-state absorption-fluorescence spectroscopic techniques. Secondly, their solubility in water and hydrogen-bonding-donor capabilities allowed to study molecular interactions as a function of the molecular structure of the CITs and/or the polarity/hydrogen-bonding capacity of the solvent (with water allowing to include high dielectric media). Finally, their molecular structure containing ionic and hydrophobic constituents, allowed studying their aggregation by means of electron paramagnetic resonance (EPR) spectroscopy, using paramagnetic probes with different ionic and hydrophobic constituents. These spectroscopic studies were complemented with other experimental (e.g. cyclic voltammetry and dynamic light scattering) and computational (e.g. DFT) techniques.

In **Paper I** it was noticed that a phosphonate [6,6]C₆₀-fullerene had strong quenching capabilities on the fluorescence of a CIT in aqueous solution. In order to further study this result, it was necessary to further characterize the solution-phase properties of the CIT. By adding homologous CITs with different side chain lengths and solvents with different polarity/H-bonding capacity, it was possible to perform an structure-function study in **Paper II**. The aims of Paper II were (i) to determine the concentration required to avoid molecular aggregation, (ii) to characterize the electronic properties of two CITs with different side chain length and (iii) to evaluate the behavior of these molecules in solvents with different polarity/H-bonding capacity. The aims of **Paper III** were to gain understanding on the effect of the structural difference on the aggregation mechanisms of the CITs in (a) solvents with different polarity/H-bonding capacity, by means of absorption-fluorescence spectroscopic techniques and (b) in presence of paramagnetic probes with probes with different ionic and hydrophobic constituents, by means of EPR spectroscopy.

Finally, the aims of **Paper IV** were to evaluate the effect of solvent polarity/H-bonding capacity on (A) the quenching mechanisms, by aid of spectroscopic and Stern-Volmer analyses, and (B) on the thermodynamics of interaction, by performing van 't Hoff analyses.

3. Experimental

3.1. Materials

The structures of the molecules used in this work are presented in Figure 7: (a) three cationic isothiuronium polythiophenes (poly-3-(N,N-diethyl-S-isothiuronium)*alkoxy*-4-methyl thiophene), with alkoxy chains of different length in the 3-position of the thiophene ring,⁹¹⁻⁹³ and (b) four [6,6]-phosphonate C₆₀-fullerene derivatives, two of which have their phosphonate (PO₃⁻), hydrogen bonding (H-bonding), acceptor functionalities, protected through alkylation.^{91,94,95}

This set up of molecules allowed to evaluate systematically the effect of molecular structure and solvent on polymer-solvent, polymer-polymer and polymer-quencher interactions.

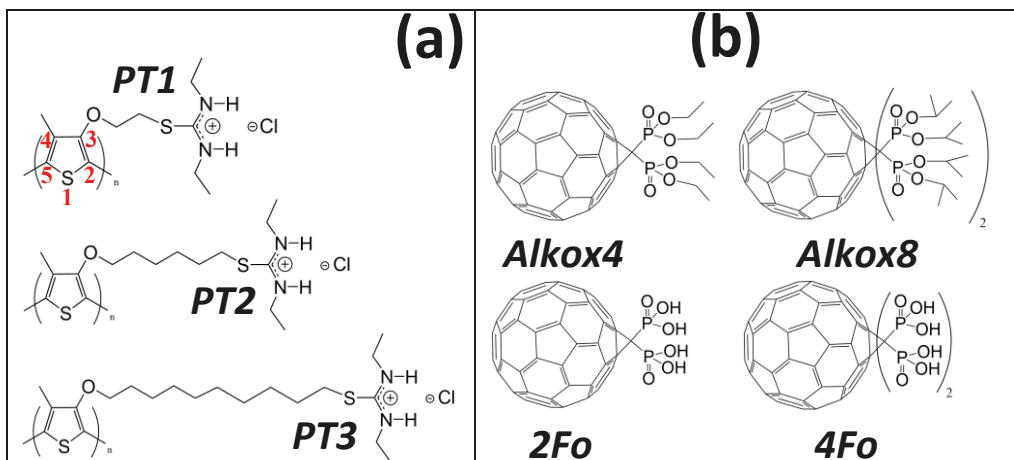


Figure 7. Structures of the poly-3-(N,N-diethyl-S-isothiuronium)*alkoxy*-4-methyl thiophenes, with *ethyloxy* (PT1), *hexyloxy* (PT2) or *decyloxy* (PT3) side chains in the 3-position of the thiophene ring, and the [6,6]-C₆₀ fullerene derivatives [6,6]-bis(diphosphonate)-bromomethanefullerene (2Fo), [6,6]-[bis(bis(diphosphonate))2-bromomethanefullerene (4Fo), [6,6]-bis(diethoxy-phosphoryl)-bromomethanefullerene (Alkox4) and [6,6]-[bis(diisopropoxyphosphoryl)]2-bromo-methanefullerene C₆₀ (Alkox8). Notice that PT1 shows the numbering (in red) of the carbon and sulphur atoms in the thiophene ring.

The control over media was further achieved by using two types of polarity agents, shown in Figure 8: (a) solvents with different polarity and H-bonding capacity or (b) paramagnetic probes with different polar and hydrophobic components (for EPR studies in aqueous solutions). The structures of these are presented in Figure 8.

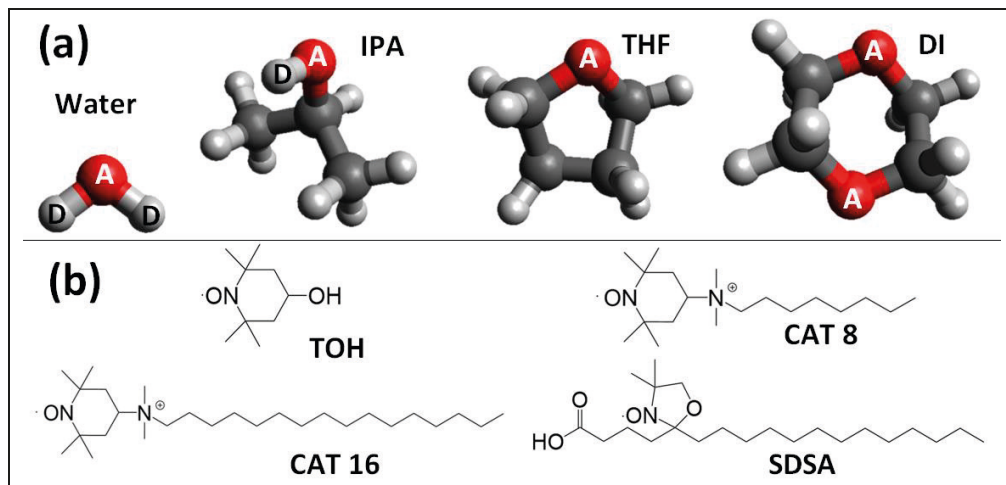


Figure 8. (a) 3D structures of the four solvents used: water, isopropanol (IPA), tetrahydrofuran (THF) and 1,4-dioxane (DI), (the labels “D” and “A” on certain atoms indicate a H-bonding donor or acceptor, respectively), and (b) skeletal formulas of the four paramagnetic spin-probes used: 4-hydroxy, 2,2,6,6 tetramethyl-piperidine-1oxyl (TOH), 4-octyl dimethylammonium, 2,2,6,6 tetramethyl-piperidine-1oxyl bromide (CAT8), 5-doxyloctyl-stearic acid (SDSA), and 4-cetyl dimethylammonium, 2,2,6,6 tetramethyl-piperidine-1oxyl bromide (CAT16).

As explained in **Papers II and III**, the three organic solvents mentioned above were chosen due to their complete miscibility with water and the properties obtained when mixed with water as cosolvents, generating *protic-protic* water-isopropanol (W-IPA), *protic-aprotic* water-tetrahydrofuran (W-THF) and *protic-non polar* water-1,4-dioxane (DI) mixtures. As shown in Table 1, this series of cosolvents represent in named order decreasing polarity, H-bonding capacity and values of the H-bonding interactive force (δH) of the Hansen solubility parameters.

Because of the properties listed in Table 1, these solvent mixtures enabled a study on specific polymer-solvent interactions, in this case by evaluating the effect of the alkoxy spacer length of PT1-3 and the polarity/H-bonding capacity of the solvent, on the specific polymer-solvent interactions (**Paper II**) and on the aggregation processes of the polymers (**Paper III**).

Table 1. Values of physical-chemical parameters relevant for the studies, from all the solvents (at 20 or 29 °C). The hydrogen bonding capacities of each *pure solvent* (according to the Hildebrand scale) are also shown. Next to each value is provided the number of the reference.

<i>Solvent</i>	<i>Density (g/cm³)</i>	<i>Dynamic Viscosity (mPa s)</i>	<i>Dielectric constant</i>	<i>Relative Polarity †</i>	<i>Refractive index</i>
Water	0.99 ⁹⁶	*0.754 ⁹⁷	80.38 ⁹⁸	1	*1.33 ⁹⁷
W-IPA	0.90 ⁹⁹	2.8 ¹⁰⁰	43.68 ¹⁰¹	0.54	1.36 ⁹⁹
W-THF	0.92 ⁹⁶	*0.79 ⁹⁷	41.21 ¹⁰²	0.51	*1.39 ⁹⁷
W-DI	1.03 ¹⁰³	*1.4 ⁹⁷	36.89 ⁹⁸	0.46	*1.40 ⁹⁷

* At 29 °C

† Ratio “Dielectric constant of cosolvent mixture/Dielectric constant of water”

Table 1-cont.

<i>Solvent</i>	<i>Hydrogen bonding capacity *</i>	<i>δD Dispersion †</i>	<i>δP Polar †</i>	<i>δH Hydrogen bonding †</i>
Water	Strong	15.5	16.0	42.3
IPA	Strong	15.8	6.1	16.4
THF	Moderate	16.8	5.7	8.0
DI	Moderate	17.5	1.8	9.0

* ¹⁰⁴

† ¹⁰⁵

Among the cosolvents used, DI is of particular interest, because besides being miscible with water in all proportions, it is a non-polar aprotic solvent with a boiling point and density similar to water, but possessing a dielectric constant significantly lower to water. Also, when used as cosolvent, DI disrupts the normal three dimensional structure of water, caused by its relatively bulky structure, the presence of 4 methylene groups and its ability to accept two hydrogen bonds without donating any (see Figure 8a).¹⁰⁶ Light scattering experiments showed that water-DI mixtures (1:3 v/v) form clusters through H-bonds.¹⁰⁷ DFT simulations also showed such complexation,¹⁰⁶ while MD simulations were used to compare the interactions and aggregation between oligomers of an anionic phenylene-fluorene copolymer in water or a 50:50 water-DI mixture. It was observed that DI forms a “coating”, displacing water from the immediate environment of the molecule, while the ionic parts are preferentially solvated by water. Such coating reduces interchain and side-chains interactions and therefore aggregation.¹⁰⁸

In Papers II and III, the mixture W-DI was used as one of the limiting experimental conditions in regard to the decrease of polarity/H-bonding capacity (pure water was

the opposite limiting condition). In Paper IV, the W-DI mixture was selected to evaluate the effect of solvent polarity/H-bonding capacity, on the interactions between a PT1:4Fo donor:acceptor pair prone to interact through H-bonding.

3.2. Methods

The techniques used in this work and the reasons behind their use are briefly described here. More details of the particular experimental/computational setups used in this project can be found in Papers I-IV.

3.2.1. UV-Vis absorption spectrophotometry

In **Paper I**, this technique was used to evaluate the effect of molecular structure on the optical properties of the four C₆₀ phosphonate derivatives in solution and as self assembled films.

In **Papers II and III** it was used to analyse the absorption maxima (λ_{max}), and also (together with complementary steady-state fluorescence measurements), quantum yields (Φ_f) and Stokes shifts ($\Delta\nu$) as a function of: (i) side chain length in PT1-PT2, and (ii) polarity/H-bonding capacity of the solvent. Additionally, an estimation of the optical bandgaps (E_{gOPT}) of PT1-PT2 could be made. In Paper II, it allowed the use of the Lippert-Mataga plot, in order to get qualitative information on polymer-solvent interactions.

In **Paper IV** this technique was used to evaluate the degree of fluorescence resonance energy transfer (FRET) and photoinduced electron transfer (PET) between a PT1:4Fo donor:acceptor pair as a function of polarity/H-bonding capacity of the solvent, and also to verify if these molecules form a ground-state complex.

3.2.2. Steady-state fluorescence spectrophotometry

In **Paper I** this technique was used to evaluate the effect of polymer functionalization on the acceptor properties of 4Fo, by analyzing the extent of fluorescence quenching in a PT1:4Fo donor:acceptor pair in water.

In **Papers II and III**, besides the analyses on quantum yields and Stokes shifts already mentioned, this technique allowed analyzing the excitation and emission maxima (λ_{ex} , λ_{em} , respectively), as a function of molecular structure, concentration, and polarity/H-bonding capacity of the solvent. In Paper III the shape of the excitation spectra as a function of solvent was used to propose a simple criterion to evaluate the type of dominant aggregation type (H- or J-like).

In **Paper IV** it was used to further study the fluorescence quenching between a PT1:4Fo donor:acceptor, extending the study in Paper I, in order to evaluate the effect of solvent (water or W-DI) on the interaction mechanisms and thermodynamics of the system.

In regard to the UV-Vis/fluorescence studies, it is important to point out the critical role of the SpectraGryph optical spectroscopy software¹⁰⁹ in this research, since it

provides a simple and efficient way to visualize, manipulate (e.g. smoothening, baseline correction, normalization), analyze and plotting large numbers of spectra, which was the case in this project.

3.2.3. Cyclic voltammetry

In **Papers I and IV**, this technique was used to evaluate the effect of polymer functionalization and phase-state on the electron-accepting properties of C₆₀.

In **Paper II**, it allowed estimating the ionization potential (I_p) of PT1-PT2, through the onset of electrochemical oxidation of drop-cast films.

3.2.4. Electron paramagnetic resonance spectroscopy (EPR)

In **Paper III**, EPR (also known as electron spin resonance) was used to study the effect of concentration of PT1 and PT2 in aqueous solutions, in presence of paramagnetic probes of different polarities, in order to evaluate the effect of the side chain length on their aggregation properties.

3.2.5. Density functional theory (DFT)

In **Paper II**, DFT calculations were performed by simulating oligomers (until hexamers), in order to evaluate qualitatively the effect of the side chain length in PT1-PT2, on the simulated frontier molecular orbitals (FMOs) and molecular conformation, simulating implicit solvation in water and dioxane.

In **Paper III**, it was used to obtain qualitative-supplementary insight on the effect of the side chain length of PT1-PT2 on the electrostatic potential maps (EPMs) of dimers of these molecules.

All calculations were carried out using the Gaussian 09 (G09) package,¹¹⁰ running in the Taito supercomputer, hosted at the CSC – IT Center for Science (Finland). The electrostatic potential surface maps were visualized using the softwares Avogadro, Open Babel Version 2.3.2.4,¹¹¹ or Jmol.¹¹²

In regard to DFT, in the electronic supplementary information of Paper II, the author clearly pointed out the boundaries of the use of this tool, as *qualitative*, and *complementary*, used for *internal comparison*. It is worth to mention that the author also performed Time-Dependent DFT (TD-DFT) and molecular dynamics (MD) studies during the duration of this project, however, only the results from DFT were successful enough to be included in this research.

3.2.6. Dynamic light scattering (DLS)

In **Paper II**, DLS (also known as photon correlation spectroscopy) was used in order to compare the particle size of aqueous solutions of PT1 and PT2 in disaggregated and aggregated states.

3.2.7. Synthesis/purification methods and ^1H -NMR

Previously, the polymers used in the present project presented challenges in regard to the estimation of regioregularity. Regardless it is known that the FeCl_3 oxidative polymerization of 3-alkoxy-4-methylthiophenes as monomers, generates mainly head-to-tail regioregularity, through 2,5-linkages (for numbering see Figure 7).^{57,75} Regardless, an attempt was made to obtain primary evidence, performing two strategies. These strategies, following the guidelines of Minami et al.,⁵⁷ were implemented in the steps pointed out by blue vertical arrows in the synthetic route shown in Figure 9.

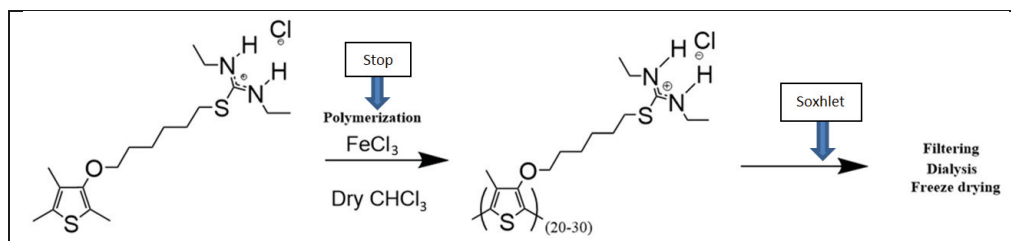


Figure 9. Polymerization step in the synthetic route of PT2. Thick blue vertical arrows indicate the modified steps.

The arrow labeled “stop” in Figure 9 indicates the step in which a time-dependent polymerization was performed in order to gain understanding on the regioregularity of the polymer, by analyzing the oxymethylene proton nuclear magnetic resonance (^1H -NMR) signals from samples taken after 1, 6 and 12 hours of polymerization. These samples were also aimed to provide information in regard to dispersity (\mathcal{D}), as detailed ahead.

On the other hand, the vertical arrow labeled “soxhlet” in Figure 9 indicates an extra purification step, consisting of a 48 hours soxhlet reflux using THF, performed, as an attempt to remove the traces of the catalyst, in order to obtain suitable ^1H -NMR spectra.

3.2.8. Time-of-flight matrix-assisted laser desorption/ionization (MALDI-TOF)

The estimation of dispersity ($\mathcal{D}=\text{Mw}/\text{Mn}$, in where Mw and Mn are the weight-average and number-average molecular weights, respectively) of cationic CPEs is very challenging due to (i) strong (and inconvenient) interactions with the chromatographic columns, and (ii) the lack of structurally-analogous polymeric standards, as discussed in **Paper II**.

Regardless of this, the author attempted to obtain primary evidence, by using MALDI-TOF, following the study of Liu et al.,¹¹³ focusing specifically at non-ionic polythiophenes and evaluating: (i) matrix, (ii) effect of laser power, and (ii) the effect of matrix/analyte ratio. For the project reported in this thesis, water-soluble matrices were used: α -Cyano-4-hydroxycinnamic or 2,5-Dihydroxybenzoic acid.

4. Results/Discussions

4.1. ^1H -NMR and MALDI-TOF

Despite of the soxhlet purification step performed in this project, the ^1H -NMR spectra from PT1 and PT2 suggested the presence of FeCl_3 , since the signals were broad and therefore not suitable for further structural analyses.

The MALDI-TOF spectra obtained did not provide information on Mw since none of them showed any clear band, regardless the matrix, laser power, and matrix/analyte ratios used.

As detailed in **Paper II**, both polymers were assumed to have similar degree of polymerization (DP), dispersity ($\text{Đ} = \text{Mw}/\text{Mn}$) and regioregularity. DP was estimated (using the polymer precursor) to be around 20-30 repeating units, value consistently obtained by this research group^{114,115} and other research groups,¹¹⁶⁻¹¹⁸ for cationic and/or anionic polythiophenes.

Finally, in regard to their regioregularity, it was assumed to be mainly head-to-tail (HT), through 2,5-linkages, since it is known that the FeCl_3 oxidative polymerization of alkyl-thiophenes minimizes 2,4-linkages.^{57,75}

4.2. Ionization potential, electron affinity and bandgap

The energy levels of PT1 and PT2 were determined either experimentally or computationally. Figure 10 shows the cyclic voltammograms (CVs) used to estimate the ionization potential (I_p). Figure 11 presents absorption and fluorescence data of all the molecules used in this project, in solution and/or solid state. The absorption spectra are used to estimate the bandgap (E_g) by means of the absorption onset or the 0-0 transition. Figure 12 shows DFT-estimated energies of the frontier molecular orbitals (FMOs) HOMO and LUMO, from dimers, tetramers and hexamers of PT1 and PT2 (labeled OT1 and OT2), together with the simulated spatial location of the electron densities in the FMOs of hexamers. Please notice that in Paper II the HOMO-LUMO values were also estimated in 1,4-dioxane, and are omitted here because the simulations in water are those that fit better to the study/case, probably because inherent limitations of the implicit solvation approach when simulating an ionic molecule within 1,4-dioxane and/or incomplete

representation of the 50:50 v/v binary mixture, which in the past has been simulated more accurately by using molecular dynamics.¹⁰⁸

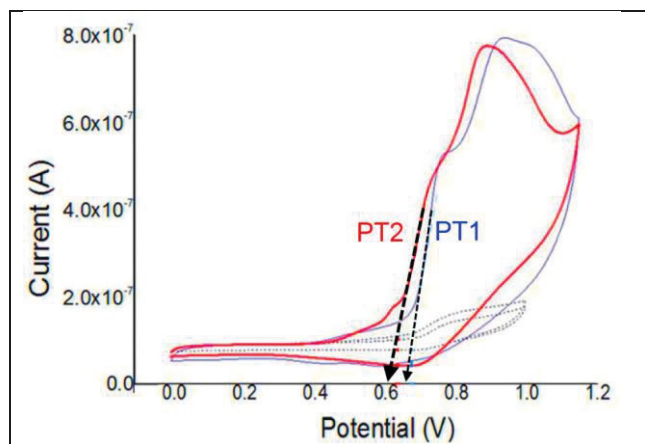


Figure 10. Cyclic voltammograms of the first cycle of oxidation of drop-casted films of PT1 and PT2 on the surface of a glassy carbon working electrode. The black dashed cyclic voltammogram shows the blank measurement. Dashed black arrows indicate the oxidation onsets.

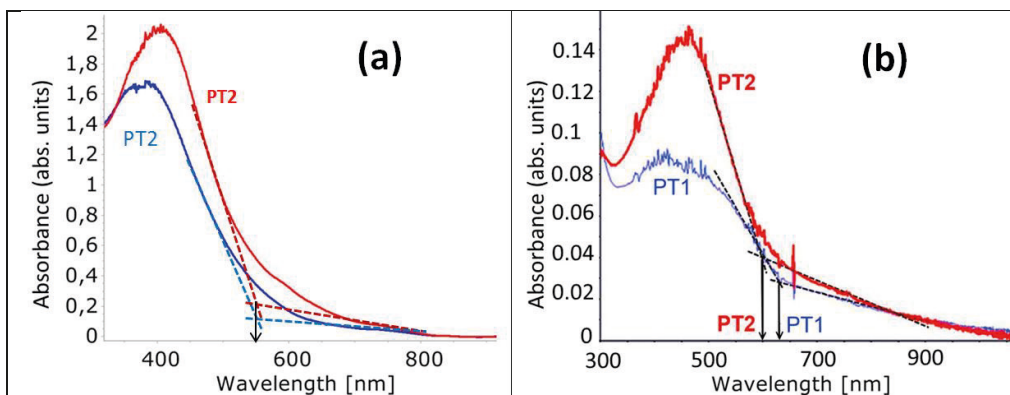


Figure 11. Absorbance of PT1 and PT2, (a) in water (1.05 M), or (b) as drop casted films on glass.

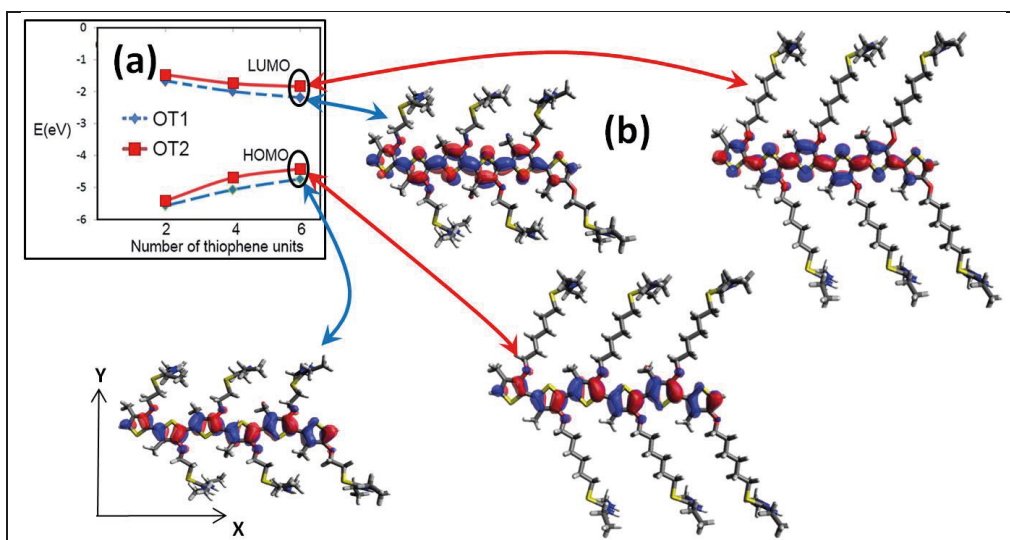


Figure 12. (a) DFT energy estimations of FMOs of di-, tetra- and hexamers of PT1 and PT2 (labeled OT1 and OT2, respectively), together with (b) images of the hexamers of OT1 and OT2, showing the spatial location of HOMO and LUMO. These oligomers lie in the x-y plane as indicated for the hexamer OT1.

Table 2 shows the experimentally and computationally estimated values of the energy levels of PT1-2.

Table 2. Energy levels estimated experimentally and by DFT (method B3LYP/6-31G**).

	SOLUTION	FILMS				DFT		
	E_{gOPT}^* (eV) Water	Oxid. onset (V)	I_p^\dagger (HOMO) (eV)	E_A^\ddagger (LUMO) (eV)	E_{gOPT} (eV)	HOMO (eV) §	LUMO (eV) §	E_g (eV)
PT1	2.35	+0.68	-5.08	-3.11	1.97	-4.77	-2.18	2.55
PT2	2.35	+0.62	-5.02	-3.02	2.06	-4.41	-1.84	2.57

*From absorption onsets in water at 1.05 M (Figure 11a).

$^\dagger I_p = -(\text{Oxid. onset} + 4.8) \text{ eV}$ (details in ESI of Paper II). Using the oxidation onsets in Figure 10.

‡ Estimated assuming $E_{gOPT} \approx I_{pCV} - E_{aOPT}$, after reference ¹¹⁹ (details ahead).

§ From DFT simulation on hexamers, 1 Hartree = 27.2114 eV

As reported in **Paper II**, in regard to the HOMO values of PT1-PT2, Table 2 shows that the I_p values estimated from the oxidation onset of drop-casted films (i.e. Figure 10), become slightly less negative for longer side chains, a trend which is in agreement with the HOMO of the simulated hexamers. Table 2 shows that the bandgap (E_g) values estimated from films (i.e. Figure 11b), indicate that the longer side chain in the 3-position of the thiophene ring of PT2, causes an increase of $\approx 0.09 \text{ eV}$ in the bandgap. This trend is in agreement with the E_g of the simulated hexamers, which predicts that a longer side chain causes an increase of $\approx 0.02 \text{ eV}$ in the bandgap.

In Paper II the LUMO values of the polymers were estimated by combining the HOMO estimation from onsets in CVs, with the optical bandgaps (E_{gOPT}) from absorption onsets of films. This approach was used after the contribution of Johansson et al. using 25 neutral polythiophenes,^{119,120} in which was shown that similar gaps are obtained from CV alone (i.e. electrochemical bandgap= $E_{gEC}=I_P-E_A$) or absorption of films (i.e. the E_{gOPT}).

It is worth to mention that in the reference cited the absorption *maxima* was used to estimate E_{gOPT} , instead of the long-wavelength onset of absorption, as reported in Paper II, after Page et al.⁸¹ This is relevant because using λ_{max} generates higher E_{gOPT} estimations and also switches the results in regard to PT1 and PT2: resulting in $E_{gOPTPT1} > E_{gOPTPT2}$. However, to the best of the author's knowledge, the onset of absorption is preferred in literature (e.g. the Tauc plot).

The energy values predicted by DFT (Table 2) show that the maximum difference between simulated and experimental data was observed in the LUMO values, for which DFT estimates values 0.93 and 1.18 eV less negative than the experimentally-estimated LUMOs of PT1 and PT2, respectively. In other words, DFT estimates less negative LUMO values than the experimental estimations, by ≈ 1 eV. The DFT estimations of HOMO and E_g differ from the experimental estimations by maximum 0.6 eV. A further discussion on the accuracy of DFT methods, for predicting actual energy values for a given system, is beyond the scope of this work. Therefore, as stated in the supporting information of Paper II, despite the actual energy values, it can be concluded that DFT, with the B3LYP/ 6-311+G* basis set, predicts the effect of the length of alkoxy side chains reasonably well, *at a qualitative level*, as was previously reported in studies of oligothiophenes.¹²¹ Also, the B3LYP/ 6-31G** level has proved to be a reasonable choice for thiophene based systems,¹²² and to correlate well with the theory and experiment for molecules with similar size to the oligomers used in this work, with estimations of bandgap ≈ 2 eV.¹²³

In Paper II DFT was also used to analyze the effects of a larger spacer on the spatial geometry of the molecules. In this regard, Figure 13 presents the x- and y-axial views of the oligomers simulated (according to the coordinate system defined in Figure 12), in water, together with the dihedral angles between the two central thiophene rings of the structures.

The angles were defined between the planes formed by each of the central thiophene rings, by measuring (with aid of the software Avogadro) Sulphur_{RING1}-Carbon(2)_{RING1}-Carbon(5)_{RING2}-Sulphur_{RING2} (following the numbering of carbons shown in the structure of PT1, in Figure 7). In Paper II, only the images from the y-axial view were presented.

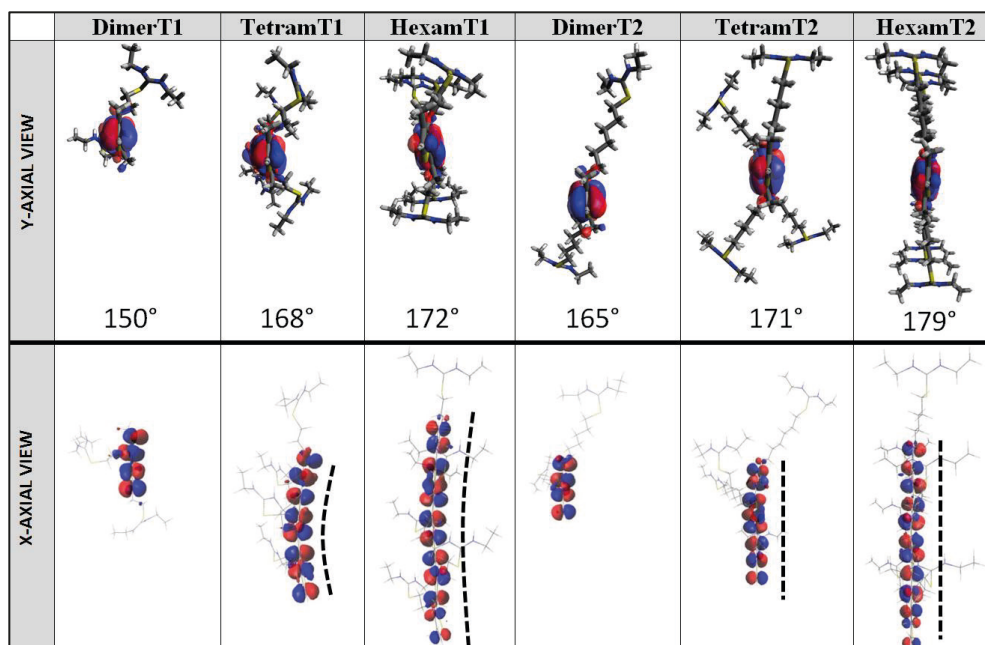


Figure 13. Y- and x-axial views of the simulated oligomers. In the y-axis a stick-like representation of the oligomers is used in order to see the bending of the side chains. The numbers shown correspond to the dihedral angle between the central-thiophene rings, this view also presents the value of the dihedral angle between the two central thiophene rings. In the x-axial view a thinner, wire-type representation of the oligomers is used in order to visualize the bending of the molecules through the HOMO electron densities. The added black-dashed lines serve also as visual guides.

As reported in **Paper II**, the X-axial views in Figure 13 show that, the longer spacers generate less bending of the polymeric chain, while the y-axial views show that shorter spacers generate larger bending of the isothiuronium group.

In this regard, the dihedral angles show that for both spacer lengths, the increase in monomer units increase the value of the dihedral angle, and that the dihedral angle values of the oligomers of PT2 are larger than those of the monomers of PT1. Notice that due to the head-to-tail nature of these simulated molecules, null twisting would be reflected in dihedral angles of 180°, while dihedral angles of 90° would indicate maximum twisting, with one thiophene ring perpendicular to the next one.

The DFT simulations suggest that PT1 has a tendency to twist and bend more than PT2. In Paper II it was mentioned that twisting of the conjugated backbone generates segments with shorter effective conjugation length, observed experimentally as blue-shifts in the absorption spectrum. Thus, the more twisted conformation of PT1 could explain its larger sensitivity to cosolvents and could be the result of specific solute–solvent interactions that only this polymer has with water.

Besides the qualitative analysis on the conformation of PT1 and PT2, this set of DFT simulations were also used in **Paper III**, to show the effect of the spacer on the molecular electrostatic potential surface (MEPS) maps of dimers. MEPS maps indicate the electrical charge cloud generated through the electrons and nuclei, at any point in the vicinity of the molecule, which can be estimated through a constant value of electron density. Such mapping over the surface of a molecule provides a qualitative visual guide about the reactivity of positively or negatively charged molecules. The MEPS maps obtained after a DFT simulation are generated according to the electronic density, while those generated without a DFT simulation, using a molecular mechanics (MM) force field, are generated according to atomic charges (see Figure 15).

Figure 14 shows the MEPS maps of oligomers of PT1 and PT2, either dimers (Dim) and also tetramers (Tetra). Please notice, the MEPS maps of dimers differ from those reported in Paper III because another visualization configuration was used.

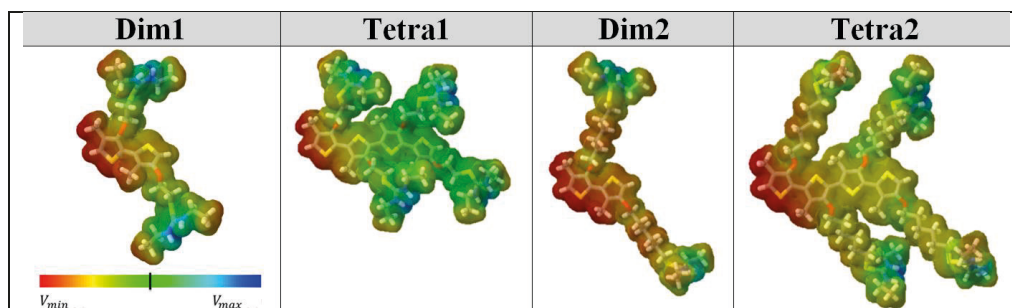


Figure 14. MEPS maps of DFT-optimized dimers and tetramers of PT1 and PT2. The qualitative scale below Dim1 shows the range of electrostatic potentials: most negative (V_{min} , red), neutral (green) and most positive (V_{max} , blue).

Figure 14 shows that the shorter spacer in the oligomers of PT1, causes a larger spreading of the cationic charge from the isothiuronium into the backbone of the oligomers (visualized as a greenish color on the thiophenes backbone) in comparison with the oligomers of PT2. This qualitative result is in agreement with previous studies on the structuring of hydrophilic ammonium-fullerenes with different spacer lengths in aqueous solution, showing that with longer spacers the influence of the charged nitrogen in the ammonium group on the fullerene is decreased (see Paper III).

Therefore, we suggested that the spacer length has an impact on the electrostatic potential of PT1 and PT2, which could partly explain the different behaviors of these polymers in solution.

Figure 15 shows the MEPS maps estimated using MM (i.e. MEPS maps due to atomic charges), with the Merck Molecular Force Field (MMFF94), for the frozen

dodecamers of PT1 and PT2. These molecules were used as inputs in the DFT calculations in Paper II (see methods section Paper II).

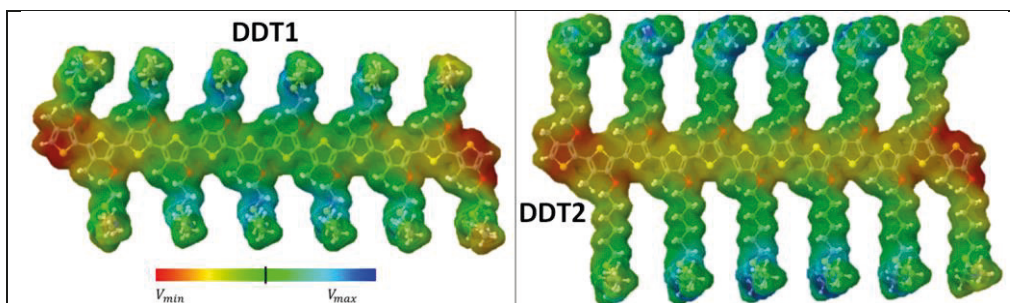


Figure 15. MEPS maps of dodecamers of PT1 (DDT1) and PT2 (DDT2). The qualitative scale below DDT1 shows the range of electrostatic potentials: most negative (V_{min} , red), neutral (green) and most positive (V_{max} , blue).

Figure 15 shows that MM predicts the same qualitative result than the DFT-optimized oligomers shown in Figure 14. The smaller spacer increases the spreading of cationic charge into the thiophenes backbone, visualized as a more greenish-blueish thiophene backbone in the oligomers of PT1.

4.3. Studies on polymer-solvent and polymer-polymer interactions

4.3.1. Disaggregated and aggregated ranges of polymer concentration

The present research work relies heavily on knowing at which concentration PT1-PT2 can be considered to be in disaggregated or aggregated state. Studies on the polymer-solvent (**Paper II**), polymer-polymer (**Paper III**) and PT1-4Fo interactions (**Paper IV**) are presented and evaluated focusing on the effect of the spacer length and/or polarity/H-bonding capacity of solvent.

Steady-state fluorescence spectroscopy was used to gain understanding on the relationship between polymer concentration ([POL]) and aggregation, by assuming that any deviation of a linear increase in the PL intensity with [POL] would indicate aggregation-driven self-quenching.

Figure 16a-d shows curves of PL *versus* [POL] obtained for PT1 and PT2 in four different solvents used in this study.

Figure 16 shows that regardless the solvent, for $[POL] \leq 0.1$ mM (monomer base), there is an almost linear, positive, dependence between PL and [POL]. Because of this, 0.084 mM was labeled as the concentration at which polymers are

disaggregated (DIS). On the other hand, at $[\text{POL}] > 0.1 \text{ mM}$, the positive, linear relationship is lost, due to aggregation self-quenching, reason why 0.4 and 1.05 mM were labeled as the concentrations which generate “middle” (CC) and “maximum” (AGG) aggregation states.

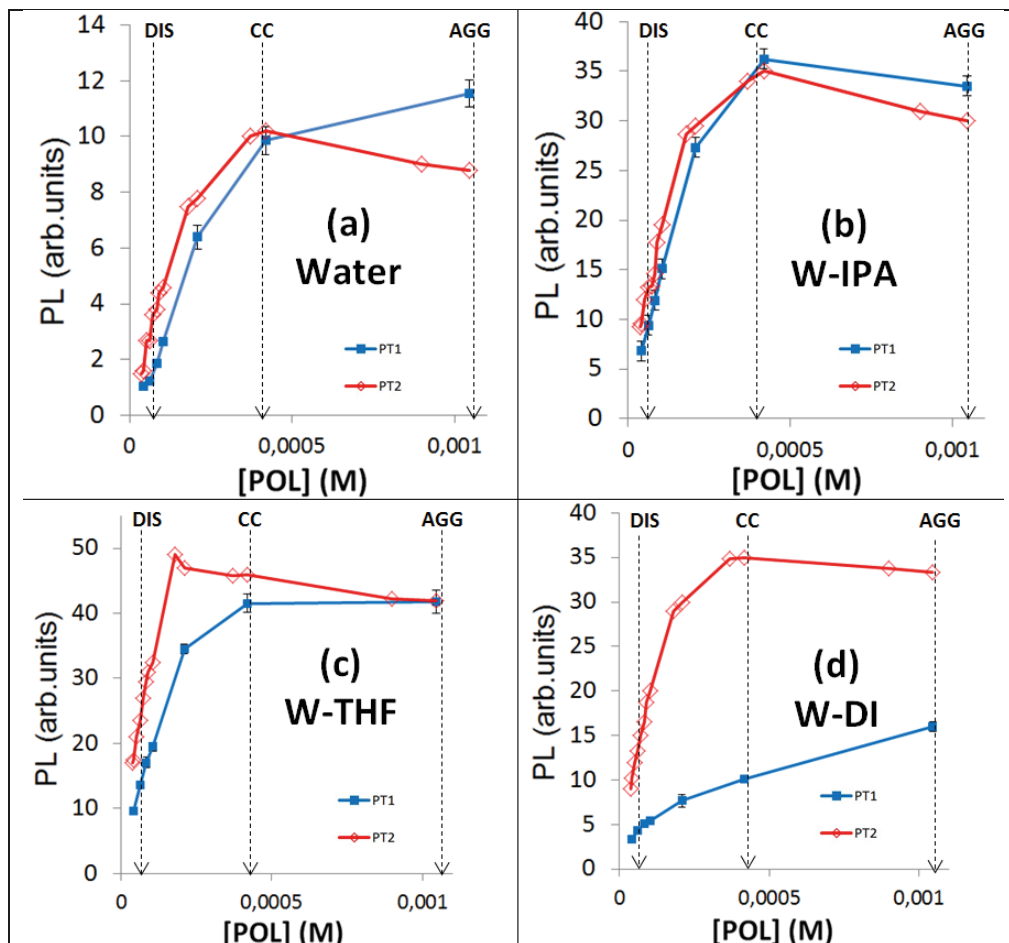


Figure 16. Plots of PL intensity versus concentration of polymer, $[\text{POL}]$, from PT1 (blue solid squares) and PT2 (red hollow diamonds) in (a) water, (b) W-IPA, (c) W-THF and (d) W-DI (Papers II and III). The reason for labeling values of $[\text{POL}]$ as “DIS”, “CC” and “AGG” is explained ahead.

4.3.2. Effect of spacer length on polymer-solvent interactions

As discussed in **Paper II**, the Lippert-Mataga equation uses the dielectric continuum model to correlate the energy difference between absorption and emission maxima (i.e. Stokes shift) to the orientation polarizability. However, after previous unsuccessful attempts of using the Lippert-Mataga, or Onsager functions, to correlate dielectric constant to the spectral shifts from anionic CPEs, this plot was

used at a qualitative level, to evaluate the effect of the spacer length. Figure 17 shows the Lippert-Mataga plot of PT1 and PT2 in the four solvents used, around “DIS” concentration (0.084 mM), as reported in Paper II.

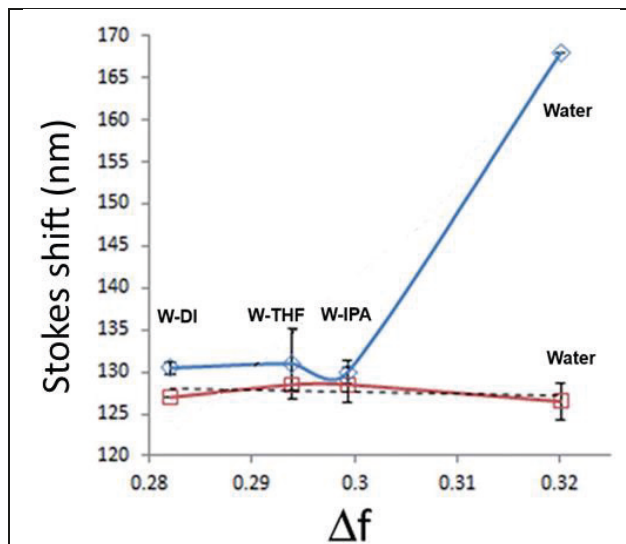


Figure 17. Lippert-Mataga plot of PT1 (blue diamonds) and PT2 (red squares), in four solvent systems, at 0.084 mM.

Figure 17 shows that the Stokes shift values for PT2 is almost constant, regardless the increase in the value of Δf , showing Stokes shift values of ≈ 127 nm, while that of PT1 shows a downward behavior in W-IPA, and a large increase in the Stokes shift, up to ≈ 170 nm, in water. As discussed in Paper II: (i) the average Stokes shifts of PT1 are slightly larger than those of PT2 (W-IPA and W-THF are statistically similar), which indicates PT1 has a larger structural difference between the S0 and S1 states; (ii) for PT1, W-IPA generates a valley in the curve. It is known that negative deviations in alcohols indicate non-specific polymer-solvent interactions in the S0 state, (e.g. hydrogen bonding); (iii) large Stokes shift of PT1 value in water, which indicates increased polymer-solvent interactions, in comparison with PT2 (see Paper II for details).

4.3.3. Effect of spacer length on relative quantum yields

The effect of spacer length and solvent on the quantum yields (of PT1 and PT2) was studied in **Paper II**. It was found that PT2 has higher quantum yields in comparison with PT1. It is known that changes in quantum yields (Φ_f) are associated with different pi-conjugation and/or triplet formation of conjugated ring molecules (e.g., thiophenes).

4.3.4. Effect of spacer length and solvent on polymer-polymer interactions

Figure 18 shows the plots with four scales reported in **Paper III**, two of the scales are the maxima of absorbance (λ_{\max}) and that of excitation (λ_{exmax}) or PL (λ_{em}), while the third and fourth scales are the wavelength and [POL]. The size of the symbols provide qualitative information on polymer concentration (i.e. the largest symbol represents the highest [POL]). A plot for each solvent is shown, using the same scale for comparative purposes.

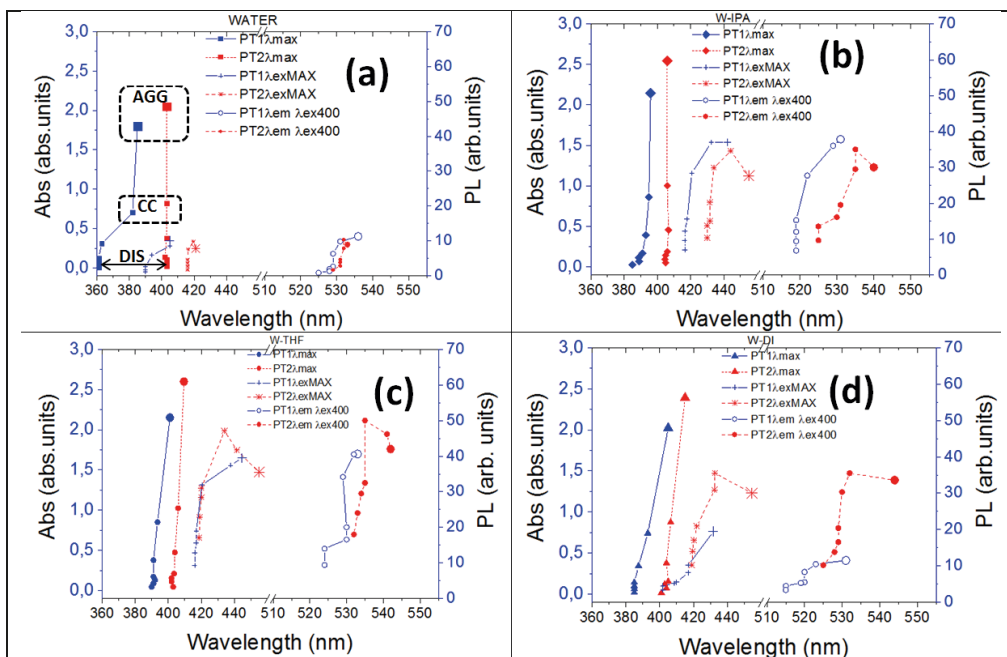


Figure 18. Plots of wavelength and intensity of λ_{\max} , λ_{exMAX} and λ_{em} from PT1 and P2, as a function of wavelength, at each [POL], in (a) water, (b) W-IPA, (c) W-THF and (d) W-DI.

4.3.4.1. λ_{\max} wavelength and excitation spectra

The data in Figure 18 were further analyzed at different levels in **Paper III**, with the first level of analyses being to analyze the effect of concentration and solvent on the *wavelength* of λ_{\max} . In this regard, in Figure 18 it is observed that regardless the solvent and concentration, the λ_{\max} of PT2 ($\lambda_{\max}^{\text{PT2}}$) is bathochromically (red) shifted with respect to $\lambda_{\max}^{\text{PT1}}$, with water maximizing this behavior.

In Paper II it was proposed that the shift of λ_{\max} due to the spacer length indicates a different ground state (S_0) in each polymer, while the role of water maximizing this difference was linked to the specific interactions of PT1 with water.

Figure 18a shows also that in water, λ_{\max} PT1 has a large and sudden red shift when concentration increases up to CC, with cosolvents decreasing the extent of this shift. On the other hand, λ_{\max} PT2 remains unchanged regardless the concentration. This indicates that PT1 goes through a clear transition in which the polymer–water interactions become weaker than polymer–polymer forces of interaction. Figure 18(b-d) adds to the assumption of PT1 having the strongest interactions with water, since it is observed that a decrease of polarity/H-bonding capacity of the solvent reduces the difference between the curves of λ_{\max} of the polymers in the disaggregated state.

Finally, the size of the red shift in wavelength of λ_{\max} (decrease in the energy of the S0 state) of each polymer, due to a change in the polarity/H-bonding capacity of the solvent is easier to visualize by plotting the difference between the absorption maxima in the three cosolvent mixtures (λ_{\max}^*) and the absorption maxima in water (λ_{\max} Water), which normalizes the data in Figure 16 with respect to water. Figure 19 shows the value of the module ($\lambda_{\max}^* - \lambda_{\max}$ Water), in the three aggregation states, as presented in the supporting information of Paper II, y-axes scales are kept the same for comparison purposes.

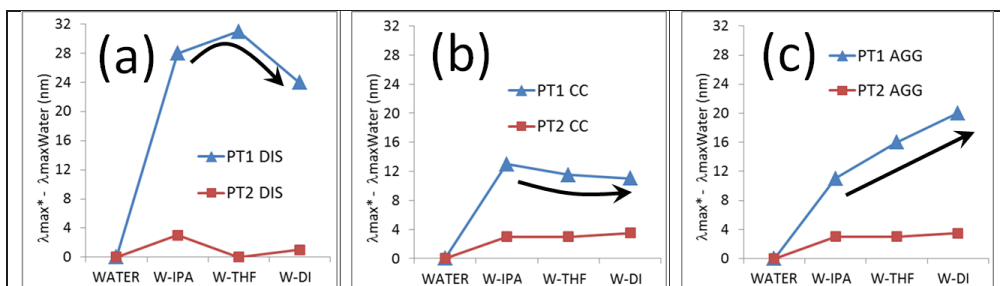


Figure 19. Shift of λ_{\max} due to a decrease in solvent polarity/H-bonding capacity at (a) DIS, (b) CC and (c) AGG. Black arrows indicate the red shift caused by W–DI in comparison with the other cosolvent mixtures in each aggregation state.

Figure 19 shows that at the three aggregation states (specially at the DIS state), the presence of cosolvents caused larger red shifts in λ_{\max} PT1 than in λ_{\max} PT2. On the other hand, λ_{\max} PT2 shows similar curves in the three aggregation states. This indicates that the energy of the S0 level in the disaggregated or aggregated chains of PT2, remained almost unchanged (with shifts of λ_{\max} smaller to 4 nm) because of a change in the polarity/H-bonding capacity of the solvent, while the S0 level of PT1 shows a larger decrease after cosolvent addition, especially in the disaggregated state. These in turn suggest that the aggregates of PT1 retained the tendency of this polymer to interact with water in a stronger way than PT2, which is a reasonable assumption. It is known that molecules in aggregates largely retain their electronic and nuclear structure. Notice that this rationalization considers that the polymer-solvent interactions between PT1 and water are associated with a twisting of the polymeric backbone,

as suggested in Paper II. As an attempt to rationalize these differences in the way the S0 levels of the polymers behave due to concentration and polarity/H-bonding capacity of the media, the use of the H-like or J-like behavior of PT1 and PT2 is used, following the contributions of Spano et al.,³¹ Zhu et al.,³² and Deng. et al.³⁶

In Paper III the effect of organic cosolvents and [POL] on the excitation spectra of PT1 and PT2 was analyzed. Figure 20 presents the normalized fluorescence excitation spectra of both polymers in the DIS and AGG states, in water and W-DI.

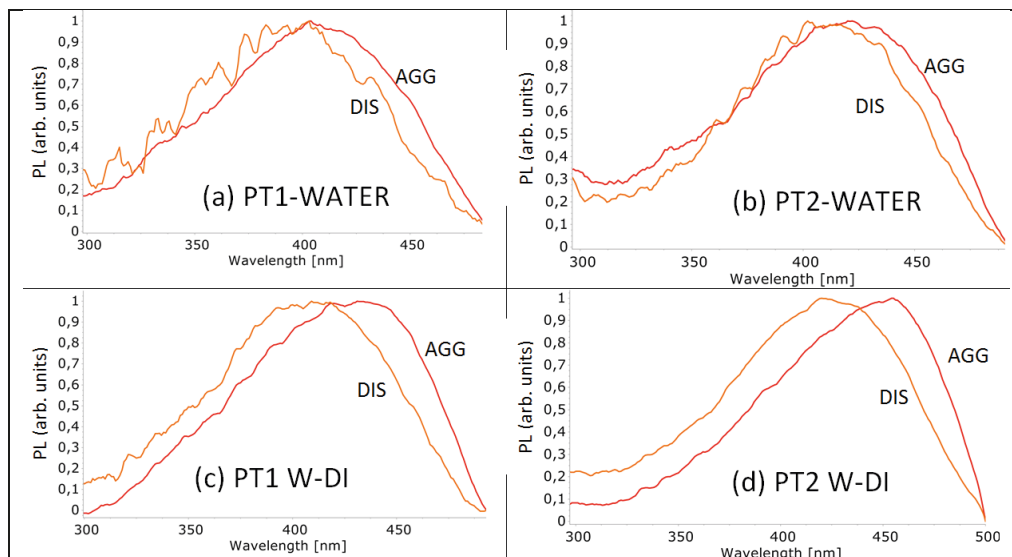


Figure 20. Normalized fluorescence excitation spectra of both polymers in the DIS and AGG states, in water (a-b) or W-DI (c-d).

Figure 20 shows that in water, the excitation spectra for both of the polymers do not show a distortion due to aggregation, which suggests that for neither polymer J-like aggregation is not the dominant form of aggregation in water. In presence of DI (or IPA or THF, see supplementary information in Paper III), a distortion in the excitation spectra is seen, which suggests a major tendency of both polymers to form J-like aggregates in presence of any of the cosolvents, following the criterion proposed by Deng et al.³⁶

In Paper III, the experimental results of the wavelength of λ_{max} and the shape of the excitation spectra, were explained using the mechanism proposed by Deng et al.: (i) in water, some aromatic groups approach each other through diffusion, forming a stable J-like aggregate with a low aggregation number because of strong pi-pi attraction. Under such conditions, there is an equilibrium between J-like aggregates and chains aggregated through forces different from pi-pi attraction. In such cases an increase in concentration do not modify the molar ratios of each type of aggregate, as demonstrated by the invariance of the excitation spectra. (ii) In the

solvent mixtures the number of J-like aggregates increases, because the presence of cosolvents cause an increase in the number of isolated aromatic groups, increasing thus the number of J-like aggregates. This in turn causes a decrease in the intensity of the excitation band at shorter wavelengths, whereas the bands at longer wavelengths are strengthening, distorting the excitation spectrum. These results suggest that in presence of cosolvents, particularly the nonprotic (i.e., W-THF and W-DI), J-like aggregation is larger than in water. This is because in the cosolvent systems: (i) both polymers, regardless of the structural difference, show distortions in the excitation spectra with changes in the concentration, and (ii) a decrease in the polarity/H-bonding capacity of the solvent causes a systematic increase in the extent of red shift of λ_{max} due to aggregation.

At the same time, the data shows that J-like aggregation does not dominate in water, since: firstly, in this solvent, both polymers show almost null distortion in the excitation spectra due to concentration, which suggests that the driving force for aggregation is a mechanism different from J-like aggregation (i.e., H-like aggregation) and secondly, a clear difference between the polymers in the effect of concentration on the S0 state is observed in water (i.e. the linear behavior of the curve of λ_{max} PT2 in Figure 18a).

In Paper III it is also proposed that in PT1 aggregates, the isothiuronium groups limit the extent of intermolecular thiophene-thiophene interactions between neighboring rings because of electrostatic repulsion, whereas the longer more flexible hexyloxy spacer of PT2 would allow other forces of interaction, with intermolecular pi-pi interactions being a possibility. In other words, when the isothiuronium functionality plays a secondary role in the interactions, pi-pi interactions dominate, forming nonsoluble aggregates (PT3 being the limiting case).

4.3.4.2. λ_{em} wavelengths

Figure 18a shows that in water, the increase in concentration causes a shift of λ_{em} PT1 and λ_{em} PT2, by 12 and 5 nm, respectively. This indicates that aggregation causes larger S1 \rightarrow S0 relaxations in PT1 than in PT2, in other words, when concentration increases, PT1 undergoes larger geometric distortion (and subsequent relaxation) due to the photons absorbed. On the other hand, the presence of any of the cosolvents nulls this difference between the polymers, generating shifts in λ_{em} PT1 and λ_{em} PT2 of ≈ 10 nm. This indicates that a reduced amount of water molecules decrease the interactions with PT1, generating a smaller difference between the polymers.

It is known that the change involved in the S0 \rightarrow S1 transition of polythiophenes involves conformational changes (e.g., from twisted aromatic into planar quinoidal geometries),^{80,124} these changes depends on the rigidity of the conjugated backbone and on the H-bonding interactions between the charged side chains of the

polymer and water. Also, as mentioned in Paper II, non-specific interactions in the S0 state, such as hydrogen bonding, become weaker in the excited state.¹²⁵

In Paper III the results are interpreted as such that when the number of water molecules decreases, the S0->S1 conformational changes are similar in both polymers, regardless of the cosolvent mixture. Conversely, pure water seems to increase the S0->S1 changes for PT1, whereas it reduces them for PT2.

In Figure 18 shows for both polymers, particularly for PT1, that the curves of λ_{em} in the cosolvent mixtures are blue shifted in comparison to those in water. These shifts were not discussed in Paper III. Previous studies on poly(2-methoxy-5-(2-ethylhexyloxy)-1,4-phenylenevinylene) (MEH-PPV), which showed blue shifts of both λ_{max} and λ_{em} when going from a “good” solvent to a “poor” solvent (in terms of solubilization) were attributed to a tighter, more twisted conformation of the backbone in the poor solvent, resulting in segments with a shorter effective conjugation length,⁸⁸ which is in agreement with the hypothesis proposed in Paper II. Another study involving an amine-PPV molecule, showed blue shifts of λ_{max} and λ_{em} due to protonation, which was rationalized to be caused by the collapse of the polymer chains due to the charge of the side groups, which decreases the conjugation length.⁸⁴ These changes in conformation, causing red shifts when going from poor to good solvents, or blue shifts when going from good to poor solvents, can be understood as an order-disorder phenomenon, regardless if they are caused by temperature or solvent.^{126,127}

4.3.4.3. Stokes shifts

In **Paper III** the effect of spacer length and solvent on the difference between the wavelengths of λ_{em} and λ_{max} (i.e. the Stokes shift, $\Delta\lambda$) are discussed. This allows to compare the relaxation energies, i.e. differences between S0 and S1 states (see Paper II).

Figure 21 shows the Stokes shift values of PT1 and PT2 at the DIS, CC and AGG states. Notice that in presence of aggregation, the Lippert-Mataga equation (i.e. Figure 17) can not be used.

Figure 21 shows that the specific interactions between PT1 and water present in the DIS state, discussed before with the Lippert-Mataga plot (i.e. Figure 17), remain in the CC and AGG states, with Stokes shift values of 150 and 145 nm respectively. In the water-cosolvent mixtures PT1 presents Stokes shift values between 120-140 nm, which are similar to those of PT2 in all the solvents, as depicted with the dashed rectangle in Figure 21.

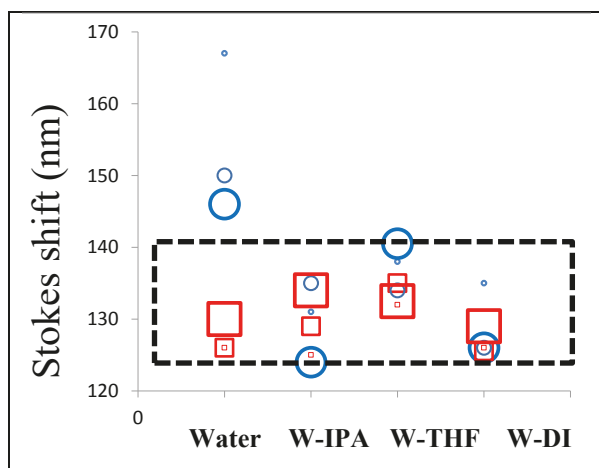


Figure 21. Stokes shift values at DIS (smaller icons), CC and AGG (largest icons) states, of PT1 (blue circles) and PT2 (red squares) in four solvent systems. Black-dashed rectangle points out the range of values common to both polymers.

Interestingly, in W-DI both polymers show Stokes shifts of around 130 nm, regardless their aggregation state. This is probably caused due to the hydrophobic-hydrophilic surface area of the aggregates at the maximum concentration becomes similarly available for interactions with the media, regardless of the length of the alkoxy spacer.

4.3.4.4. Absorbance and PL intensities

Besides the wavelengths of λ_{\max} and λ_{em} , the effect of spacer length and solvent on the *intensities* of absorption and fluorescence was analyzed in **Paper III**. These provide information on the oscillator strengths associated with the $S_0 \rightarrow S_1$ and $S_1 \rightarrow S_0$ transitions, respectively.

Figure 18 shows that regardless the solvent, PT1 shows absorbances smaller than those of PT2, which indicates that the oscillator strength of PT2 is larger than that of PT1 in all solvents.

It is also observed that presence of any cosolvent increases the absorbance (i.e. oscillator strength) of both polymers (see Paper III, Figure S1-b).

The effect of spacer length and solvent on the PL intensities can be seen in Figure 18. The PL intensity of both polymers increase with concentration, however, for concentrations close to the aggregated state (AGG), the intensity of PT1 keeps increasing while that of PT2 decreases, which indicate that the aggregates of PT2 undergo self-quenching to a larger extent.

In polar protic solvents (i.e. water and W-IPA), both polymers generate similar intensities in the aggregated states. Aprotic cosolvents generate larger PL intensities of PT2 in comparison to PT1, in W-DI the PL intensities of PT1 are similar to those obtained in water, despite that high polarities decrease the PL

intensity. In Paper III it was concluded that PT1 shows an unusually low S1->S0 relaxation in W-DI.

The ratio between the PL values obtained at the n-th increasing concentration (PL[n]) and the lowest concentration (PL[1]), for both polymers, in water and W-DI is discussed in **Paper III**. This comparison allows to see “how many times” the PL intensity changes (increases or decreases) due to a specific increase in concentration. For a molecule which self-quenches, this approach is analogous to that of the Stern-Volmer plot which normalizes the changes in the PL intensity of a fluorophore due to a specific change in mass of a particular quencher. Thus, these plots were used as an attempt to normalize the effects of the cosolvents on the PL intensities of both polymers. Figure 22 shows PL[n]/PL[1] versus [POL] plots of both polymers in the four solvent systems. The same scale is maintained for comparison purposes.

Figure 22 shows that in the disaggregated regime, PL[n]/PL[1] curves of the polymers are similar in all solvents, which suggest that the difference in spacer length does not play a major role in the “kinetics” of photophysical intermolecular deactivation processes. On the other hand in water, at aggregated conditions, the values of PL[n]/PL[1] for PT1 are almost twice as those for PT2 (which means that aggregation doubles the PL intensity of PT1 compared to PT2). The presence of cosolvents with decreasing polarity/H-bonding capacity cause a systematic reduction of the difference between the curves of the two polymers with respect to the differences observed in water. Due to this, the plots of both polymers are almost the same in W-DI. This phenomenon is less pronounced in the plots of PT2, i.e. water promotes larger concentration-driven increases in the PL of PT1 in comparison with PT2.

The study of the interactions between PT1 or PT2 with a common quencher molecule, in water and W-DI should provide information on the role of the spacer and solvent on polymer-quencher interactions which would be useful in rationalizing the results presented so far about aggregation. In this regard, **Paper IV** studies the interactions between PT1 and 4Fo, in water and W-DI.

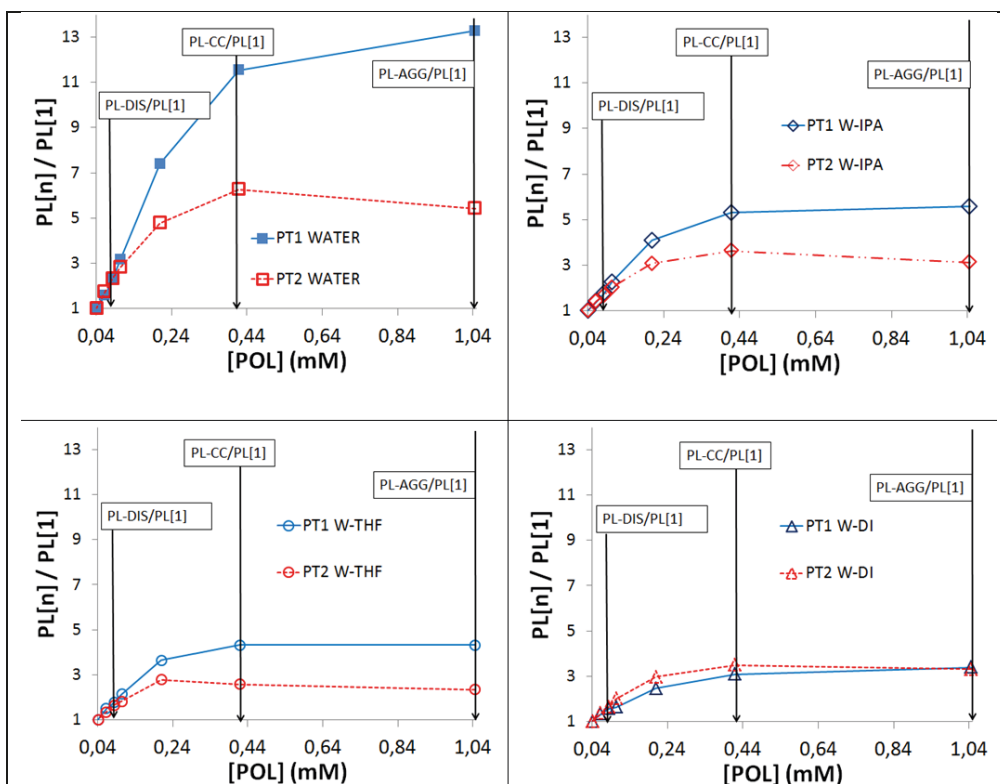


Figure 22. Ratios $PL[n]/PL[0]$ for both polymers, in different $[POL]$, in (a) water, (b) W-IPA, (c) W-THF and (d) W-DI. The labels indicate the values obtained at using DIS, CC or AGG.

4.3.5. EPR study on the effect of spacer length on the concentration-driven aggregation in water

A computer-aided EPR study is presented in **Paper III** with the intent to follow the aggregation and interacting ability of PT1 and PT2 with paramagnetic probes containing different polar and dispersive constituents: TOH, CAT8, CAT16 and 5DSA, shown in Figure 8b.

Figure 23 presents the effect of $[POL]$ on the EPR-intensity variation (measured as double integral of the spectra) and the microviscosity (interaction) parameter (τ) of TOH, CAT8 and CAT16, which are the probes containing hydrophilic and hydrophobic groups. Since the completely hydrophobic probe (5DSA) generated results that do not follow the same trend, these results are discussed separately in Paper III. Notice that, differently from Paper III, Figure 23 uses the same scales of intensity or τ , for comparison purposes.

Figures 23(a-c) show that all the probes generate a maximum intensity at $[\text{POL}] \approx 0.25 \text{ mM}$, which suggests increased probe solubility at this $[\text{POL}]$. As discussed in Paper III, the hydrophilic/hydrophobic nature of these probes allow considering increases in intensity as proof of formation of micellar aggregates, in which the hydrophobic parts of the polymers are condensing, surrounded by the hydrophilic parts.

Figure 23a shows that the intensity from the probe without a hydrophobic alkyl chain (TOH), generates almost identical solubility (i.e. intensity values) with both polymers, while the probes with a hydrophobic portion (alkyl chains) generates larger increases in solubility (i.e. intensity values). Such probes also generate larger intensity values for PT2, in comparison with PT1.

The results with TOH indicate that this probe interacts mainly with the cationic isothiuronium group in both polymers, regardless of whether PT2 forms a slightly larger hydrophobic core, because of the hydrophobic interactions between the packed hexyloxy chains within the pi-pi cores of the micelles.

In resume, these results suggest that around 0.25 mM, larger spacers generate larger hydrophobic surface area in the aggregates and that the aggregates possess similar hydrophilic surface area, regardless of the spacer.

Figure 23 also shows that regardless the probe, at 0.05 mM similar intensities of the polymers are obtained. This suggests that in the disaggregated regime both polymers have similar hydrophobic/hydrophilic areas available for the probes to interact with.

The decrease in EPR-intensity values for $[\text{POL}] > 0.25 \text{ mM}$ indicates that high values of $[\text{POL}]$ generate less organized aggregates.

Figure 23(d-f) show that for all the probes, the curves of the microviscosity (interaction) parameter (τ), as a function of $[\text{POL}]$, display a maximum. Higher microviscosity values were observed for PT1 with respect to PT2, inversely to the EPR-intensity values, which is explained by that the shorter spacer chain in PT1 forms aggregates where the stronger hydrophilic interactions with the probes prevail in respect to the weaker hydrophobic ones.

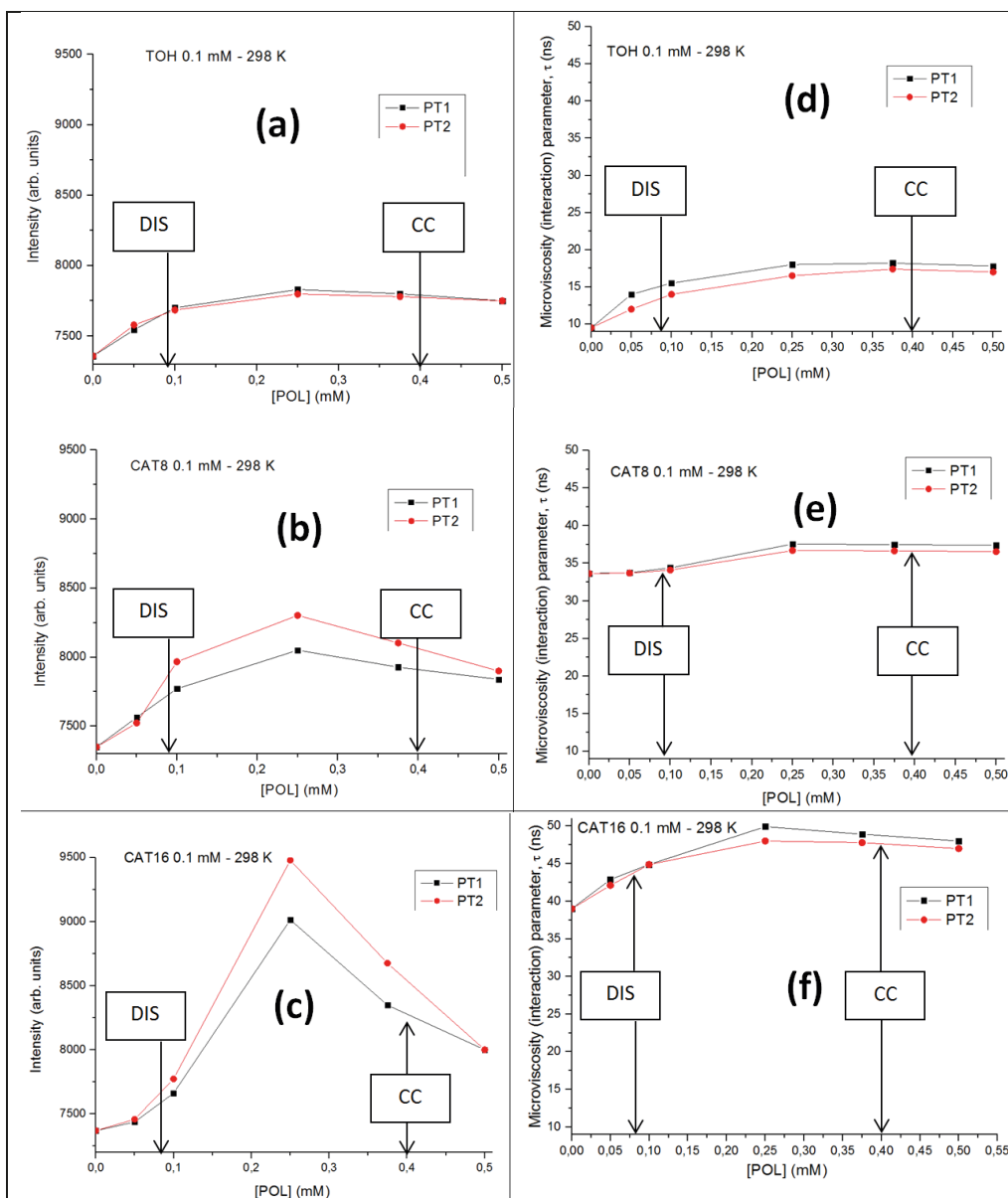


Figure 23. EPR spectral intensity (measured as double integral of the spectra) as a function of concentration of PT1 (black squares) and PT2 (red circles) in the presence of 0.1 mM TOH (a), CAT8 (b), and CAT16 (c), together with the microviscosity (interaction) parameter (τ), as a function of concentration of PT1 (black squares), PT2 (red circles) in presence of 0.1 mM TOH (d), CAT8 (e), and CAT16 (f). The labels “DIS” and “CC” refer to the concentrations defined with steady-state fluorescence spectroscopy (Figure 16).

Figure 23d shows that the microviscosity of PT2 increases until reaching [POL] of about 0.35 mM when using TOH, due to weak interactions with the isothiuronium groups. Interactions are quite independent on the aggregate formation, but largely

depended on the aggregate size. Figures 23e-f show that CAT8 and CAT16 show a maximum at [POL] 0.25 mM, for both polymers.

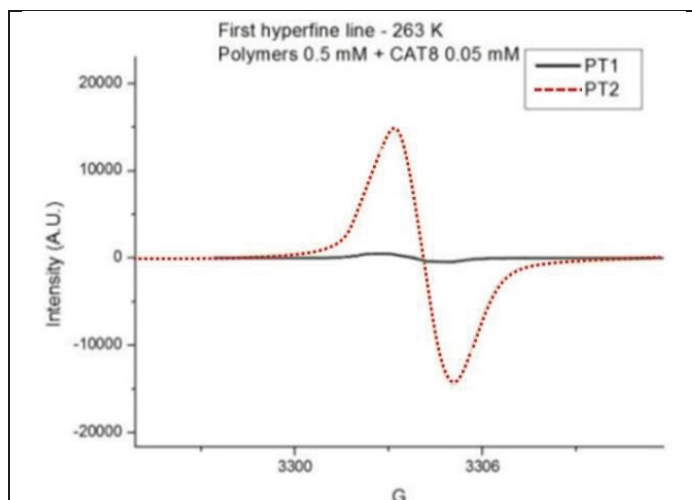


Figure 24. First hyperfine line of the EPR-spectra of CAT8 in presence of PT1 and PT2 (both 0.5 mM), at -9.15 °C (263 K)

Figure 24 shows that, at high concentrations (0.5 mM), the EPR intensity for PT1 decreases up to 95% in comparison to PT2. This indicates that PT1 forms smaller aggregates than PT2, with the latter being able to create a protected region to host CAT8, avoiding a phase separation of the probe from the solution. PT1 forms aggregates that host CAT8 poorly and therefore is not possible to avoid a separation of a large fraction of probes due to freezing of the solution.

However, as discussed in Paper III, spectral computations on the microviscosity (interaction) parameter τ for CAT8 under these conditions (i.e. [POL] = 0.5 mM, at 263 K), show a stronger interaction of CAT8 with PT1 ($\tau = 215$ ps) than with PT2 ($\tau = 180$ ps). Therefore, the EPR spectrum for PT1 in such conditions was generated by the nonfrozen fraction of CAT8, trapped in few small aggregates in solution showing stronger interactions than in the more fluid and larger PT2 aggregates.

Figure 25 shows the experimental and computed spectra of CAT16 at 264 K, with [PT1]=0.5 mM (computation was obtained by adding two spectral components at about 50%), together with the experimental and computed broad spectral component, only present for PT2 (15%), which was extracted from the overall spectrum after subtraction of the spectrum for PT1.

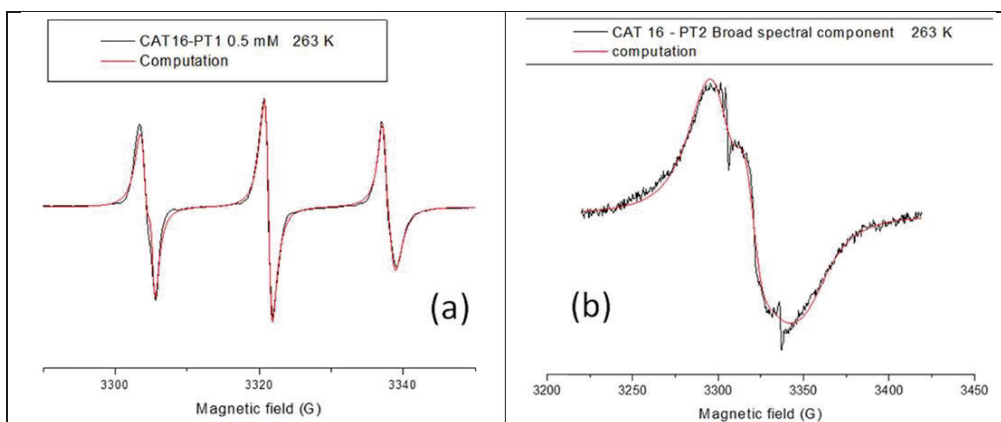


Figure 25. (a) Experimental and computed spectra for CAT16 with [PT1]=0.5 mM at ≈ 10 °C (263 K). Computation was obtained by adding two spectral components at about 50%; (b) experimental and computed broad spectral component only present for PT2 (15%).

Figure 25 shows that at [POL]=0.5 mM, 263 K, CAT16 distributes the signal in three different regions. For PT1, the spectrum (Figure 25a) was constituted by 50% of a component, which (according to the computation parameters), arose from a fluid region ($\tau = 52$ ps), at middle/low polarity ($A_{ii} = 6, 6, 36.6$ G). This fluid region probably is the interphase at the surface of the polymer aggregates.

The other 50% of the spectrum for PT1 was characteristic of slightly less fluid character ($\tau = 74$ ps) but more polar ($A_{ii} = 6, 6$, and 39.3 G) region, which was probably the water solution trapped in the polar head groups of the polymers. On the other hand, Figure 25b shows that the PT2 spectrum contained a broad spectral component at a relative percentage of 15%, computational parameters indicated a middle/low polar ($A_{ii} = 6, 6, 36.6$ G) region, quite microviscous ($\tau = 4200$ ps) and well-packed (line width = 12.5 G), formed inside the polymer aggregates.

As mentioned before, the completely hydrophobic spin probe (5DSA) generated results different from TOH and CAT8-16. Firstly, no spectrum could be recorded for PT1 in the entire concentration range, while a low-intensity spectrum was recorded for PT2 at the highest concentrations (mainly above 0.25 mM). This indicates that the alkoxy chain in PT1 was not long enough to interact with the hydrophobic 5DSA, which provides further evidence to the fact that the interactions observed between PT1 and the other probes were mainly hydrophilic.

Figure 26 shows the experimental EPR spectra at ≈ 25 °C (298 K), for (a) CAT16 probe (0.05 mM) in solution of [PT2]= 0.1 mM and (b) 5DSA probe at [PT2]= 0.5 mM, together with their computations (red lines).

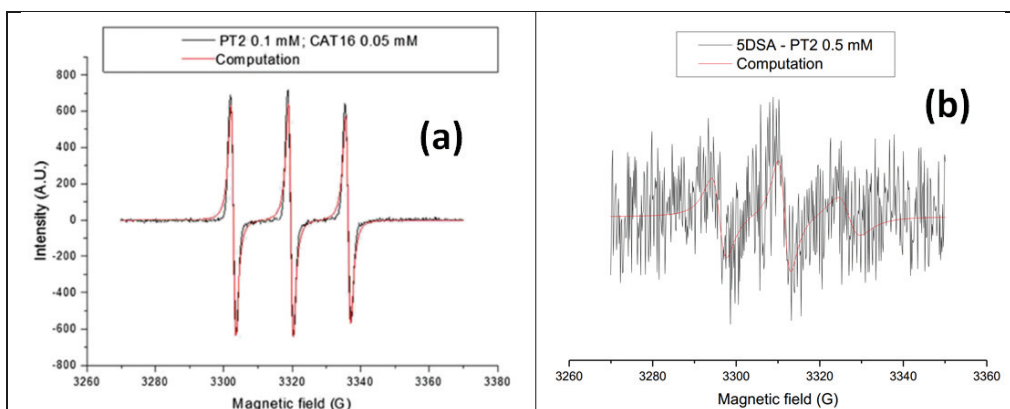


Figure 26. Experimental EPR spectrum at $\approx 25^\circ\text{C}$ (298 K) for (a) CAT16 probe (0.05 mM) in solution of $[\text{PT2}]=0.1$ mM and its computation (red line) and (b) 5DSA (0.1 mM) with $[\text{PT2}]=0.5$ mM and its computation (red line).

The spectra obtained with either CAT16 or 5DSA in a solution of PT2 show a high noise level, which is caused by the low solubility of 5DSA in this system, in which the probe only solubilizes into the hydrophobic region formed by polymer aggregates, but is repulsed by the charged polymer heads.

The computed spectrum in Figure 26b generates the parameters $A_{ii} = 6, 6, 35$ G, and $\tau = 1.3$ ns, which interestingly indicate the radical group (at position 5 of the stearic chain) was located in a region of low polarity and quite high microviscosity, as expected for the hydrophobic core of a lipid aggregate.

Figure 27 shows the hydrodynamic radius (R_h) distributions of PT1 and PT2 in water at $[\text{POL}]=0.084, 0.2$, and 0.4 mM, at room temperature.

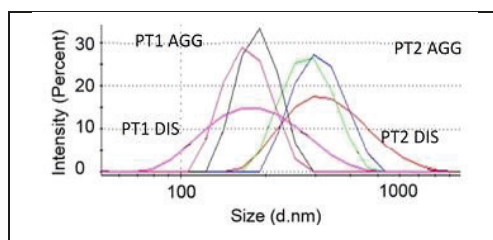


Figure 27. Hydrodynamic radius (R_h) distributions of PT1 and PT2 in water at $[\text{POL}]=0.084, 0.2$ and 0.4 mM, at room temperature.

Figure 27 shows that for both polymers, the highest concentration generates a broader distribution with lower intensity, with hydrodynamic radii (R_h) values of around 190 and 200 nm for PT1 and PT2, respectively. The broader nature of the profiles at higher concentrations indicate the presence of smaller and larger aggregates, maintaining the average R_h unchanged.

In regard to the possible micellar-like aggregation discussed in the EPR studies, the fluorescence data shown in Figure 16 can be replotted showing the values of [POL] in a logarithmic scale, as shown in Figure 28. This is made following previous studies on micelle formation of water-soluble block copolymers, using pyrene as fluorescent probe,^{37,38} or following the intrinsic fluorescence of a polythiophene graft polyampholyte³⁹ in order to estimate the *apparent* critical micelle concentration (CMC).

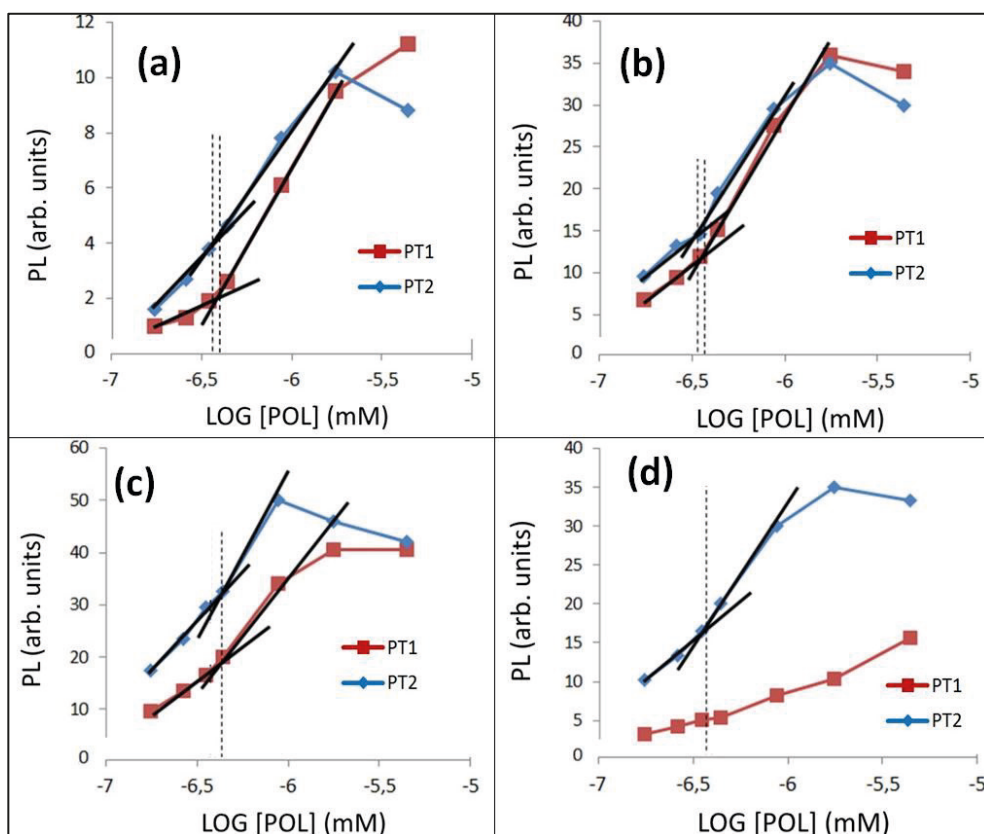


Figure 28. Logarithmic arrangement of the x-axis shown in Figure 16. Dashed vertical lines indicate the value of log[POL] at the intersection of slopes, used to estimate the CMC of PT1 (red squares) and PT2 (blue diamonds) in (a) water, (b) W-IPA, (c) W-THF and (d) W-DI.

The plots in Figure 28 are similar to those reported previously^{37–39} and show that the replotting of the data in Figure 19 clearly exposes the change in the slopes observed at low concentrations. It is observed that both polymers show almost identical CMC values, additionally, in W-DI, PT2 does not show a clear transition.

4.4. Effect of solvent polarity and hydrogen-bonding capacity on the solution interactions between the PT1:4Fo pair

The PT1:4Fo donor:acceptor pair is used as a starting point to study the possible H-bonding-driven interactions as a function of the polarity/H-bonding capacity of the solvent, by using water or the W-DI mixture.

PT1 and 4Fo offer a good model system because it allows a two-point H-bonding interaction, due to the topological complementarity between the Y-shaped isothiuronium functionality when interacting with phosphates, carboxylates or spherical anions,^{65,128} which is a principle exploited to allow ideal anion recognition in water for sensing applications.¹²⁹

The fullerene derivatives, 2Fo, Alkoxy4 and Alkoxy8 were not chosen due to poor solubility.

In **Paper IV** all the possible interaction phenomena between the PT1:4Fo pair are analyzed, which, due to the nature of the pair, could include: fluorescence resonance energy transfer (FRET), photoinduced electron transfer (PET), static and/or dynamic quenching.

Figure 29 shows some of the absorption/fluorescence spectra and SV plots (generated by using equation 3) used in Paper IV to analyze the donor:acceptor interactions.

As shown in Figure 29a and discussed in Paper IV, in water, the addition of aliquots of 4Fo causes a decrease of approximately 80% in the PL of PT1, when the concentration of 4Fo ($[4Fo]$) is $\approx 2 \times 10^{-5}$ M. This indicates a strong interaction between these molecules. In the supplementary information of Paper IV it is shown that this also occurs in W-DI.

The largest overlapping, between the PL of PT1 and absorption of 4Fo, observed in W-DI (pointed out as the dashed area in Figure 29b) indicates that in this solvent the extent of FRET is expected to be larger.

PET is expected to occur due to the strong electron-acceptor nature of fullerene. As mentioned before the Rehm-Wheller equation (equation 2) allows estimating the extent of PET in each solvent. As discussed in Paper IV, the parameter “C” in this equation can be ignored in water. The zero-zero (0-0) vibronic transition of PT1 can be estimated by the intersection point of the absorption and PL emission spectra of PT1, since at such energy there is no Stokes shift between the absorption and emission bands.¹⁴ Figure 29c shows that in both solvents PT1 has practically the same intersection points between the absorption and PL, at around 475 nm (i.e. a 0-0 transitions of around 2.61 eV) in both solvents.

The $E_{ox}(PT1)$ and $E_{red}(4Fo)$ are $\approx +0.78$ and ≈ -0.81 V, respectively (according to Papers I and II) (considering 1 e-, i.e. 1V=1eV). Thus, equation 2 predicts

$\Delta G_{csWater} = \Delta G_{csW-DI} = -1.02$ eV. This indicates that in both solvents, PET can occur spontaneously, at a similar extent in both solvents. This is expected, since as mentioned before, PET does not require close molecular contact, and can occur over larger distances.

These results also suggest that PET remains similar regardless of the presence or not of a H-bonding. These values are also similar to the $\Delta G_{cs} \approx -1$ eV reported by Fox et al.,¹⁴ estimated for a water-soluble poly(fluorene–thiophene):phosphate-nucleotides donor:acceptor system, regardless the fact that such system does not possess H-bonding capabilities.

In regard to the possible ground-state complexing between the PT1:4Fo pair, the intermediate absorption spectra observed in Figure 29d, caused by increasing concentrations of 4Fo, together with the lack of an isosbestic point, indicate that ground-state complexing is occurring in some extent, and also to possible aggregation and possible multiple site binding (notice that similar features are observed in W-DI, as shown in Paper IV Figure S3). In this regard, Figure 29e shows that in both solvents, the values of the SV plots from the PT1:4Fo pair correlate inversely with temperature, which gives further evidence of the presence of ground-state, static quenching.

This figure also shows that in both solvents, the SV plots lose linearity when [4Fo] increases, particularly in water, which in turn gives evidence of the presence of dynamic quenching.

Thus, the spectra and SV plots suggest the occurrence of both static and dynamic quenching mechanisms, which is known to happen in pairs containing polythiophenes.

The shape of the SV plots in Figure 29e also indicate that the dominance of this mechanisms varies as a function of [4Fo], regardless the solvent, reason why three characteristic [4Fo] were defined according to the changes observed in different regions of the SV plots in Figure 29e Q1 stands for values of $[4Fo] \leq 1 \times 10^{-5}$ M, since it defines an almost linear region, Q2 stands for $[4Fo] \leq 1.7 \times 10^{-5}$ M, conditions that generates an upward region, and Q3 means $[4Fo] \leq 2.1 \times 10^{-5}$ M.

Figure 29e shows that above Q3 the SV plots obtained in water show a downward behavior, while those obtained in W-DI show an upward behavior, which indicate completely different mechanisms in each case. As discussed in Paper IV, the downward behavior has been related to possible micelle-formation between the donor:acceptor pair, and/or saturation of the H-bonding donor units of a water-soluble polythiophene:fullerene pair with three-point H-bonding capabilities.

On the other hand, the upward behavior of the SV plots in W-DI indicate that DI delays some of the mechanisms PT1 undergoes when in water.

In Paper IV the range of $[4Fo]$ below Q1, which generates a linear behavior (depicted in Figure 29f) was analyzed by the regular SV model (equation 1). The range below Q2 was analyzed by the Perrin model, by plotting $[4Fo]$ versus $LN(PL_0 / PLI)$, and the whole range of $[4Fo]$ was analyzed with the general static quenching (GSQ) model, by plotting $1/[4Fo]$ versus $PL_0/(PL_0-PL)$ (see supplementary information in Paper IV for further details on these models). The Perrin model was also used for the whole range of $[4Fo]$ in W-DI, since in this solvent a downwards behavior was not observed for values of $[4Fo] > Q3$.

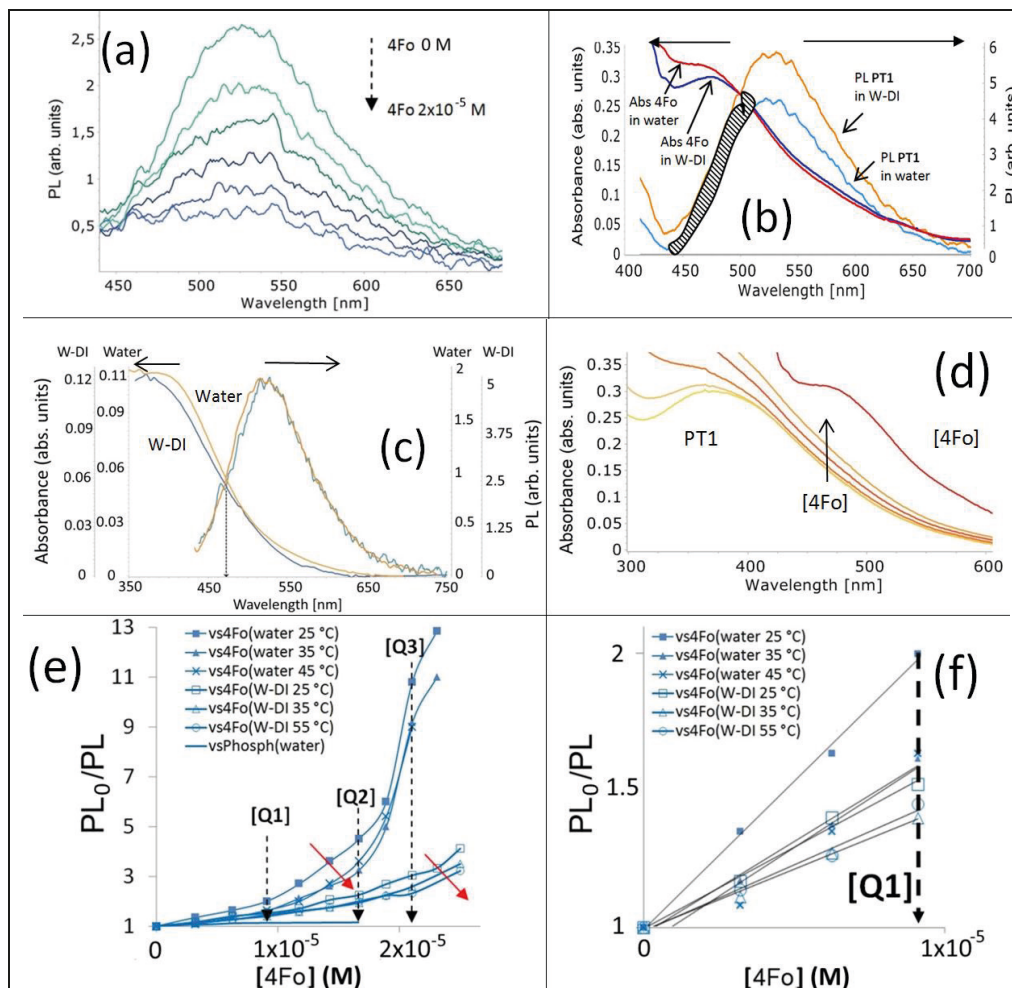


Figure 29. (a) PL spectra of PT1 in water upon addition of 4Fo; (b) PL of PT1 and absorbance spectra of 4Fo, in water and W-DI (the dashed area points out the extra overlapping area in W-DI compared with that present in water); (c) normalized absorbance and PL intensity of PT1, in water and W-DI (vertical arrows indicate an estimation of the zero-zero (0-0) transition of PT1 in each solvent); (d) absorption spectra of PT1 and 4Fo, together with the intermediate spectra of their mixtures in water (dashed inclined black arrow indicates increasing amounts of 4Fo); (e) SV plots of the PT1:4Fo pair, in water and

W-DI, at three different temperatures, and the PT:phosphoric acid pair at 25 °C (dashed black vertical lines indicate the three characteristic concentrations of quencher, as defined ahead, while continuous inclined red arrows indicate increase in temperature); and (f) SV plots of the PT1:4Fo pair until [Q1], showing the fittings to equation 3.

Table 3 shows the values of interaction kinetic constants (K's) and quenching sphere radii in the PT1:4Fo system, estimated by using regular SV model, and Perrin and GSQ models, for both polymers in both solvent systems, and two different temperatures. All fittings generate correlation coefficients (R^2) ≥ 0.98 (see supplementary information in Paper IV).

Table 3. Interaction constants estimated in the different ranges of [4Fo].

Region of [4Fo] fitted		$\leq Q1$	$\leq Q2$	$\leq Q2$	Whole	Whole	Whole
Model		SV	Perrin	Perrin	GSQ	Perrin	Perrin
Solvent	T (°C)	K _{sv} (1/M)	k _p (1/M)	R _s	K _s (1/M)	k _p (1/M)	R _s
Water	25	1.1x10 ⁵	9.2x10 ⁴	33.1	1x10 ⁵		
Water	35	6.7x10 ⁴	7.7x10 ⁴	31.3	5x10 ⁴		
W-DI	25	5.9x10 ⁴	4.9x10 ⁴	26.8	5x10 ⁴	5.6X10 ⁴	28.1
W-DI	35	4.5x10 ⁴	4.1x10 ⁴	25.4	3.3x10 ⁴	5X10 ⁴	27.1

As detailed in **Paper IV**, the K_{sv}=1.1x10⁵ estimated in water at 25 °C is similar to previously reported donor:acceptor systems involving a CIT,⁵⁷ polythiophene:fullerene pairs with three-point H-bonding capabilities,⁷⁴ aminopurine:uracil-C₆₀ pair with two-point H-bonding capabilities,⁵³ anthracenyl polymer:DNA pair,⁴⁸ and polythiophene:Cu+2 pair.⁵¹

Table 3 shows that the presence of DI decreases the value of K_{sv} by 46%, which could be related to either a saturation of available H-bonding donors in the fluorophore, as reported before for a water-soluble polythiophene:fullerene pair with three-point H-bonding capabilities,⁷⁴ and/or related to the viscosity of the W-DI mixture, which is 40% more viscous than water (see Table 1). This is particularly important in the region below Q1, since the linear behavior observed in this region indicates dominance of dynamic quenching, which depends on diffusion-controlled collisions in the S1 state.

In regard to viscosity, it is possible to analyze its effect under the assumption of dominant static or dynamic quenching (regardless Figures 29d-e suggest dominance of static quenching). Assuming static quenching, larger viscosities would be expected to increase the PT1:4Fo complexing. However water generates larger K_{sv} values than W-DI, which is 40% more viscous than water (see Table 1). This suggests that water promotes larger PT1:4Fo complexing due to the other parameters differing from W-DI, namely dielectric constant and H-bonding capacity. On the other hand, in regard to assuming dominant dynamic quenching, in Paper IV, a brief parameter-sensitivity analysis is performed using the experimental value of the ratio K_{sv}Water/K_{sv}W-DI=1.86 as a constraint. It demonstrated that the larger viscosity in the W-DI mixture

can not explain the decrease in the Ksv value observed, which suggests that the polarity/H-bonding capacity also play a role in such decrease of Ksv.

Table 3 shows that in water at 25 °C, the kp value estimated from the region below Q2 is similar to that estimated with the data below Q1. The kp value is also similar to previous studies involving a water-soluble tetraphenyl polymer:nitroaromatics pairs.⁶⁰ In regard to the whole range of [4Fo], Table 3 shows that the K value estimated at 25 °C is similar to the values estimated in the other two regions.

In regard to the values of the radius of the quenching sphere (Rs), the values below Q2, at 25 °C shown in Table 3, are 1 order of magnitude smaller to previous estimations involving CPEs (sphere-of-action with radius ~ 400 Å)⁴⁶ or a fluorescent porous organic polymer (radii of quenching sphere ~ 150 Å).⁶⁰ A possible reason for this difference is the slightly different methodology used in these references, which use correction factors. Regardless, the Rs values estimated in Paper IV are meant to be used for internal comparison in regard to the effect of DI. On the other hand, Table 3 shows that when the data from the region above Q3 is included (only from W-DI, since in water the SV plots are downward shaped), the values of Rs increase 5 and 7%, at 25 and 35 °C, respectively, suggesting that the quenching sphere increases with temperature. It is also observed that at all temperatures, the presence of DI decreases Rs in around 20%, suggesting that this solvent reduces the interaction between the isothiuronium and phosphate functionalities in the system. Therefore, a larger sphere of action in water would be the result of more available isothiuronium groups, while the presence of 1,4-dioxane would disrupt the H-bonding of the media, due to its two H-bonding donor oxygens, without any H-bonding donor hydrogens.

In order to analyze the thermodynamics of the system, the van 't Hoff model (equation 4) was used to gain insight on the dominant binding forces between PT1 and 4Fo, in both solvents, at different concentrations of 4Fo, using the kinetic interaction values listed in Table 3.

The thermodynamic parameters estimated from the van 't Hoff plots are resumed in Table 4. Please notice that the van 't Hoff plots are shown in the supplementary information of Paper IV.

Table 4. Thermodynamic parameters of PT1 and PT2 in water and W-DI, at 25 and 35 °C.

Model (range) ->			SV (4Fo<Q1)			PERRIN (4Fo<Q2)			General static quenching (whole range of 4Fo)		
Row	COLUMN		A	B	C	D	E	F	G	H	I
	Solvent	T (K)	ΔH (KJ/M)	ΔS (J/K)	ΔG (KJ/M)	ΔH (KJ/M)	ΔS (J/K)	ΔG (KJ/M)	ΔH (KJ/M)	ΔS (J/K)	ΔG (KJ/M)
1	Water	298,15	-31,78	-10,23	-28,74	-13,43	49,97	-28,33	-52,95	-81,86	-28,54
2	W-DI	298,15	-21,44	19,49	-27,25	-12,45	47,97	-26,75	-30,97	-13,92	-26,82
3	Water	308,15	-31,78	-10,23	-28,63	-13,43	49,97	-28,83	-52,95	-81,86	-27,72
4	W-DI	308,15	-21,44	19,49	-27,44	-12,45	47,97	-27,23	-30,97	-13,92	-26,65

Table 4 shows that in each solvent the enthalpy change (ΔH) does not vary significantly in the temperature range studied, which is known to be a criterion of validity to the use of the van't Hoff equation to study changes of enthalpy (ΔH) and entropy (ΔS).¹³⁰ Table 4 shows that in water, at a $[4Fo] \leq Q1$, a $\Delta H = -31.78$ KJ/M was estimated (row 1 column A), which is similar to previous studies on a polythiophene-CPEs:Cu+2 pair and a water-soluble poly-anthracene:DNA pair^{48,51} (see Paper IV).

In Table 4 was also shown that regardless solvent and $[4Fo]$, $\Delta G < 0$ values are estimated. This indicates spontaneous binding/complexing. Water generates the largest negative values, while W-DI generates similar values to the other two ranges of $[4Fo]$.

Rows 1-2 in Table 4 show that for all the ranges of $[4Fo]$, ΔH represents most of the value of ΔG . When ΔS is the main contribution to ΔG (i.e. for the opposite case to these results), hydrophobic interactions dominate over H-bonding and electrostatic interactions.¹³¹ Therefore, apparently, at any of the $[4Fo]$, H-bonding and electrostatic interactions dominate in both solvents. However, the imbalance in the H-bonding acceptors and donors that DI causes is enough to cause the big difference in the SV plots shown in Figure 29e.

Table 4 shows that at $[4Fo] < Q1$ positive and negative values of ΔS are estimated for water and W-DI, respectively. In water ΔH and ΔS are both negative (i.e. row 1 columns A-B), which suggests the presence of H-bonding or van der Waals forces.^{48,51} On the other hand, the data from W-DI generates values of $\Delta H < 0$ and $\Delta S > 0$. This combination of values was previously interpreted as an indication of dominance of electrostatic interactions, in studies using bovine serum albumin.^{54,130,131} Also, very low values (positive or negative) of ΔH , together with $\Delta S > 0$, have been associated with electrostatic interactions in donor:acceptor systems involving CPEs.⁵¹

It is known that the electrostatic contribution of a H-bond is the one less affected by an increase in the bond length.⁶² This causes a dominance of electrostatic interactions at relatively long H-bonding distance. Therefore, these results suggest that in W-DI, at $[4Fo] < Q1$, the importance of electrostatic interactions increase, while water would promote other interactions (e.g. H-bonding).

Table 4 shows that the three models generate similar values of ΔH and ΔG , but that those of ΔS clearly vary when using data from each model, particularly when using Perrin's model, case in which positive ΔS values are estimated.

In regard to the effect of solvent, Table 4 shows that, according to the three models, the presence of DI decreases the values of ΔH and ΔG .

Figure 30 shows the molecular electrostatic potential surface (MEPS) maps (as estimated with the UFF MM force field, with aid of the software Avogadro) of mono- and tetra-mer of PT1 and a bisphosphonate C_{60} fullerene (2Fo), either alone or next to each other, by placing them arbitrarily within ≈ 6 Å in between the isothiuronium and phosphonate functionalities.

Figures 30a-d show that when alone, the electrostatic potential of the monomer and tetramer of PT1 exhibits a negative (reddish) charge over the thiophene ring, and a positive (bluish-greenish) charge over the isothioronium group(s). 2Fo on the other hand exhibits a charged nature within the biphosphonate group. C_{60} does not present partial charges at all.

Figures 30f and 30h show that when in presence of 2Fo, the mono- and tetra-mers of PT1 become the positively charged constituent of the complex thiophene:2Fo. This indicates a distribution of positive charge over the monomer (or oligomer),¹³² while the fullerene sphere remains relatively less charged. On the other hand, Figures 30e and 30g show that in presence of bare C_{60} the effect of distribution of positive charge over the monomer (or oligomer) is less pronounced.

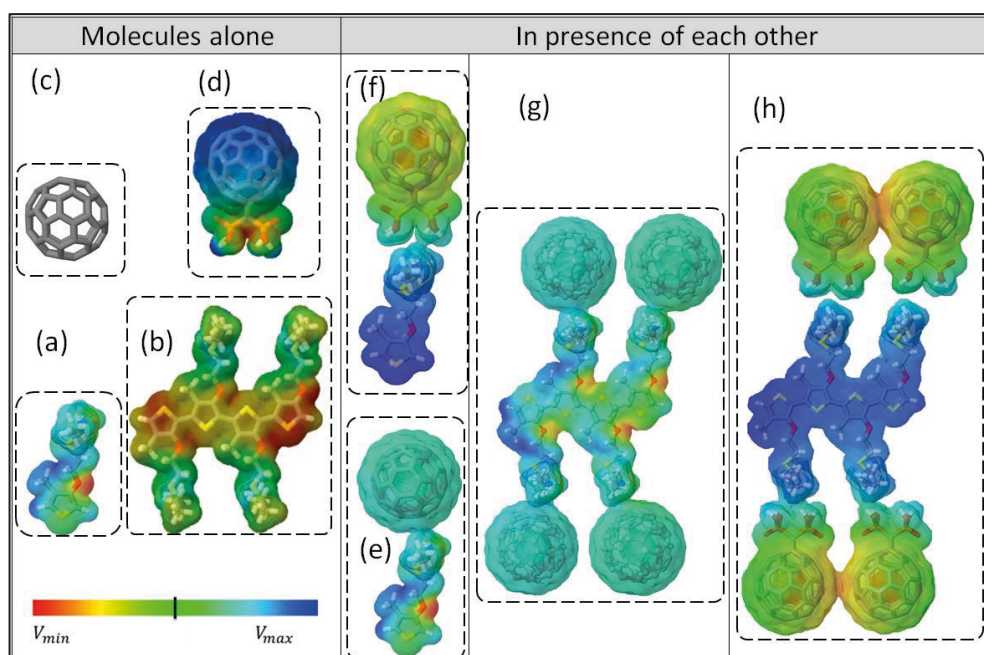


Figure 30. MM simulations of MEPS maps of alone molecules: (a) monomer of PT1, (b) tetramer of PT1, (c) bare C_{60} and (d) 2Fo, together with the MEPS maps of the monomer of PT1 in presence (at around 6 Å) of (e) bare C_{60} or (f) 4Fo, and the MEPS maps of a tetramer of PT1 in presence (at around 6 Å) of (g) bare C_{60} or (h) 4Fo. Dashed rectangles indicate a single MM simulation. The qualitative scale below (a) and (b) shows the range of electrostatic potentials: most negative (V_{min} , red), neutral (green) and most positive (V_{max} , blue).

5. Conclusions

The optical and structural properties of homologous cationic isothiuronium polythiophenes (CITs) with H-bonding donor capabilities were exploited in order to perform solution-phase, structure-function spectroscopic studies on electronic properties and H-bonding-influenced (i) polymer-solvent, (ii) polymer-polymer and (iii) polymer-quencher interactions. The first two of these studies were performed by controlling polymer concentration and the polarity/H-bonding capacity of the solvent, and also by using paramagnetic probes with different ionic and hydrophobic constituents. The latter study was performed using as quencher a phosphonate fullerene with topological complementarity to the isothiuronium group, promoting a two-point H-bonding interaction, and solvents with clearly different polarity/H-bonding capacity. In all cases, DFT and MM provided complementary information.

When in disaggregated state, the side chain length causes the isothiuronium polymers to have different electronic properties (λ_{max} , λ_{em} , molar absorption coefficient, quantum yield and Stokes shift). The polymer with a shorter spacer shows higher energy of the S0 state, as shown by the red shift in water. This shift is more than double in the polymer with a shorter spacer in comparison with the polymer with a longer spacer.

In the cosolvent mixtures both polymers show similar values of Stokes shift. However, in water these molecules present a dramatic difference. This indicates larger geometry changes for the shorter-spacer polymer in water. Empirical data also suggests that shorter spacers increase the ionization potential and decrease the band gap.

DFT simulations suggest that shorter spacers promote a more twisted and bent conformation of the polymers, and also a larger effect of the cationic isothiuronium group on the thiophene backbone. The latter is also predicted by MM simulations. This could explain the empirically observed largest specific water-polymer interactions of the polymer with the shortest spacer, and the largest sensitivity of this polymer with the shortest spacer to the presence of cosolvents.

Regardless if this assumptions based on DFT or MM are correct, the studies in aggregated state show that the largest interactions with water of the polymer with shorter spacer remain in the aggregated state, as shown by the largest extent of polymer–water interactions in comparison with polymer –polymer interactions.

Regardless the spacer length, the presence of cosolvents causes the polymers to have practically the same relaxation energies in the aggregated state.

During aggregation, the cosolvent with smaller polarity/H-bonding capacity (1,4-dioxane), generates an equivalent increase in PL for the two polymers. This suggests

that a decrease in water content decreases the effect of the isothiuronium groups on aggregation, favored by pi-pi interactions. These results confirm that H-bonding is maximized in water in the presence of a shorter spacer, with the electrostatic potential surface probably playing a role.

Following reported studies on lignosulfonates, the distortion (or not) of the excitation spectra due to aggregation, was used as a simple criterion to classify the aggregates in the framework of H- and J-like aggregation. Thus, water seems to minimize aggregation through pi-pi interactions, while the presence of organic cosolvents promote J-like pi-pi interactions.

Absorption, fluorescence, electron paramagnetic resonance and photon correlation spectroscopic results show that the aggregates of the polymer with shorter spacer have smaller inner cavities and hydrodynamic radius, suggesting that the water inside the aggregate still has an effect on the twisting of the polymeric backbone, causing higher energy of the S0 state and relaxation energies (Stokes shifts).

Electron paramagnetic resonance spectroscopy also shows that the polymer with a shorter spacer has larger hydrophilic interactions because their surface has smaller hydrophobic areas, which are larger in the aggregates of PT2 probably due to the exposure of the hexyloxy chains.

Electrochemical measurements indicate a difference in the packing between polymers, with the polymer having longer spacer being more easily p-dopable and de-dopable.

The use of the polymer with shorter spacer (PT1) as fluorophore in studies of quenching by a phosphonate C₆₀-fullerene allowed to gain insight on different aspects of the interaction of this water-soluble pair with H-bonding capabilities, as a function of solvent polarity, viscosity and H-bonding capacity, by studying their interaction in water and W-DI.

The possibility of PET remains the same despite the solvent, while that of FRET increases, mainly due to the higher quantum yield PT1 has in the W-DI mixture.

This pair seems to interact through a mixture of static and dynamic quenching, which however depend on the concentration of 4Fo. At low concentrations of 4Fo the presence of DI seems to increase the distance between the isothiuronium and phosphonate functionalities, increasing the electrostatic nature of the complex and decreasing the value of the Stern-Volmer (SV) constant K_{sv}. The effect of DI seems to be mostly related with the decrease of the polarity/H-bonding capacity of the media, instead of the increase in viscosity.

At higher concentrations of 4Fo, the quenching sphere of 4Fo seems to increase, particularly in water. Also, the sphere of action radii values decrease due to the presence of DI, which also delays the formation of aggregates.

The data from both solvents, particularly from water, generate similar K values regardless the model used.

The estimations of ΔH and ΔG are similar regardless the model, however those of ΔS seem to be quite more model-dependent.

Apparently, the H-bonding present in water increases the sphere of action radii, generating the larger PT1:4Fo complexing, despite the similar thermodynamics to those present in W-DI, and despite the fact that in W-DI FRET is expected to be larger.

6. Future perspectives

As future perspectives must be considered those studies also performed during the duration of this project, using the CITs (PT1 and PT2) and also other cationic polythiophenes: (i) solution-phase solvent-dependent spectroscopic studies on HJ-like aggregation; (ii) quenching of the CITs by non-conjugated quenchers; (iii) cationic-anionic polymeric complexation; (iii) MD computational studies on conformation and aggregation of oligomers, and also DFT and/or MD donor-acceptor interactions, and (iv) solid-state studies focused on the surface free energy and morphology of films made of cationic polythiophenes.

Another future perspective is the evaluation of these cationic polythiophenes as electrode selective buffer layers (through a collaboration with a group specialized in OSCs), applied from different solvents, in well-investigated polymer–fullerene solar cell systems, in normal and/or inverted device architectures.

7. List of references

- (1) David P. Stay, Stephen G. Robinson,; and Mark C. Lonergan; David P. Stay, Stephen G. Robinson,; and Mark C. Lonergan. 3. Development and Applications of Ion-Functionalized Conjugated Polymers. In *Iontronics Ionic Carriers in Organic Electronic Materials and Devices*.
- (2) Scherf, U.; Evans, R. C.; Gutacker, A.; Bazan, G. C. All-Conjugated Rod–Rod Diblock Copolymers Containing Conjugated Polyelectrolyte Blocks. In *Conjugated Polyelectrolytes*; John Wiley & Sons, Ltd, 2013; pp 65–89. <https://doi.org/10.1002/9783527655700.ch2>.
- (3) Burrows, H. D.; Knaapila, M.; Fonseca, S. M.; Costa, T. Aggregation Properties of Conjugated Polyelectrolytes. In *Conjugated Polyelectrolytes*; John Wiley & Sons, Ltd, 2013; pp 127–167. <https://doi.org/10.1002/9783527655700.ch4>.
- (4) Li, H.; Yang, R.; Bazan, G. C. Fluorescence Energy Transfer to Dye-Labeled DNA from a Conjugated Polyelectrolyte Prequenched with a Water-Soluble C60derivative. *Macromolecules* **2008**, *41* (4), 1531–1536. <https://doi.org/10.1021/ma702102v>.
- (5) Patil, A. O.; Ikenoue, Y.; Wudl, F.; Heeger, A. J. Water-Soluble Conducting Polymers. *Journal of the American Chemical Society* **1987**, *109* (6), 1858–1859. <https://doi.org/10.1021/ja00240a044>.
- (6) S. Sundaresan, N.; Basak, S.; Pomerantz, M.; R. Reynolds, J. Electroactive Copolymers of Pyrrole Containing Covalently Bound Dopant Ions: Poly{pyrrole-Co-[3-(Pyrrol-1-Yl)Propanesulphonate]}. *Journal of the Chemical Society, Chemical Communications* **1987**, *0* (8), 621–622. <https://doi.org/10.1039/C39870000621>.
- (7) Wang, S.; Lv, F. Chapter 1. Introduction. In *Functionalized Conjugated Polyelectrolytes: Design and Biomedical Applications*; SpringerBriefs in Molecular Science; Springer-Verlag: Berlin Heidelberg, 2013.
- (8) EUNKYUNG JI. CONJUGATED POLYELECTROLYTES: SYNTHESIS, PHOTOPHYSICAL STUDIES AND APPLICATIONS TO SENSORS AND BIOCIDAL ACTIVITY, UNIVERSITY OF FLORIDA, 2009.
- (9) Shu Wang,; Fengting Lv. 1. Introduction. In *Functionalized Conjugated Polyelectrolytes Design and Biomedical Applications*.
- (10) Pu, K.-Y.; Wang, G.; Liu, B. 1. Design and Synthesis of Conjugated Polyelectrolytes. In *Conjugated Polyelectrolytes*; John Wiley & Sons, Ltd, 2013; pp 1–64. <https://doi.org/10.1002/9783527655700.ch1>.
- (11) Carreon, A. C.; Santos, W. L.; Matson, J. B.; So, R. C. Cationic Polythiophenes as Responsive DNA-Binding Polymers. *Polym. Chem.* **2014**, *5* (2), 314–317. <https://doi.org/10.1039/C3PY01069D>.

- (12) Wu, D.; Yang, J.; Feng, F.; Schanze, K. S. Sensing via Quenching of Conjugated Polyelectrolyte Fluorescence. In *Conjugated Polyelectrolytes*; John Wiley & Sons, Ltd, 2013; pp 169–200. <https://doi.org/10.1002/9783527655700.ch5>.
- (13) Lakowicz, J. R. *Principles of Fluorescence Spectroscopy*, 3rd ed.; Springer US, 2006.
- (14) Willis-Fox, N.; Gutacker, A.; Browne, M. P.; Khan, A. R.; Lyons, M. E. G.; Scherf, U.; Evans, R. C. Selective Recognition of Biologically Important Anions Using a Diblock Polyfluorene-Polythiophene Conjugated Polyelectrolyte. *Polymer Chemistry* **2017**, 8 (46). <https://doi.org/10.1039/c7py01478c>.
- (15) Brown, D. M.; Yang, J.; Strach, E. W.; Khalil, M. I.; Whitten, D. G. Size and Substitution Effect on Antimicrobial Activity of Polythiophene Polyelectrolyte Derivatives Under Photolysis and Dark Conditions. *Photochemistry and Photobiology* **2018**, 94 (6), 1116–1123. <https://doi.org/10.1111/php.13013>.
- (16) Lee, W.; Seo, J. H.; Woo, H. Y. Conjugated Polyelectrolytes: A New Class of Semiconducting Material for Organic Electronic Devices. *Polymer (United Kingdom)* **2013**, 54 (19), 5104–5121. <https://doi.org/10.1016/j.polymer.2013.07.015>.
- (17) Hu, S.; Zhong, C.; Wu, H.; Cao, Y. Organic Optoelectronic Devices Containing Water/Alcohol-Soluble Conjugated Polymers and Conjugated Polyelectrolytes*. In *Conjugated Polyelectrolytes*; John Wiley & Sons, Ltd, 2013; pp 345–388. <https://doi.org/10.1002/9783527655700.ch11>.
- (18) Lee, S.; Nguyen, T. L.; Lee, S. Y.; Jang, C. H.; Lee, B. R.; Jung, E. D.; Park, S. Y.; Yoon, Y. J.; Kim, J. Y.; Woo, H. Y.; et al. Conjugated Polyelectrolytes Bearing Various Ion Densities: Spontaneous Dipole Generation, Poling-Induced Dipole Alignment, and Interfacial Energy Barrier Control for Optoelectronic Device Applications. *Adv. Mater. Weinheim* **2018**, 30 (14), e1706034. <https://doi.org/10.1002/adma.201706034>.
- (19) Langenhorst, F.; Campione, M. Ideal and Real Structures of Different Forms of Carbon, with Some Remarks on Their Geological Significance. *Journal of the Geological Society* **2018**, jgs2018-056. <https://doi.org/10.1144/jgs2018-056>.
- (20) Körner, C. Oligothiophene Materials for Organic Solar Cells - Photophysics and Device Properties. **2013**.
- (21) Seidler, N. Polythiophene Nanofibres for Optoelectronic Applications. Doctoral, UCL (University College London), 2014.
- (22) *Electronic Structure of Organic Semiconductors*. <https://doi.org/10.1088/2053-2571/aaddd8>.
- (23) Lemieux, É. J.; Leclerc, M. Sensing via Conformational Changes of Conjugated Polythiophenes. In *Conjugated Polyelectrolytes*; John Wiley & Sons, Ltd, 2013; pp 231–261. <https://doi.org/10.1002/9783527655700.ch7>.
- (24) Wang, S.; C. Bazan, G. Solvent -Dependent Aggregation of a Water-Soluble Poly(Fluorene) Controls Energy Transfer to Chromophore -Labeled DNA. *Chemical Communications* **2004**, 0 (21), 2508–2509. <https://doi.org/10.1039/B410002F>.
- (25) Lavigne, J. J.; Broughton, D. L.; Wilson, J. N.; Erdogan, B.; Bunz, U. H. F. “Surfactochromic” Conjugated Polymers: Surfactant Effects on Sugar-Substituted PPEs. *Macromolecules* **2003**, 36 (20), 7409–7412. <https://doi.org/10.1021/ma0348167>.
- (26) Tan, C.; R. Pinto, M.; S. Schanze, K. Photophysics, Aggregation and Amplified Quenching of a Water-Soluble Poly(Phenylene Ethynylene). *Chemical Communications* **2002**, 0 (5), 446–447. <https://doi.org/10.1039/B109630C>.
- (27) Burrows, H. D.; Lobo, V. M. M.; Pina, J.; Ramos, M. L.; Seixas de Melo, J.; Valente, A. J. M.; Tapia, M. J.; Pradhan, S.; Scherf, U. Fluorescence Enhancement of the Water- Soluble

- Poly{1,4-Phenylene-[9,9-Bis- (4-Phenoxybutylsulfonate)]Fluorene-2,7-Diyl} Copolymer in n-Dodecylpentaerythritol Glycol Ether Micelles. *Macromolecules* **2004**, *37* (20), 7425–7427. <https://doi.org/10.1021/ma048780+>.
- (28) Garcia, A.; Nguyen, T.-Q. Effect of Aggregation on the Optical and Charge Transport Properties of an Anionic Conjugated Polyelectrolyte. *J. Phys. Chem. C* **2008**, *112* (17), 7054–7061. <https://doi.org/10.1021/jp711462p>.
 - (29) Fang, J.; Wallikewitz, B. H.; Gao, F.; Tu, G.; Müller, C.; Pace, G.; Friend, R. H.; Huck, W. T. S. Conjugated Zwitterionic Polyelectrolyte as the Charge Injection Layer for High-Performance Polymer Light-Emitting Diodes. *J. Am. Chem. Soc.* **2011**, *133* (4), 683–685. <https://doi.org/10.1021/ja108541z>.
 - (30) Scherf, U. Counterion Pinning in Conjugated Polyelectrolytes for Applications in Organic Electronics. *Angewandte Chemie International Edition* **2011**, *50* (22), 5016–5017. <https://doi.org/10.1002/anie.201101643>.
 - (31) Spano, F. C.; Silva, C. H- and J-Aggregate Behavior in Polymeric Semiconductors. *Annual Review of Physical Chemistry* **2014**, *65* (1), 477–500. <https://doi.org/10.1146/annurev-physchem-040513-103639>.
 - (32) Zhu, J.; Han, Y.; Kumar, R.; He, Y.; Hong, K.; Bonnesen, P. V.; Sumpter, B. G.; Smith, S. C.; Smith, G. S.; Ivanov, I. N.; et al. Controlling Molecular Ordering in Solution-State Conjugated Polymers. *Nanoscale* **2015**, *7* (37), 15134–15141. <https://doi.org/10.1039/C5NR02037A>.
 - (33) Baghgar, M.; Labastide, J. A.; Bokel, F.; Hayward, R. C.; Barnes, M. D. Effect of Polymer Chain Folding on the Transition from H- to J-Aggregate Behavior in P3HT Nanofibers. *J. Phys. Chem. C* **2014**, *118* (4), 2229–2235. <https://doi.org/10.1021/jp411668g>.
 - (34) Dimitriev, O. P.; Blank, D. A.; Ganser, C.; Teichert, C. Effect of the Polymer Chain Arrangement on Exciton and Polaron Dynamics in P3HT and P3HT:PCBM Films. *J. Phys. Chem. C* **2018**, *122* (30), 17096–17109. <https://doi.org/10.1021/acs.jpcc.8b05155>.
 - (35) Agbolaghi, S.; Zenoozi, S. A Comprehensive Review on Poly(3-Alkylthiophene)-Based Crystalline Structures, Protocols and Electronic Applications. *Organic Electronics* **2017**, *51*, 362–403. <https://doi.org/10.1016/j.orgel.2017.09.038>.
 - (36) Deng, Y.; Feng, X.; Yang, D.; Yi, C.; Qiu, X. Pi-Pi Stacking of the Aromatic Groups in Lignosulfonates. *BioResources* **2012**, *7* (1), 1145–1156. <https://doi.org/10.15376/biores.7.1.1145-1156>.
 - (37) Zhao, C. L.; Winnik, M. A.; Riess, G.; Croucher, M. D. Fluorescence Probe Techniques Used to Study Micelle Formation in Water-Soluble Block Copolymers. *Langmuir* **1990**, *6* (2), 514–516. <https://doi.org/10.1021/la00092a038>.
 - (38) Wilhelm, M.; Zhao, C. L.; Wang, Y.; Xu, R.; Winnik, M. A.; Mura, J. L.; Riess, G.; Croucher, M. D. Poly(Styrene-Ethylene Oxide) Block Copolymer Micelle Formation in Water: A Fluorescence Probe Study. *Macromolecules* **1991**, *24* (5), 1033–1040. <https://doi.org/10.1021/ma00005a010>.
 - (39) Ghosh, R.; Das, S.; Chatterjee, D. P.; Nandi, A. K. Surfactant-Triggered Fluorescence Turn “on/off” Behavior of a Polythiophene-Graft-Polyampholyte. *Langmuir* **2016**, *32* (33), 8413–8423. <https://doi.org/10.1021/acs.langmuir.6b01928>.
 - (40) Ottaviani, M. F.; Cangiotti, M.; Fiorani, L.; Barnard, A.; Jones, S. P.; Smith, D. K. Probing Dendron Structure and Nanoscale Self-Assembly Using Computer-Aided Analysis of EPR Spectra. *New J. Chem.* **2012**, *36* (2), 469–476. <https://doi.org/10.1039/C1NJ20685K>.

- (41) Santeusano, S.; Attanasi, O. A.; Majer, R.; Cangiotti, M.; Fattori, A.; Ottaviani, M. F. Effect of Hydrogenated Cardanol on the Structure of Model Membranes Studied by EPR and NMR. **2013**.
- (42) Gao, J.; Stein, B. W.; Thomas, A. K.; Garcia, J. A.; Yang, J.; Kirk, M. L.; Grey, J. K. Enhanced Charge Transfer Doping Efficiency in J-Aggregate Poly(3-Hexylthiophene) Nanofibers. *J. Phys. Chem. C* **2015**, *119* (28), 16396–16402. <https://doi.org/10.1021/acs.jpcc.5b05191>.
- (43) Geddes, C. D. Optical Halide Sensing Using Fluorescence Quenching: Theory, Simulations and Applications - a Review. *Meas. Sci. Technol.* **2001**, *12* (9), R53. <https://doi.org/10.1088/0957-0233/12/9/201>.
- (44) Heinlein, T.; Knemeyer, J.-P.; Piestert, O.; Sauer, M. Photoinduced Electron Transfer between Fluorescent Dyes and Guanosine Residues in DNA-Hairpins. *J. Phys. Chem. B* **2003**, *107* (31), 7957–7964. <https://doi.org/10.1021/jp0348068>.
- (45) Pace, N. A.; Reid, O. G.; Rumbles, G. Delocalization Drives Free Charge Generation in Conjugated Polymer Films. *ACS Energy Lett.* **2018**, *3* (3), 735–741. <https://doi.org/10.1021/acsenenergylett.8b00108>.
- (46) Wang, J.; Wang, D.; Miller, E. K.; Moses, D.; Bazan, G. C.; Heeger, A. J. Photoluminescence of Water-Soluble Conjugated Polymers: Origin of Enhanced Quenching by Charge Transfer. *Macromolecules* **2000**, *33* (14), 5153–5158. <https://doi.org/10.1021/ma000081j>.
- (47) Campbell, K.; Zappas, A.; Bunz, U.; Thio, Y. S.; Bucknall, D. G. Fluorescence Quenching of a Poly(Para-Phenylene Ethynylenes) by C60 Fullerenes. *Journal of Photochemistry and Photobiology A: Chemistry* **2012**, *249*, 41–46. <https://doi.org/10.1016/j.jphotochem.2012.08.015>.
- (48) Deiana, M.; Mettra, B.; Matczyszyn, K.; Piela, K.; Pitrat, D.; Olesiak-Banska, J.; Monnereau, C.; Andraud, C.; Samoc, M. Interactions of a Biocompatible Water-Soluble Anthracenyl Polymer Derivative with Double-Stranded DNA. *Phys. Chem. Chem. Phys.* **2015**, *17* (45), 30318–30327. <https://doi.org/10.1039/C5CP05381A>.
- (49) Goutam, P. J.; Singh, D. K.; Iyer, P. K. Photoluminescence Quenching of Poly(3-Hexylthiophene) by Carbon Nanotubes. *J. Phys. Chem. C* **2012**, *116* (14), 8196–8201. <https://doi.org/10.1021/jp300115q>.
- (50) Stern, O., V., M. On the Quenching-Time of Fluorescence. *Physik Zeitschr* **20**, 183–188.
- (51) Liu, Y.; Meng, X.; Pei, M.; Zhang, G.; Li, H. Sensitive Fluorescence “off-on” Switch System for Catechins Detection Based on Water-Soluble Polythiophene Derivatives. *Anal. Methods* **2014**, *6* (15), 5812–5817. <https://doi.org/10.1039/C4AY00937A>.
- (52) Ncube, P.; Krause, R. W.; Mamba, B. B. Fluorescent Sensing of Chlorophenols in Water Using an Azo Dye Modified β -Cyclodextrin Polymer. *Sensors (Basel)* **2011**, *11* (5), 4598–4608. <https://doi.org/10.3390/s110504598>.
- (53) D’Souza, F.; Gadde, S.; Islam, D.-M. S.; Pang, S.-C.; Schumacher, A. L.; Zandler, M. E.; Horie, R.; Araki, Y.; Ito, O. Photoinduced Electron Transfer in a Watson–Crick Base-Paired, 2-Aminopurine:uracil-C60 Hydrogen Bonding Conjugate. *Chem. Commun.* **2007**, *0* (5), 480–482. <https://doi.org/10.1039/B611217J>.
- (54) Hu, Y.-J.; Ou-Yang, Y.; Dai, C.-M.; Liu, Y.; Xiao, X.-H. Binding of Berberine to Bovine Serum Albumin: Spectroscopic Approach. *Mol Biol Rep* **2010**, *37* (8), 3827–3832. <https://doi.org/10.1007/s11033-010-0038-x>.

- (55) Lehrer, S. Solute Perturbation of Protein Fluorescence. Quenching of the Tryptophyl Fluorescence of Model Compounds and of Lysozyme by Iodide Ion. *Biochemistry* **1971**, *10* (17), 3254–3263. <https://doi.org/10.1021/bi00793a015>.
- (56) Agudelo-Morales, C. E.; Silva, O. F.; Galian, R. E.; Pérez-Prieto, J. Nitroanilines as Quenchers of Pyrene Fluorescence. *ChemPhysChem* **2012**, *13* (18), 4195–4201. <https://doi.org/10.1002/cphc.201200637>.
- (57) Minami, T.; Kubo, Y. Fluorescence Sensing of Phytate in Water Using an Isothiuronium-Attached Polythiophene. *Chemistry - An Asian Journal* **2010**, *5* (3), 605–611. <https://doi.org/10.1002/asia.200900444>.
- (58) Molecular Fluorescence: Principles and Applications, 2nd Edition <https://www.wiley.com/en-us/Molecular+Fluorescence%3A+Principles+and+Applications%2C+2nd+Edition-p-9783527328376> (accessed Feb 12, 2019).
- (59) Fang, H.; Mighri, F.; Ajji, A. Fluorescence Quenching of Phenanthrene and Anthracene by Maleic Anhydride and N-Octadecenylsuccinic Anhydride in Solution and in Bulk Polypropylene. *Polymer Engineering & Science* **2007**, *47* (2), 192–199. <https://doi.org/10.1002/pen.20691>.
- (60) Deshmukh, A.; Bandyopadhyay, S.; James, A.; Patra, A. Trace Level Detection of Nitroanilines Using a Solution Processable Fluorescent Porous Organic Polymer. *J. Mater. Chem. C* **2016**, *4* (20), 4427–4433. <https://doi.org/10.1039/C6TC00599C>.
- (61) Airinei, A. T.; RI; Rusu, E.; Dorohoi, DO. FLUORESCENCE QUENCHING OF ANTHRACENE BY NITROAROMATIC COMPOUNDS. *Digest Journal of Nanomaterials and Biostructures* **2011**, *6* (3), 1265–1272.
- (62) Steiner, T. The Hydrogen Bond in the Solid State. *Angewandte Chemie International Edition* **2002**, *41* (1), 48–76. [https://doi.org/10.1002/1521-3773\(20020104\)41:1<48::AID-ANIE48>3.0.CO;2-U](https://doi.org/10.1002/1521-3773(20020104)41:1<48::AID-ANIE48>3.0.CO;2-U).
- (63) Smith, P. J.; Reddington, M. V.; Wilcox, C. S. Ion Pair Binding by a Urea in Chloroform Solution. *Tetrahedron Letters* **1992**, *33* (41), 6085–6088. [https://doi.org/10.1016/S0040-4039\(00\)60012-6](https://doi.org/10.1016/S0040-4039(00)60012-6).
- (64) Fan, E.; Van Arman, S. A.; Kincaid, S.; Hamilton, A. D. Molecular Recognition: Hydrogen-Bonding Receptors That Function in Highly Competitive Solvents. *J. Am. Chem. Soc.* **1993**, *115* (1), 369–370. <https://doi.org/10.1021/ja00054a066>.
- (65) Li, A.-F.; Wang, J.-H.; Wang, F.; Jiang, Y.-B. Anion Complexation and Sensing Using Modified Urea and Thiourea-Based Receptors. *Chemical Society Reviews* **2010**, *39* (10), 3729–3729. <https://doi.org/10.1039/b926160p>.
- (66) Kubo, Y.; Tsukahara, M.; Ishihara, S.; Tokita, S. A Simple Anion Chemosensor Based on a Naphthalene–Thiuronium Dyad. *Chemical Communications* **2000**, *0* (8), 653–654. <https://doi.org/10.1039/B000352M>.
- (67) Kubo, Y.; Ishihara, S.; Tsukahara, M.; Tokita, S. Isothiuronium-Derived Simple Fluorescent Chemosensors of Anions. *Journal of the Chemical Society, Perkin Transactions 2* **2002**, *0* (8), 1455–1460. <https://doi.org/10.1039/B202953G>.
- (68) Dormidontova, E. E. Role of Competitive PEO–Water and Water–Water Hydrogen Bonding in Aqueous Solution PEO Behavior. *Macromolecules* **2002**, *35* (3), 987–1001. <https://doi.org/10.1021/ma010804e>.
- (69) Li, A.-F.; Wang, J.-H.; Wang, F.; Jiang, Y.-B. Anion Complexation and Sensing Using Modified Urea and Thiourea-Based Receptors. *Chemical Society Reviews* **2010**, *39* (10), 3729–3729. <https://doi.org/10.1039/b926160p>.

- (70) Yeo, W.-S.; Hong, J.-I. Oxoanion Recognition by a Thiouronium Receptor. *Tetrahedron Letters* **1998**, 39 (44), 8137–8140. [https://doi.org/10.1016/S0040-4039\(98\)01806-1](https://doi.org/10.1016/S0040-4039(98)01806-1).
- (71) Nishizawa, S.; Cui, Y.-Y.; Minagawa, M.; Morita, K.; Kato, Y.; Taniguchi, S.; Kato, R.; Teramae, N. Conversion of Thioureas to Fluorescent Isothiuronium-Based Photoinduced Electron Transfer Sensors for Oxoanion Sensing. *Journal of the Chemical Society, Perkin Transactions 2* **2002**, 0 (5), 866–870. <https://doi.org/10.1039/B201704K>.
- (72) Briseno, A. L.; Holcombe, T. W.; Boukai, A. I.; Garnett, E. C.; Shelton, S. W.; Fréchet, J. J. M.; Yang, P. Oligo- and Polythiophene/ZnO Hybrid Nanowire Solar Cells. *Nano Lett.* **2010**, 10 (1), 334–340. <https://doi.org/10.1021/nl9036752>.
- (73) Chen, Y.-Z.; Wu, L.-Z.; Tung, C.-H.; Yang, Q.-Z. Hydrogen Bonding-Controlled Photoinduced Electron and Energy Transfer. In *Hydrogen Bonded Supramolecular Materials*; Li, Z.-T., Wu, L.-Z., Eds.; Lecture Notes in Chemistry; Springer Berlin Heidelberg: Berlin, Heidelberg, 2015; pp 1–42. https://doi.org/10.1007/978-3-662-45780-1_1.
- (74) Li, F.; Yang, J.; Qin, Y. Synthesis and Characterization of Polythiophene Block Copolymer and Fullerene Derivative Capable of “Three-Point” Complementary Hydrogen Bonding Interactions and Their Application in Bulk-Heterojunction Solar Cells. *J. Polym. Sci. Part A: Polym. Chem.* **2013**, 51 (16), 3339–3350. <https://doi.org/10.1002/pola.26731>.
- (75) Malika Jeffries-El, R. D. M. 9. Regioregular Polythiophenes. In *Handbook of Conducting Polymers Third Edition CONJUGATED POLYMERS THEORY, SYNTHESIS, PROPERTIES, AND CHARACTERIZATION*; Terje A. Skotheim, J. R. R., Ed.; CRC Press Taylor & Francis Group, 2007.
- (76) Yamamoto, T.; Sanechika, K.; Yamamoto, A. Preparation of Thermostable and Electric-Conducting Poly(2,5-Thienylene). *Journal of Polymer Science: Polymer Letters Edition* **1980**, 18 (1), 9–12. <https://doi.org/10.1002/pol.1980.130180103>.
- (77) McCullough, R. D.; Ewbank, P. C.; Loewe, R. S. Self-Assembly and Disassembly of Regioregular, Water Soluble Polythiophenes: Chemoselective Ionchromatic Sensing in Water. *Journal of the American Chemical Society* **1997**, 119 (3), 633–634. <https://doi.org/10.1021/ja963713j>.
- (78) Wang, E.; Bergqvist, J.; Vandewal, K.; Ma, Z.; Hou, L.; Lundin, A.; Himmelberger, S.; Salleo, A.; Müller, C.; Inganäs, O.; et al. Conformational Disorder Enhances Solubility and Photovoltaic Performance of a Thiophene–Quinoxaline Copolymer. *Advanced Energy Materials* **2013**, 3 (6), 806–814. <https://doi.org/10.1002/aenm.201201019>.
- (79) Zhao, F.; Wang, C.; Zhan, X. Morphology Control in Organic Solar Cells. *Advanced Energy Materials* **2018**, 8 (28), 1703147. <https://doi.org/10.1002/aenm.201703147>.
- (80) Ma, Y.-Z.; Shaw, R. W.; Yu, X.; O'Neill, H. M.; Hong, K. Excited-State Dynamics of Water-Soluble Polythiophene Derivatives: Temperature and Side-Chain Length Effects. *J Phys Chem B* **2012**, 116 (49), 14451–14460. <https://doi.org/10.1021/jp304526h>.
- (81) Page, Z. A.; Duzhko, V. V.; Emrick, T. Conjugated Thiophene-Containing Polymer Zwitterions: Direct Synthesis and Thin Film Electronic Properties. *Macromolecules* **2013**, 46 (2), 344–351. <https://doi.org/10.1021/ma302232q>.
- (82) Worfolk, B. J.; Rider, D. A.; Elias, A. L.; Thomas, M.; Harris, K. D.; Buriak, J. M. Bulk Heterojunction Organic Photovoltaics Based on Carboxylated Polythiophenes and PCBM on Glass and Plastic Substrates. *Advanced Functional Materials* **2011**, 21 (10), 1816–1826. <https://doi.org/10.1002/adfm.201100049>.
- (83) Burrows, H. D.; Tapia, M. J.; Silva, C. L.; Pais, A. A. C. C.; Fonseca, S. M.; Pina, J.; De Melo, J. S.; Wang, Y.; Marques, E. F.; Knaapila, M.; et al. Interplay of Electrostatic and

- Hydrophobic Effects with Binding of Cationic Gemini Surfactants and a Conjugated Polyanion: Experimental and Molecular Modeling Studies. *Journal of Physical Chemistry B* **2007**, *111* (17), 4401–4410. <https://doi.org/10.1021/jp070100s>.
- (84) Wang, M.; Zou, S.; Guerin, G.; Shen, L.; Deng, K.; Jones, M.; Walker, G. C.; Scholes, G. D.; Winnik, M. A. A Water-Soluble PH-Responsive Molecular Brush of Poly(N,N-Dimethylaminoethyl Methacrylate) Grafted Polythiophene. *Macromolecules* **2008**, *41* (19), 6993–7002. <https://doi.org/10.1021/ma800777m>.
- (85) Hansen, C. M.; Smith, A. L. Using Hansen Solubility Parameters to Correlate Solubility of C60 Fullerene in Organic Solvents and in Polymers. *Carbon* **2004**, *42* (8), 1591–1597. <https://doi.org/10.1016/j.carbon.2004.02.011>.
- (86) Zalar, P.; Nguyen, T.-Q. Charge Injection Mechanism in PLEDs and Charge Transport in Conjugated Polyelectrolytes. In *Conjugated Polyelectrolytes*; John Wiley & Sons, Ltd, 2013; pp 315–344. <https://doi.org/10.1002/9783527655700.ch10>.
- (87) Kamps, A. C. Synthesis and Self-Assembly of Polymeric Hybrid Nanomaterials Synthesis and Self-Assembly of Polymeric Hybrid Nanomaterials. **2012**.
- (88) Nguyen, T.-Q.; Doan, V.; Schwartz, B. J. Conjugated Polymer Aggregates in Solution: Control of Interchain Interactions. *J. Chem. Phys.* **1999**, *110* (8), 4068–4078. <https://doi.org/10.1063/1.478288>.
- (89) McDowell, C.; Abdelsamie, M.; Toney, M. F.; Bazan, G. C. Solvent Additives: Key Morphology-Directing Agents for Solution-Processed Organic Solar Cells. *Advanced Materials* **2018**, *30* (33). <https://doi.org/10.1002/adma.201707114>.
- (90) Jain, N.; Chandrasekaran, N.; Sadhanala, A.; Friend, R. H.; McNeill, C. R.; Kabra, D. Interfacial Disorder in Efficient Polymer Solar Cells: The Impact of Donor Molecular Structure and Solvent Additives. *J. Mater. Chem. A* **2017**, *5* (47), 24749–24757. <https://doi.org/10.1039/C7TA07924A>.
- (91) Damlin, P.; Hätönen, M.; Domínguez, S. E.; Ääritalo, T.; Kivelä, H.; Kvarnström, C. Study of the Electrochemical and Optical Properties of Fullerene and Methano[60]Fullerenediphosphonate Derivatives in Solution and as Self-Assembled Structures. *RSC Adv.* **2014**, *4* (16), 8391–8401. <https://doi.org/10.1039/C3RA46740F>.
- (92) Domínguez, S. E.; Meriläinen, M.; Ääritalo, T.; Damlin, P.; Kvarnström, C. Effect of Alkoxy-Spacer Length and Solvent on Diluted Solutions of Cationic Isothiuronium Polythiophenes. *RSC Adv.* **2017**, *7* (13), 7648–7657. <https://doi.org/10.1039/C6RA21451G>.
- (93) Domínguez, S. E.; Cangiotti, M.; Fattori, A.; Ääritalo, T.; Damlin, P.; Ottaviani, M. F.; Kvarnström, C. Effect of Spacer Length and Solvent on the Concentration-Driven Aggregation of Cationic Hydrogen-Bonding Donor Polythiophenes. *Langmuir* **2018**, *34* (25), 7364–7378. <https://doi.org/10.1021/acs.langmuir.8b00808>.
- (94) Mirakyan, A. L.; Wilson, L. J. Functionalization of C60 with Diphosphonate Groups: A Route to Bone-Vectored Fullerenes. *J. Chem. Soc., Perkin Trans. 2* **2002**, *0* (6), 1173–1176. <https://doi.org/10.1039/B200145D>.
- (95) Nuretdinov, I. A.; Gubskaya, V. P.; Shishikina, N. I.; Fazleeva, G. M.; Berezhnaya, L. Sh.; Karaseva, I. P.; Sibgatullina, F. G.; Zverev, V. V. Reactions of Carbanions of Bis(Dialkoxyphosphoryl)Bromomethane with Fullerenes C60 and C70. *Russian Chemical Bulletin* **2002**, *51* (2), 337–341. <https://doi.org/10.1023/A:1015472114103>.
- (96) Belandria, V.; Mohammadi, A. H.; Richon, D. Volumetric Properties of the (Tetrahydrofuran + Water) and (Tetra-n-Butyl Ammonium Bromide + Water) Systems: Experimental Measurements and Correlations. *Journal of Chemical Thermodynamics* **2009**, *41* (12), 1382–1386. <https://doi.org/10.1016/j.jct.2009.06.014>.

- (97) Nayak, J.; Aralaguppi, M.; Naidu, B. V.; Aminabhavi, T. Thermodynamic Properties of Water + Tetrahydrofuran and Water + 1,4-Dioxane Mixtures at (303 . 15 , 313 . 15 , and 323 . 15) K. *J. Chem. Eng. Data* **2004**, 49, 468–474.
- (98) Critchfield, F. E.; Gibson Jr., J. A.; Hall, J. L. Dielectric Constant for the Dioxane—Water System from 20 to 35°. *Journal of the American Chemical Society* **1953**, 75 (8), 1991–1992. <https://doi.org/10.1021/ja01104a506>.
- (99) Chu, Kwang-Yu, Thompson, R. Densities and Refractive Indices of Alcohol-Water Solutions. *Journal of Chemical & Engineering Data* **1962**, 7 (3), 358–360. <https://doi.org/10.1021/jc60014a011>.
- (100) Rudakov, O. B.; Rudakova, L. V.; Podolina, E. A.; Barsukova, L. G. Penetration Isotherms of Binary Mobile Phases for Liquid Chromatography. *Russ. J. Phys. Chem.* **2009**, 83 (11), 1972–1975. <https://doi.org/10.1134/S0036024409110272>.
- (101) Akerlof, G. Dielectric Constants of Some Organic Solvent-Water Mixtures at Various Temperatures. *Journal of the American Chemical Society* **1932**, 54, 4125–4139. <https://doi.org/10.1021/ja01350a001>.
- (102) Critchfield, F. E.; Gibson Jr., J. A.; Hall, J. L. Dielectric Constant and Refractive Index from 20 to 35° and Density at 25° for the System Tetrahydrofuran—Water. *Journal of the American Chemical Society* **1953**, 75 (23), 6044–6045. <https://doi.org/10.1021/ja01119a509>.
- (103) Omota, L.-M.; Iulian, O.; Omota, F.; Ciocirlan, O. DENSITIES AND DERIVED PROPERTIES OF WATER, 1,4-DIOXANE AND DIMETHYL SULFOXIDE BINARY AND TERNARY SYSTEMS AT TEMPERATURES FROM 293.15 K TO 313.15 K. *Revue Roumaine de Chimie* **2009**, 54 (1), 63–73.
- (104) Barton, A. F. M. *CRC Handbook of Solubility Parameters and Other Cohesion Parameters, Second Edition*, Second.; Barton, A. F. M., Ed.; CRC Press, 1991. <https://doi.org/9780849301766> - CAT# 176.
- (105) Hansen, C. M. *Hansen Solubility Parameters: A User's Handbook, Second Edition*; Hansen, C. M., Ed.; 2007.
- (106) Kris, M. R. EFFECT OF 1,4-DIOXANE ON THE COMPLEXATION OF LANTHANIDES WITH α -HYDROXY- ISOBUTYRATE By MARIA REBECCA KRIZ A Dissertation Submitted in Partial Fulfillment of the Requirements for the Degree of DOCTOR OF PHILOSOPHY Department of Chemistry DECEMBER 2010. **2010**, No. December.
- (107) Ying Guang Wu; Masaaki, T.; Toshiyuki, T. A Local Solvent Structure Study on 1,4-Dioxane-Water Binary Mixtures by Total Isotropic Rayleigh Light Scattering Method. *Journal of Molecular Liquids* **2001**, 94 (3), 273–282. [https://doi.org/10.1016/S0167-7322\(01\)00275-6](https://doi.org/10.1016/S0167-7322(01)00275-6).
- (108) Burrows, H. D.; Fonseca, S. M.; Silva, C. L.; Pais, A. A. C. C.; Tapia, M. J.; Pradhan, S.; Scherf, U. Aggregation of the Hairy Rod Conjugated Polyelectrolyte Poly{1,4-Phenylene-[9,9-Bis(4-Phenoxybutylsulfonate)]Fluorene-2,7-Diyl} in Aqueous Solution: An Experimental and Molecular Modelling Study. *Phys Chem Chem Phys* **2008**, 10 (30), 4420–4428. <https://doi.org/10.1039/b800773j>.
- (109) Menges, F. *Spectragryph - Optical Spectroscopy Software*; 2017.
- (110) Trucks, G. W. Schlegel, H. B.; Frisch, M. J. *Gaussian 09*; Gaussian, Inc., 2009.
- (111) Hanwell, M. D.; Curtis, D. E.; Lonie, D. C.; Vandermeersch, T.; Zurek, E.; Hutchison, G. R. Avogadro: An Advanced Semantic Chemical Editor, Visualization, and Analysis

- Platform. *Journal of Cheminformatics* **2012**, 4 (8), 1–17. <https://doi.org/10.1186/1758-2946-4-17>.
- (112) *Jmol: An Open-Source Java Viewer for Chemical Structures in 3D* [Http://Www.Jmol.Org/](http://www.jmol.org/).
- (113) Liu, J.; Loewe, R. S.; McCullough, R. D. Employing MALDI-MS on Poly(Alkylthiophenes): Analysis of Molecular Weights, Molecular Weight Distributions, End-Group Structures, and End-Group Modifications. *Macromolecules* **1999**, 32 (18), 5777–5785. <https://doi.org/10.1021/ma9905324>.
- (114) Lukkari, K.; Salomaki, M.; Viinikanoja, A.; Aaritalo, T.; Paukkunen, J.; Kocharova, N.; Kankare, J. Polyelectrolyte Multilayers Prepared from Water-Soluble Poly(Alkoxythiophene) Derivatives. *J. Am. Chem. Soc.* **2001**, 123 (14), 6083–6083. <https://doi.org/10.1021/ja0043486>.
- (115) Viinikanoja, A.; Areva, S.; Kocharova, N.; Ääritalo, T.; Vuorinen, M.; Savunen, A.; Kankare, J.; Lukkari, J. Structure of Self-Assembled Multilayers Prepared from Water-Soluble Polythiophenes. *Langmuir* **2006**, 22 (14), 6078–6086. <https://doi.org/10.1021/la060519u>.
- (116) Knaapila, M.; Evans, R. C.; Garamus, V. M.; Almásy, L.; Székely, N. K.; Gutacker, A.; Scherf, U.; Burrows, H. D. Structure and “Surfactochromic” Properties of Conjugated Polyelectrolyte (CPE): Surfactant Complexes between a Cationic Polythiophene and SDS in Water. *Langmuir: the ACS journal of surfaces and colloids* **2010**, 26 (19), 15634–15643. <https://doi.org/10.1021/la102591b>.
- (117) Chayer, M.; Faïd, K.; Leclerc, M. Highly Conducting Water-Soluble Polythiophene Derivatives. *Chem. Mater.* **1997**, 9 (12), 2902–2905. <https://doi.org/10.1021/cm970238v>.
- (118) Ho, H.-A.; Boissinot, M.; Bergeron, M. G.; Corbeil, G.; Doré, K.; Boudreau, D.; Leclerc, M. Colorimetric and Fluorometric Detection of Nucleic Acids Using Cationic Polythiophene Derivatives. *Angewandte Chemie* **2002**, 114 (9), 1618–1621. [https://doi.org/10.1002/1521-3757\(20020503\)114:9<1618::AID-ANGE1618>3.0.CO;2-2](https://doi.org/10.1002/1521-3757(20020503)114:9<1618::AID-ANGE1618>3.0.CO;2-2).
- (119) Johansson, T.; Mammo, W.; Svensson, M.; Andersson, M. R.; Inganäs, O. Electrochemical Bandgaps of Substituted Polythiophenes. *J. Mater. Chem.* **2003**, 13 (6), 1316–1323. <https://doi.org/10.1039/B301403G>.
- (120) Cardona, C. M.; Li, W.; Kaifer, A. E.; Stockdale, D.; Bazan, G. C. Electrochemical Considerations for Determining Absolute Frontier Orbital Energy Levels of Conjugated Polymers for Solar Cell Applications. *Advanced Materials* **2011**, 23 (20), 2367–2371. <https://doi.org/10.1002/adma.201004554>.
- (121) Lévêque, P.; Biniek, L.; Fall, S.; Chocos, C. L.; Leclerc, N.; Heiser, T. Alkoxy Side Chains in Low Band-Gap Co-Polymers: Impact on Conjugation and Frontier Energy Levels. *Energy Procedia* **2012**, 31, 38–45. <https://doi.org/10.1016/j.egypro.2012.11.163>.
- (122) Irfan, A.; Al-Sehemi, A. G.; Muhammad, S. Towards Rational Designing of Efficient Sensitizers Based on Thiophene and Infrared Dyes for Dye-Sensitized Solar Cells <https://www.hindawi.com/journals/jqc/2014/796790/> (accessed May 28, 2019). <https://doi.org/10.1155/2014/796790>.
- (123) Ko, S.; Hoke, E. T.; Pandey, L.; Hong, S.; Mondal, R.; Risko, C.; Yi, Y.; Noriega, R.; McGehee, M. D.; Brédas, J.-L.; et al. Controlled Conjugated Backbone Twisting for an Increased Open-Circuit Voltage While Having a High Short-Circuit Current in Poly(Hexylthiophene) Derivatives. *J. Am. Chem. Soc.* **2012**, 134 (11), 5222–5232. <https://doi.org/10.1021/ja210954r>.

- (124) Rasmussen, S. C.; Evenson, S. J.; McCausland, C. B. Fluorescent Thiophene-Based Materials and Their Outlook for Emissive Applications. *Chem. Commun.* **2015**, 51 (22), 4528–4543. <https://doi.org/10.1039/C4CC09206F>.
- (125) Hermenegildo, B. F.; Pereira, G.; Abreu, A. S.; Castanheira, E. M. S.; Ferreira, P. M. T.; Queiroz, M. J. R. P. Phenanthrenyl-Indole as a Fluorescent Probe for Peptides and Lipid Membranes. *Journal of Photochemistry and Photobiology A: Chemistry* **2011**, 221 (1), 47–57. <https://doi.org/10.1016/j.jphotochem.2011.04.022>.
- (126) Gutacker, A.; Koenen, N.; Scherf, U.; Adamczyk, S.; Pina, J.; Fonseca, S. M.; Valente, A. J. M.; Evans, R. C.; Seixas de Melo, J.; Burrows, H. D.; et al. Cationic Fluorene-Thiophene Diblock Copolymers: Aggregation Behaviour in Methanol/Water and Its Relation to Thin Film Structures. *Polymer* **2010**, 51 (9), 1898–1903. <https://doi.org/10.1016/j.polymer.2010.03.010>.
- (127) Goldoni, F. F. Thiophene-Based Pi-Conjugated Polymers: Synthetic Design towards the Control of Their Supramolecular Architecture. **2000**. <https://doi.org/10.6100/IR533019>.
- (128) Gómez, D. E.; Fabbrizzi, L.; Licchelli, M.; Monzani, E. Urea vs. Thiourea in Anion Recognition. *Org. Biomol. Chem.* **2005**, 3 (8), 1495–1500. <https://doi.org/10.1039/B500123D>.
- (129) Bazzicalupi, C.; Bencini, A.; Lippolis, V. Tailoring Cyclic Polyamines for Inorganic/Organic Phosphate Binding. *Chemical Society Reviews* **2010**, 39 (10), 3709–3709. <https://doi.org/10.1039/b926161n>.
- (130) SHARMA, R. N.; PANCHOLI, S. S. PROTEIN BINDING INTERACTION STUDY OF OLMESARTAN MEDOXOMIL AND ITS METABOLITE OLMESARTAN BY FLUORESCENCE SPECTROSCOPY. **6**, 4.
- (131) Rashid, M. A.; Islam Rabbi, S. N. Fluorescence Spectroscopic Study of Interaction between Olanzapine and Bovine Serum Albumin. *Pharmaceutica Analytica Acta* **2015**, 06 (08). <https://doi.org/10.4172/2153-2435.1000408>.
- (132) Samanta, P. N.; Das, K. K. Noncovalent Interaction Assisted Fullerene for the Transportation of Some Brain Anticancer Drugs: A Theoretical Study. *Journal of Molecular Graphics and Modelling* **2017**, 72, 187–200. <https://doi.org/10.1016/j.jmgm.2017.01.009>.

Original Publications

Sergio Ulises Espinosa Domínguez

Study of the electrochemical and optical properties of fullerene and methano[60]-fullerenediphosphonate derivatives in solution and as self-assembled structures

2014 January; 11 pp.

Effect of alkoxy-spacer length and solvent on diluted solutions of cationic isothiuronium polythiophenes

2017 January; 10 pp.

Effect of Spacer Length and Solvent on the Concentration-Driven Aggregation of Cationic Hydrogen-Bonding Donor Polythiophenes

2018 May; 15 pp.

Hydrogen-bonding mediated interactions between a water-soluble polythiophene-fullerene pair with two-point hydrogen-bonding capabilities, as a function of fullerene concentration and polarity and hydrogen-bonding capacity of the solvent

Submitted manuscript; 16 pp.